Study on the Charge Transport Mechanism of Natural Dye Based Organic Schottky Diodes

A thesis submitted for the Degree of Doctor of Philosophy (Science)

Of

Jadavpur University

by

Aloke Kumar Das

Condensed Matter Physics Research Centre

Department of Physics

Jadavpur University

Kolkata 700032

2024

To the memory of my grandparents

To my parents and teachers

To my family and friends

To my wife and daughter

Declaration by the Author

I, **ALOKE KUMAR DAS**, hereby declare that this thesis titled, **Study on charge transport mechanism of natural dye based organic semiconductor Schottky diodes**, and the work presented in it are my own. I confirm that:

This work was completed entirely or mostly while pursuing a degree at this university. It has been made known if any portion of this thesis has ever been submitted for credit towards a degree or other qualification at this university or another. Whenever I have referenced someone else's published work, I always provide due credit. I have always cited my sources when I have used their words in my writing. This thesis is entirely my own work, with the exception of such quotes. I have given credit to all primary sources of support. If the thesis is based on work I did in collaboration with others, I have explicitly stated what I contributed and what others did.

(ALOKE KUMAR DAS)

Date:

Place:

CERTIFICATE FROM THE SUPERVISOR(S)

This is to certify that the thesis entitled **"Study on the charge transport mechanism of natural dye based organic Schottky diodes"**, Submitted by **Sri Aloke Kumar Das** who had got his name registered on 9th June 2022 for the award of Ph. D. (Science) Degree of Jadavpur University, is absolutely based upon his own work under the supervision of Prof. Dr. Dulal Krishna Mandal and Prof. Dr. Nabin Baran Manik and that neither this thesis nor any part of it has been submitted for either any degree / diploma or any other academic award anywhere before.

…….

……..

(Signature of the Supervisor(s) date with official seal)

Acknowledgments

I want to start by expressing my gratitude to my supervisor, Prof. Dulal Krishna Mandal, for his inspiration and leadership. Also, I would like to thank Prof. Nabin Baran Manik, another supervisor, for his encouragement and unwavering support and guidance throughout the course of this research. Your expertise and insights have been invaluable to my work. A special thank you is extended to Dr. Ratan Mandal for his insightful comments that he provided during my study.

I am also thankful to Dr. Partha Pratim Roy, Prof. Kalyan Kumar Chattopadhyay and Prof. Subinay Chakraborty whose feedback and suggestions greatly enriched my study.

Most of the measurements were carried out using the equipment of the School of Energy Studies and department of physics lab at the Jadavpur University in Kolkata. I would want to thank both the labs of Jadavpur University.

Dr. Marc Burgelman (University of Gent) provided the simulation software SCAPS is used in the simulation study of this work, which the authors gratefully acknowledge.

Finally, I would want to thank the previous and present members of the Organic Semiconductors group for the enjoyable gatherings we had at Jadavpur University.

My sincere appreciation goes to my loving parents, friends and family for their encouragement and understanding.

This thesis would not have been possible without the contributions of each individual mentioned above, as well as many others who have supported me along this journey.

List of Tables

List of Figures

List of Abbreviations

Ag	Silver
Al	Aluminum
Al-M	Aluminum coated Myler
BHJ	Bulk heterojunction
CB	Conduction Band
CT	Charge transfer
CTE	Charge transfer exciton
CU	Copper
DAD	Donor acceptor donor
DFT	Density functional theory
DT	Direct tunnelling
E_c	Trap Energy
EET	Electronic energy transfer
EL	Electroluminescence
EQE	External quantum efficiency
ETL	Electron transport layer
FC	Franck Condon
FNT	Fowler-NordheimTunneling
G (I, V)	(d logI)/ (d logV)
GD	Gaussian Distribution
HOMO	Highest occupied molecular orbital
HT	Herzberg Teller
HTL	Hole transport layer
IPV	Inorganic photovoltaics
IRF	Instrument response function
LUMO	Lowest unoccupied molecular orbital
MG	Malachite green

MR	Methyl Red
NP	Nanoparticles
OPV	Organic Photovoltaic
PVA	Polyvinyl alcohol
PFE	Poole-Frenkle emission
R_J	Differential resistance or junction resistance
RR	Rectification ratio or asymmetry of the diode = $F_{ASYM} = I_F/I_R$
Rs	Series Resistance
SCLC	Space charge limited current
SE	Schottky emission
Tc	Characteristics temperature
VB	Valance band
β_{PF}	Poole-Frenkle emission lowering coefficient
β_{PF}	Schottky emission lowering coefficient

Contents

Chapter 3

Electrical Characteristics of Turmeric dye-based organic device

Chapter 4

The current transport mechanism of Beetroot and indigo dye-based organic semiconductor Schottky diodes

Chapter 5

Quantum tunnelling in beetroot, turmeric and indigo dye-based Schottky diodes

Chapter 6

Impact of ZnO nanoparticles on electrical characteristics of organic Beetroot, Turmeric and Indigo Schottky diodes

Chapter 7

The impact of shape of zinc oxide nanoparticles on electrical parameters of Beetroot Schottky diode

Chapter 8

Conclusion

Preface

In the realm of semiconductor physics and organic electronics, the pursuit of efficient, ecofriendly and sustainable materials for electronic devices has become increasingly vital. This journey led to the exploration of natural dyes as promising candidates for organic semiconductor applications. The study presented in this thesis delves deep into understanding the "**Charge transport mechanism of natural dye-based organic Schottky diodes"**, aiming to unravel their potential in next-generation electronic devices.

Researchers discovered the electrical conductivity of some organic materials and polymers such as Polyacetylene. But there is not so much study on the conductivity of natural dye-based organic materials. So, in this thesis we have discussed the semiconducting behaviour of some natural herbal dyes and charge transport mechanism through them. For this purpose, we have chosen Indigo, Turmeric and Beetroot dyes in this work. To measure and analyse the electrical parameters of any metal-semiconductor junction based electronic devices dark I-V characteristics is very important. For this reason, we have fabricated Al / Indigo / Cu, Al / Turmeric / Cu and Al / Beetroot / Cu devices and observed the dark I-V characteristics. Then using this dark I-V we have measured the electrical parameters and analyse them. We have also observed the absorption spectra of dye solutions and using this we have measured the band gap of the respective dye molecules which lying in the range of semiconductor. Finally, we have discussed the charge transport mechanism through natural dye-based organic Schottky diodes.

Devices based on these natural dye-based organic materials are more advantageous than those based on inorganic materials because of their low cost, easy fabrication processes, and simple electrical and optical characteristic adjustment. Modifying the electrical and optoelectronic properties of organic materials is also an easy process. At the same time the low mobility, the presence of traps, the effects of dampness, etc., impose some limitations. Low efficiency in organic devices is a big issue because of these restrictions.

The conductivity and performance of the devices produced by organic semiconductors are poor, despite the fact that these materials have many desired features. The overall current in organic devices has been found to be substantially lower than in inorganic devices; nevertheless, in order to comprehend this finding, a thorough analysis of the charge transport mechanism through an organic semiconductor Schottky diode based on natural dye is required. Therefore, studying the

current-voltage characteristics is crucial to understand the mechanism of charge transport in organic devices based on natural dyes.

This thesis explores the charge transport mechanism of organic semiconductor Schottky diodes based on natural dyes, with the goal of maximizing their potential for use in next-generation electronic devices. Natural dyes with donor-acceptor-donor chromophore behavior, found in plants like indigo, beetroot, and curcumin, have special qualities. They are perfect for Schottky devices and metal-insulator-metal (MIM) devices due to their low dielectric constants.

This thesis undertakes a thorough analysis to clarify the complex interactions of charge carriers inside the organic semiconductor matrix by combining theoretical understanding with experimental confirmation. The journey starts with a comprehensive review of organic semiconductors, electrical properties of ZnO nanoparticles and the emerging field of organic electronics. The discussion then moves smoothly to the characterization of natural dyes, looking at their molecular makeup, optoelectronic characteristics, and applicability in semiconductor applications.

The clarification of charge transport mechanisms inside the organic semiconductor matrix is essential to this research. The study examines the dynamics of charge carriers, their mobility, and the impact of different factors on charge transport efficiency through rigorous experimentation and sophisticated theoretical modelling. Furthermore, in order to understand its influence on device performance, the interface between the metal electrode in the Schottky diode configuration and the organic semiconductor based on natural dye is carefully examined. We use simulations and experimental studies in our investigation. Using Poisson's equation, we extract the mobility, carrier concentration, and trap density in Al/beetroot/Cu Schottky diodes. The mobility is notable for reaching 124.54 $cm^2/V \cdot s$, indicating effective charge transport. The diode is a potential rectifier due to its sensitivity, nonlinearity, and asymmetric current-voltage characteristics. Additionally, we propose a one-dimensional Al/organic semiconductor/Cu diode with low capacitance, expanding the design possibilities.

Furthermore, we compare various natural dye-based diodes, including Al/indigo/Cu, Al/turmeric/Cu, and Al/beetroot/Cu. The parabolic behavior observed in the dI/dV vs. V plot suggests the influence of quantum tunneling phenomena. Finally, simulations enhance our understanding of the physical mechanisms governing these devices.

At last, our investigation centers around the incorporation of zinc oxide (ZnO) nanoparticles with the natural dyes used in this work. By altering the morphology of ZnO, we observe significant changes in the Schottky diodes characteristics. Specifically, we explore the impact on series resistance (Rs), barrier height, ideality factor, and trap energy. These parameters play a crucial role in determining the device performance.

The research and findings discussed here are not just theoretical; they have significant ramifications for the development of organic electronics. Through a thorough comprehension of the charge transport mechanism of organic semiconductor Schottky diodes based on natural dyes, we can pave the way for the development and enhancement of electronic devices that will be more efficient, sustainable, and functional in the future.

The commitment, inquisitiveness, and spirit of cooperation exhibited by everyone engaged in the search for scientific truth is demonstrated by this thesis. My genuine wish is that the knowledge gained from this study will spur more developments in the field of organic electronics and encourage upcoming generations of scientists to keep pushing the frontiers of knowledge.

Chapter 1

Motivation of the present work and thesis outline

1.1 Introduction

1.2 Motivation of the present work

1.3 Objective of the present work

1.4 Thesis outline

1.5 References

1.1 Introduction

Recently, organic polymers have drawn considerable attention from researchers for their promising opto-electronics properties. Organic materials have advantages over inorganic materials due to their low cost and high availability [1]. In addition, due to the decrease in fossil fuels and similar energy sources, which are being reduced day by day, this inherently generates the requirement to develop renewable energy technologies. Organic dye-based devices have gained much importance for its easy fabrication techniques and numerous advantages over conventional silicon-based crystalline electronic devices [2–7]. For a superior diode, the asymmetry (i.e., rectification ratio), nonlinearity and responsivity should be large, and this can be achieved via thermionic emission and quantum mechanical tunnelling [8]. Therefore, it is undoubtedly very important to select an optically active semiconductor dye material to better improve the electrical parameters of devices and to use them as an alternative to inorganic diode-like devices. Dyes have the potential to play a role as a photosensitizer, and they also possess several excellent film-forming properties.

Researchers identified the electrical conductivity of certain organic compounds and polymers, including Polyacetylene. However, there has been relatively little research on the conductivity of natural dye-based organic electronic devices. So, in this thesis, we looked at the semiconducting properties of various natural herbal dyes, as well as the charge transport mechanism that takes place through them.

1.2 Motivation of the work

The motivation behind this thesis is rooted in the burgeoning interest and pressing need for sustainable solutions in semiconductor technology. Conventional semiconductor materials, while widely used, often rely on rare or environmentally harmful resources for their production, posing significant challenges in terms of both resource availability and ecological impact. In light of these concerns, the exploration of alternative materials and device architectures has become imperative.

Natural dye-based organic semiconductor Schottky diodes offer a promising avenue for addressing these challenges. By harnessing organic compounds derived from renewable sources, such as plant

extracts, these materials not only mitigate reliance on finite resources but also present opportunities for eco-friendly device fabrication. Furthermore, the unique optical and electronic properties inherent in natural dyes make them intriguing candidates for a variety of electronic applications.

The primary motivation driving this thesis is to observe the semiconductor behaviour of natural dyes and unravel the intricate charge transport mechanisms governing the operation of natural dye-based organic semiconductor Schottky diodes. Understanding these mechanisms is crucial for optimizing device performance and unlocking their full potential for practical applications. By elucidating the fundamental principles underlying charge transport in these systems, this research aims to contribute to the advancement of sustainable semiconductor technology.

In addition, research on Schottky diodes, which are organic semiconductors based on natural dyes, has important ramifications for a number of recently developed industries, such as organic electronics, photovoltaics, and sensor technologies. This thesis aims to advance our fundamental understanding of organic semiconductor physics and to pave the way for the creation of next-generation, environmentally friendly electronic devices with improved functionality and performance by clarifying the underlying mechanisms driving charge transport in these devices.

Organic semiconductors, such as herbal dyes, offer an alternative solution for solar cell applications, as they have advantages over inorganic semiconductors, such as low cost, easy fabrication, flexibility and tunability of optical and electrical properties [1-10]. The natural herbal dyes have potential to play a role as photosensitizer and also possess some excellent film forming properties. The donor-acceptor (D-A) type chromophores with low band gap are particularly of interest [11-20]. Organic Schottky diodes are one type of organic solar cells that use a metal-organic junction to create a built-in electric field that separates the photogenerated charge carriers. However, organic Schottky diodes also face some challenges, such as high barrier height, high series resistance, high trap energy and low current conduction at the metal-organic interface. These factors limit their performance and efficiency in converting sunlight into electricity.

Therefore, there is a need to improve the electrical characteristics of organic Schottky diodes by modifying the organic layer or the metal-organic interface. One possible way to achieve this is to incorporate nanoparticles, such as zinc oxide (ZnO), into the organic layer. ZnO nanoparticles have unique properties, such as high electron mobility, high transparency and broad bandgap, that

can enhance the electrical characteristics of the organic Schottky diode. For example, ZnO nanoparticles can lower the barrier height, series resistance, trap energy and threshold voltage of the device, while increasing the current conduction in the bulk regime.

In essence, this thesis is motivated by the imperative to explore and harness the potential of natural dye-based organic semiconductor Schottky diodes as sustainable alternatives to conventional semiconductor materials. Through systematic investigation and analysis, it aims to contribute to the advancement of green electronics and pave the way for the realization of a more environmentally sustainable technological future.

1.3 Objective of the present work

The primary objective of this thesis is to explore the semiconducting properties of natural dye-based organic materials and investigate the charge transport mechanisms in natural dye-based organic semiconductor Schottky diodes. To achieve the desired electrical characteristics, we intend to develop and optimize Schottky diodes using organic semiconductors derived from natural dyes. To study the charge transport mechanism of natural dye based organic Schottky diode and also the type of conductivity in presence of different nanoparticles like ZnO, we have selected natural dyes like Turmeric, Indigo, and Beetroot. We have studied the absorption spectra to measure the band gap of dye molecule and temperature dependent I-V characteristics to analyse the semiconducting behaviour. We have also studied I-V characteristics and analyse it to find different electrical parameters.

The I-V characteristics and Norde function measurements will be used to evaluate the electrical characteristics of the devices. The results will be compared with those of pure herbal dye based organic Schottky diodes and conventional TiO_2 based Schottky diode. For current transport mechanism we want to discuss SE, PFE, GD and quantum tunnelling. And finally, we want to observe which process is more dominant for natural herbal dye based Schottky devices. We want to find out the insulating temperature of our fabricated Al/Beetroot/Cu device. Again, a simulation study was run using the SCAPS 1d program to confirm the findings of the experiment.

High values of barrier height, series resistance, trap energy and low current conduction at the metal-organic interface limit natural dye-based organic semiconductor devices performance and its applications in optoelectronics. One way to overcome these challenges is to incorporate nanoparticles, such as zinc oxide (ZnO), into the organic layer. This thesis looks into how ZnO nanoparticles affect the electrical characteristics of organic Schottky diodes derived from herbal dyes. Finally, we want to study the impact of the shape of the ZnO nano particles on electrical parameters of natural dye based FTO/Beetroot/Al Schottky diode.

The results of this research will be beneficial for future studies involving these dyes. Our initial efforts should inspire the characterization of other new materials. Additionally, the findings will help address issues related to herbal dye-based organic semiconductor Schottky diodes. This study will aid in developing a simple and cost-effective technique to enhance device performance. Furthermore, our work on the charge transport mechanism in natural dye-based organic semiconductor Schottky diodes may be applicable to other organic or inorganic electronic systems as well.

1.4 Thesis outline

The present work is presented in different chapters. In ***Chapter 1***, the thesis outlines the general intro duction, motivation and objectives of the entire study. The importance of the present work is also described. The organisation of the whole thesis work has also been described.

In ***Chapter 2*** we have discussed the overview on conductivity of organic materials and charge transportation in organic semiconductor Schottky diodes. Chemical structure of organic polymer-based semiconductor and their electrical structure also discussed. In order to understand the charge transport mechanism, it is very important to have a knowledge about the energy band diagram of semiconductor material. Here we have discussed about the energy band diagram in polymer-based organic semiconductor molecules. Here we have also discussed the basics of charge transfer exciton generation (CTE) and its dissociation. In the charge transport mechanism carrier recombination occurs, which we have also discussed in this chapter. Here we have discussed the basic of organic semiconductor Schottky diode. Trap energy and barrier height of organic semiconductor Schottky diode is very high. To reduce this and increase the conductivity we have used ZnO nanoparticles of different morphology. We have discussed a short review on ZnO nanoparticles in organic electronic devices. Finally, we have discussed on some earlier works on organic semiconductor and the natural herbal dyes we have used to fabricate thin film devices in this thesis.

From ***Chapter 3*** to ***Chapter 7*** we mentioned the fabrication and characterization of natural dye-based devices and charge transportation through them.

In ***Chapter 3*** we have discussed about the electrical Characteristics of a turmeric dye-based organic thin film device and the effect temperature on barrier height. Al/turmeric/Cu diode, which is thin film electronic device, made by fabricating and characterising herbal (turmeric) dye. The parameters of the temperature-dependent current-voltage (I-V) were assessed under various circumstances. The thermionic emission theory was used to calculate the ideality factor (n), series resistance (R_S), and shunt resistance (R_{sh}) of the Al/turmeric/Cu diode. The fact that the series resistance reduced with temperature as a result of the current research was an intriguing finding, demonstrating the semiconducting behaviour of the natural herbal dye source at disposal.

In ***Chapter 4*** we have discussed about the current transport mechanism of beetroot and indigo dye-based organic semiconductor Schottky diodes. An organic thin-film diode based on beetroot has been developed and characterised. A thermionic emission technique is used to extract the diode's electronic properties from its I-V characteristics. Additionally, using the Cheung and Cheung functions, the ideality factor (n), barrier height (ϕ), and series resistance (R_s) of Al/Beetroot/Cu were calculated respectively. The band gap of betanin which is present in the beetroot dye and the temperature dependency of n, ϕ and R_s support the hypothesis that beetroot root behaves like semiconductor. For Al/Beetroot/Cu, we have discussed charge transport mechanism using quantum tunnelling and thermionic emission. We have also discussed Poole-Frenkle emission for the Al/Beetroot/Cu diode, using the G(V) vs V plot. We also determined the trap energy (E_c) of the device, which is significantly lower than that of Al/Turmeric/Cu organic diode. Al/Beetroot/Cu's insulation temperature is theoretically predicted in this chapter.

Chapter 5 describes the trap density (N_t), density of carriers (n_o) and mobility in Al/Beetroot/Cu Schottky diode using the Poisson's equation. The device shows highly asymmetric current-voltage characteristics with a good degree of nonlinearity. In this chapter we have discussed change of nonlinearity and sensitivity of the beetroot, turmeric and indigo dye-based devices. We also proposed a one-dimensional Al/ organic semiconductor/ Cu diode with low capacitance. This chapter also reports the comparative study between a series of natural dyes-based diodes and finally the comparison with our fabricated inorganic Al/TiO_2/Cu diode. The impact of quantum tunnelling phenomena in charge transport mechanism through natural dyes-based diodes also discussed here. Finally, the simulation was utilized to develop a predicted behaviour and a better understanding of the physical mechanisms determining the effectiveness of the device under research.

In *Chapter 6* we have discussed about the effect of ZnO nanoparticles on the electrical properties of an organic Schottky diode based on herbal dyes. An herbal dye-based organic Schottky diode's electrical characteristics, including as barrier height (ϕ), series resistance (Rs), threshold voltage (V_{th}), and trap energy (Ec), were examined. We looked at how the presence of zinc oxide (ZnO) nanoparticles affected the results of the aforementioned factors. It has been noted that ZnO nanoparticles also had an impact on the aforementioned features. Based on I-V characteristics, it has been estimated and demonstrated the impact of ZnO nanoparticles on the charge transport

mechanism of Al/Beet/Cu. We have also used Norde function to analyse the electrical parameters. Consequently, there is good agreement between the results obtained using the two different approaches indicated above. It has also been investigated how ZnO nanoparticles affect several natural dyes, like indigo and turmeric. A larger range of applicability for the current work is revealed by the validation of the results for experimental dyes.

In *Chapter 7* we have discussed about the impact of the shape of zinc oxide nanoparticles on electrical parameters of natural dye-based FTO/Beetroot/Al Schottky diode. For this, we have developed FTO/ZnO/Al and herbal dye-based FTO/Beet+ZnO/Al Schottky diodes using spherical and cylindrical zinc oxide (ZnO) nanoparticles. To determine the impact of ZnO nano shape on the performance of the reported organic Schottky diode, various electrical parameters were examined. In this chapter we have used two different methods to determine the electrical parameters. It was discovered that these methods were highly consistent with one another.

Chapter 8 describes as overall summary and conclusion of the work. A description of semiconducting behaviour of turmeric, indigo, and beetroot dyes and the charge transport mechanism has been included in the overall research work conclusions in order to improve the performance of natural dye-based organic semiconductor Schottky diodes by lowering the ideality factor (n), series resistance (R_s), trap energy (E_t) and barrier height (ϕ). Even though this thesis aims to reflect a compact substantial work, there are still numerous avenues that this research study did not cover. Potential areas of additional research include photovoltaic performance, transient response, career lifetime measurement, and performance of various optoelectronic devices composed of such natural components. In this chapter, certain unresolved issues have been mentioned. As a result, these studies were accessible for further investigation into this fascinating subject.

1.5 References

1. Klauk H (Ed.) (2006), Organic Eletronics: Materials, Manufacturing and Applications 2006, Wiley-VCH, Weinheim. Print ISBN 9783527312641.

2. Klauk H (Ed.) (2006) Organic Eletronics: Materials, Manufacturing and Applications 2006, Wiley-VCH, Weinheim. Print ISBN 9783527640218.

3. Barbec CJ, Sariciftci NS, Hummelen JC (2001) Plasticsolar cells. Adv. Funct, Mater.11: 15-26.

4. Kawano K, Sakai J,Yahiro M, Adachi C (2009) Effect of solvent on fabrication of active layersin organic solar cells based on poly (3-hexylthiophene) and fullerene derivatives. Solar EnergyMaterials and Solar Cells 93: 514-518.

5. Yu G, Jeeger AJ, Charge separation and photovoltaic conversion in polymer composites with internal donor / acceptor heterojunctions. Journal of Applied Physics78

6. Feron K, Belcher WJ, Fell CJ, Dastoor PC (2012) Organic solar cells: understanding the role offorster resonance energy transfer. International Journal of Molecular Sciences 13: 17019-17047.

7. Benanti TI, Venkataraaman D (2006) organic solar cells: an overview focusing on active layermorphology. Photosynth Research 87:73-81.

8. Haldar A, Maity S, Manik NB (2008) Effect of back electrode on photovoltaic properties of crystal-violet-dye-doped solid-state thin film. lonics14: 427-432.

9. Thompson BC, Frechet JMJ (2008) Ploymer-fullerence composite solar cells. Angewandt Chemie International Edition 47: 58-77.

10. Elumalai NK, Saha A, Vijila C, Rajan Jose R, Zhang Jie Z, Ramakrishna S (2013) Enhancingthe stability of polymer solar cells by improving the conductivity of the nanostructured MoO_3hole transport layer. Physical Chemistry Chemical Physics15: 6831-6841.

11. Alimardani N, Conley JF Jr (2014) Enhancing metal-insulator-insulator-metal tunnel diodes via defect enhanced direct tunneling J. Appl, phys. 105: 082902.

12. Alimardani N, Conley JF Jr (2013) Step tunneling enhanced asymmetry in asymmetric electrode metal-insulator-metal tunnel diodes. Applied Physics Letters102: 143501.

13. Maraghechi P, Foroughi-Abari A, CadienK, Elezzabi AY (2011) Enhanced rectifying response from metal-insulator-metal junctions. Applied Physics Letters99: 253503

14. Grover S, Moddel G (2012) Engineering the current voltage characteristics of metal-insulator-metal diodes using double insulator tunnel barriers. Solid state electron67: 94-99.

15. Aydinoglu F, Alhazmi M, Cui B, Ramahi OM, Irannejad M, Brzezinski A, Yavuz M (2014) Higher performance metal-insulator-metal diodes using multiple insulator layers. Austin Journal of Nanomedicine&Nanotechnology1(1): 1004

16. Maraghechi P, Foroughi-Abari A, CadienK, Elezzabi AY (2012) Observation of reson at tunneling phenomenon in metal-insulator-insulator-insulator-metal electron tunnel devices.Applied Physics Letters100:113503

17. Gaddala MN, Abdei-Rahman M, Shamim A (2014) Design, optimization and fabrication of a 28.3 THz nano-rectenna for infrared detection and rectification. Scientific Report4 (1): 1-9.

18. Grover S,Moddel G (2011) Applicability of metal/insulator/metal (MIM) diodes to solar rectennas. IEEE Journal of Photovoltaics1(1): 78-83.

19. Weerakkody AD, SedghiN,MitrovicIZ,Zalinge HV, Noureddine IN, Hall S, Wrench JS, Chalker PR, Phillips LJ, TreharneR, Durose K (2015) Enhance low voltage nonlinearity in resonant tunneling metal-insulator-insulator-metal nanostructures. Microelectronic Engineering 147: 298-301.

20. Rad MNS, Sharbati MT, S. Behrouz S, A.R. Nekoei AR (2015) Fabrication of non-doped red organic light emitting diode using naturally occurring Curcumin as donor-acceptor-donor (D-A-D) emitting layer with very low turn-on voltage. Iranian Journal of Science & Technology 39A3: 297-304

Chapter 2

Overview on charge transportation in organic semiconductor Schottky diodes

2.1 Introduction

In the modern era, emerging concepts and techniques have been successfully utilized in semiconductors at the micro- to nanoscale level. Over the past 20 years, the field in question has demonstrated remarkable potential. The investigations focused on the optical, magnetic, and electrical characteristics of mainly on the inorganic semiconducting materials. But the discovery of charge conductivity in organic materials has created a new and exciting area of study. Organic materials differ from inorganic materials in optoelectronic properties. Studies on these materials have given material scientists a brand-new opportunity to use them as active materials in the construction of various gadgets. The availability, low cost, the simplicity of the film fabrication process, and flexibility spur more interest to study its applicability in optoelectronic devices. Even so, there are several fundamental restrictions on the materials' extensive use in device applications. When exposed to high current for an extended period of time, some devices composed of the organic materials show low stability. Furthermore, the disordered nature of organic semiconductors, which leaves them prone to traps, is one of the main reasons for their poor current conduction. When trapping states are present, conduction into the materials has a high value of series resistance. With the trap states there are so many reasons for high series resistance and high value of ideality factor for organic semiconductor Schottky diodes. Therefore, it is important to focus on the current conduction mechanism through natural dye-based organic semiconductor Schottky diodes. It is also important to find out the ways to reduce the series resistance and trap energy for good charge conduction through natural dye-based organic semiconductor Schottky diodes. The author's interest in conducting an examination into the matter is piqued by the following point of view. In several chapters of the thesis, the results of the research on this topic have been discussed.

2.2 Organic semiconductor polymers

There are many organic polymers, oligomers, and single molecules can be used as organic semiconductor materials [1-2]. Out of all the organic semiconductive materials, semiconducting polymers are used in organic printed electronics. Organic macromolecules known as conjugated

polymers have an alternating double- and single-bond backbone chain. Conjugated polymers serve as one-dimensional semiconductors because of their overlapping p-orbitals produce conjugated π-electrons. Conjugated electrons typically have excitation energies in the visible range and do not belong to a single valence band, resulting in conjugated polymers that are optically active [3]. Section 2.7 examines the conductivity and the charge transport mechanism in conjugated polymers. Another method for creating charges on the backbone chain of a conjugated polymer is controlled by impurities, or "doping" procedures. The conductivity of organic semiconductor may also be controlled by doping like inorganic semiconductor materials. By suitable doping of polyacetylene, the electrical conductivity may change significantly.

The conductivity in oxidized and iodine-doped polyacetylene was reported in 1977 by Alan J. Heeger, Alan MacDiarmid, and Hideki Shirakawa [4]. They discovered that when polyacetylene thin films were exposed to iodine vapours, their conductivity significantly increased. The conductivity varies widely, ranging from semiconducting range to those of metals [4]. The conductivity variations of polyacetylene are shown in Figure 2.1. Scientists were given the Chemistry Nobel Prize in 2000 "for the discovery and development of conductive polymers" [5].

Due to its instability in air and the difficulty of making films with it, polyacetylene, which is the first and most basic conjugated polymer, was never used in practical applications [3]. But scientists were intrigued by this peculiar finding, and it led to a flurry of research and development. Subsequently, stable materials that can be processed from solution or even melt were discovered and produced through appropriate chemical modifications [3]. Organic semiconductors have advantages over their inorganic counterparts due to their low cost, mechanical flexibility, and ease of fabrication.

All devices that can be made from inorganic semiconductors, such as transistors and diodes, can theoretically also be made from conjugated polymers. Indeed, organic semiconductors are currently employed as active materials in optoelectronic devices, including organic light-emitting diodes (OLEDs) [6, 7], organic solar cells [7], organic field-effect transistors (OFETs) [8, 9], electrochemical transistors [10], and more recently, biosensing methods [11, 12].

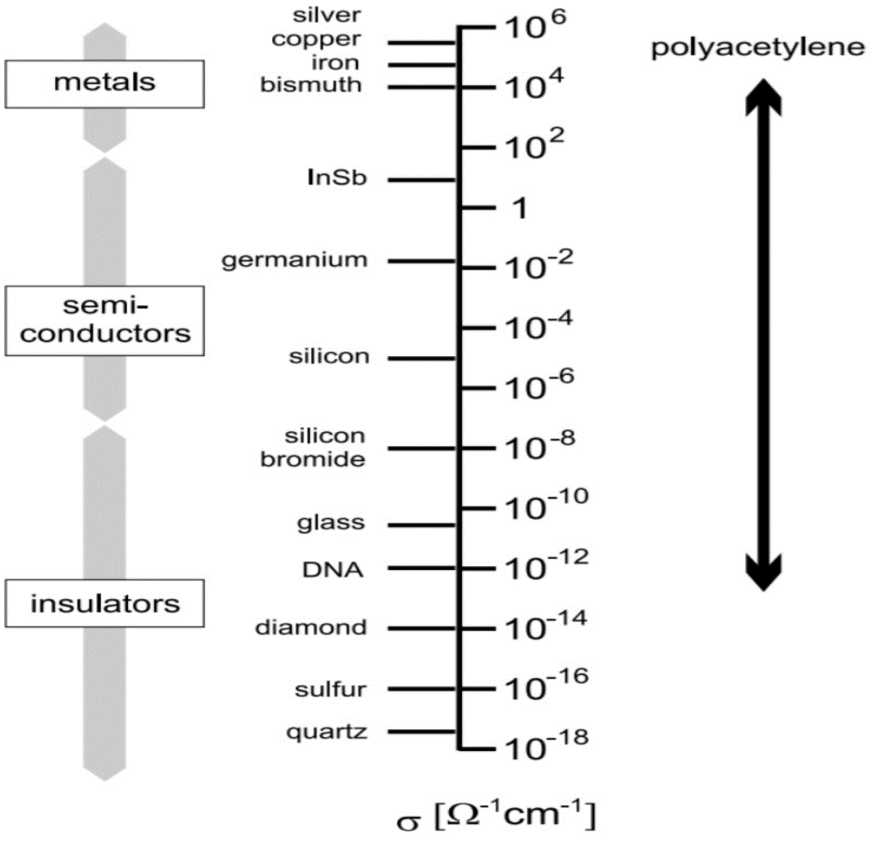

Fig. 2.1 Comparing the range of conductivities that doped polyacetylene covers to that of other materials [3]

2.3 Chemical properties of organic semiconductors

All organic semiconducting compounds contain carbon atoms as a common component. The covalent bond is what firmly holds carbon atoms (C) together. There may be partial ionic interactions with other atomic elements. Carbon has an electrical orientation of He2s22p2. In such a structure, the valence band's four electrons, or the p ones, are arranged in different bonds. Experimental research indicates that carbon can only form up to four equivalent bonding, whereas a structure like this would only form two. The theory of valence band hybridization is used to solve the issue.

Conjugated compounds are organic semiconductors exhibiting sp2 hybridization, which can change both double and single bonds. The electrons referred to as being above and below the

molecular plane delocalize upon conjugation between the bonds. In this plane, π bonds are labelled as HOMO when they are loaded with electrons, or as empty (LUMO).

There are two categories of organic semiconductors: organic polymers and small molecule organic compounds. Repetition of a basic monomer forms polymeric molecules, which progressively dissolve in solvents dependent on organic content. Molecular materials are the name given to such substances. The structures of a few polymers and molecular compounds are displayed below in Fig 2.2.

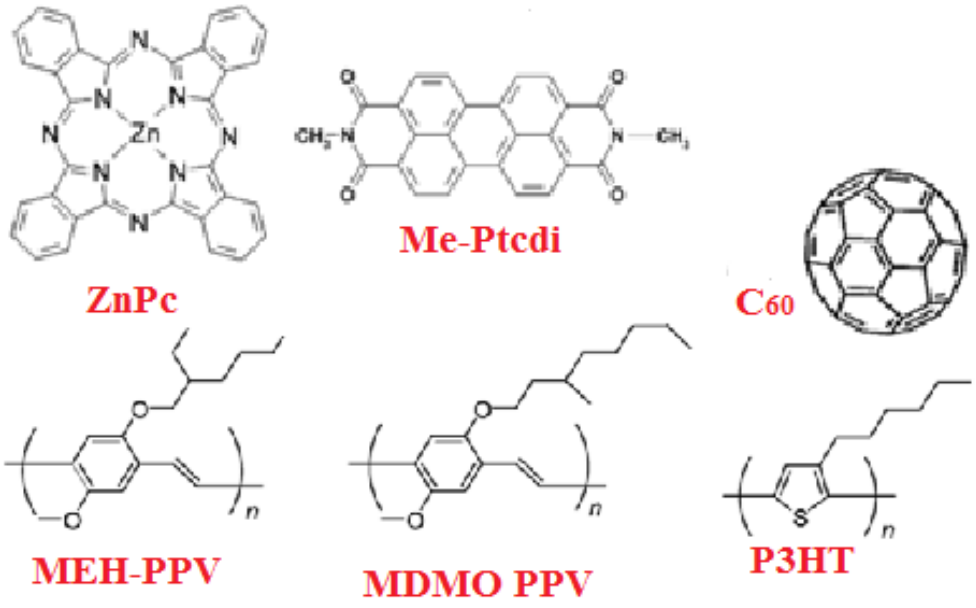

Fig. 2.2 Chemical structure of some organic semiconductors

Organic semiconductors can be classified into two groups: N-type and p-type semiconductors. However, a direct comparison of the two types of materials shouldn't be useful in this context because of the significant differences in the doping mechanisms of organic semiconductors and inorganic materials. MDMO-PPV, P3HT, and PFB behave like p-type organic semiconductors, whereas MEH-PPV, F8BT, C60, and Me-Ptcdi act as n-type organic semiconductors. Based on their chemical properties, the polymers have been found to be amenable to solution processing.

Such p-type polymer mixtures and, usually, n-type small molecule components that are handled by the solution may be advantageous for photosensitive devices [13, 14].

2.4 Electrical structure of organic semiconductors

We must work with an ideal molecular system made up of two atoms in order to show the electrical structures of organic semiconducting materials. The molecular system is described by the molecular orbital model. The model states that when two atoms of the same energy contact, their levels of energy are separated by forming two different energy states, one of which remains lower than the initial energy state and the other of which belongs in a higher energy state. The Linear Combination of Atomic Orbital concept (LCAO) approximates such molecular states. Molecule orbitals can be compared to single atoms, as demonstrated by LCAO. There is the expression of the wave-function of two hydrogen atoms:

$$\Psi_{\pm} = \Psi_{1s}(A) + \Psi_{1s}(B) \qquad (2.1)$$

Here $\Psi_{1s}(A) = \sqrt{\frac{1}{\pi a_0^3}} e^{-r_A/a_0}$, A and B are considered as atom and r_A is the distance between atom A and electron and r_B is the distance between electron and atom B.

From the linear combination of wave functions for both A and B, two molecular orbitals may be obtained. There are two types of molecular orbitals: anti-bonding orbitals (abbreviated ABO), Ψ_-, and bonding orbitals (abbreviated BO), Ψ_±. Figure 2.3 shows such atomic and molecular orbitals. Atomic orbitals are added to produce the BO. BO contains two nuclei with a high electron density. This orientation increases the atomic bond's energy and is sufficiently advantageous because it has a lower energy E+ than an isolated atomic orbital. Conversely, the difference between the atomic orbitals yields ABO. Given that this orientation's energy E-is higher than an isolated atomic orbital, it is highly unfavourable in terms of molecule stability.

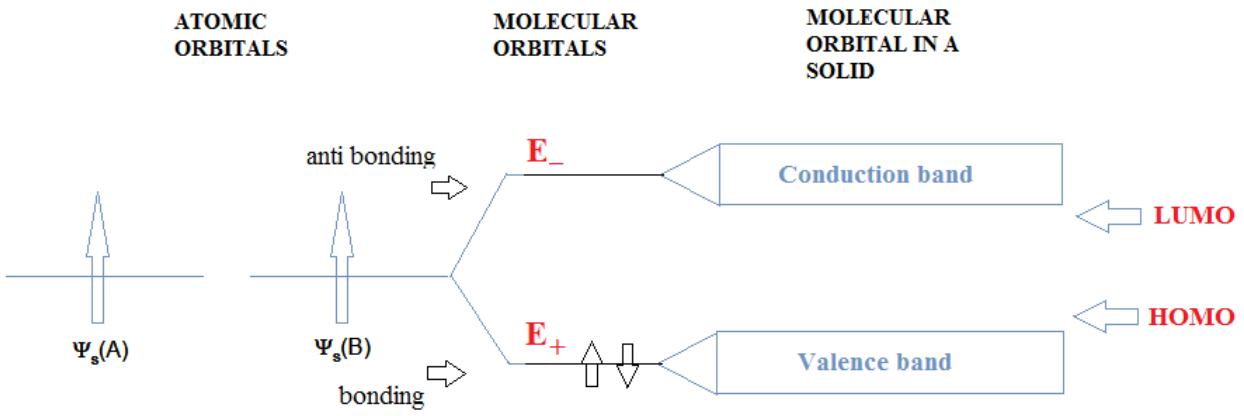

Fig. 2.3 Schematic representation of energy levels of two distinct atoms, one bi-atomic molecule and a solid

In compounds resembling polymer chains with several covalently bonded atoms, superposition takes place for every molecular orbital. Further splitting results from this interaction, as seen in Fig. 2.3, where the energy gap (Eg) is represented by the difference between the HOMO and LUMO.

The energy diagrams of linear organic molecules and crystalline inorganic compounds, which include prohibited gaps with distinct energy bands, resemble each other quite a bit. However, the energy map of many solids based on organic molecules shows a notable change. Compared to intramolecular interactions that are covalently constrained, intermolecular interactions in organic solids are substantially weaker.

2.5 Energy bands in polymer based organic semiconductor molecules

In conjugated polymers, electrons are similarly limited to specific energy and excluded from other energies. An electron has a range, or band, of possible energies in the conjugated polymer, which is the main distinction between the situation of an electron in a conjugated polymer and that of an electron in a monomer. In actuality, the conjugated polymer's discrete monomer energy levels dispersed into two bands of energy, each divided by an energy gap that excludes electrons from occupying any energy levels. The lower band is referred to as the valence band, and the upper band as the conduction band. The electrons are not always localised at a specific carbon atom once they are released from the valence band and enter the conduction band. Rather, they are unconfined and

able to travel about freely inside the molecule. The double bonds in this instance are dispersed throughout the polymer chain.

If every carbon atom in the polyacetylene were the same distance apart, the material would behave as a metallic conductor according to this concept. Actually, a metal-like, half-filled band with no energy gap is produced by the delocalized π-electrons along the polyacetylene's main chain. However, Pierels' theorem states that a metallic construction with an equidistant linear chain cannot be stable. In actuality, a structural distortion known as the Pierels transition will occur in the molecular geometry of the polyacetylene, resulting in a deformation of alternating longer and shorter double bonds. Figure 2.4 illustrates how this bond length alternation causes a limited band gap for polyacetylene. The band gap and imaginary energy band generation in polyacetylene are shown in Figure 2.4.

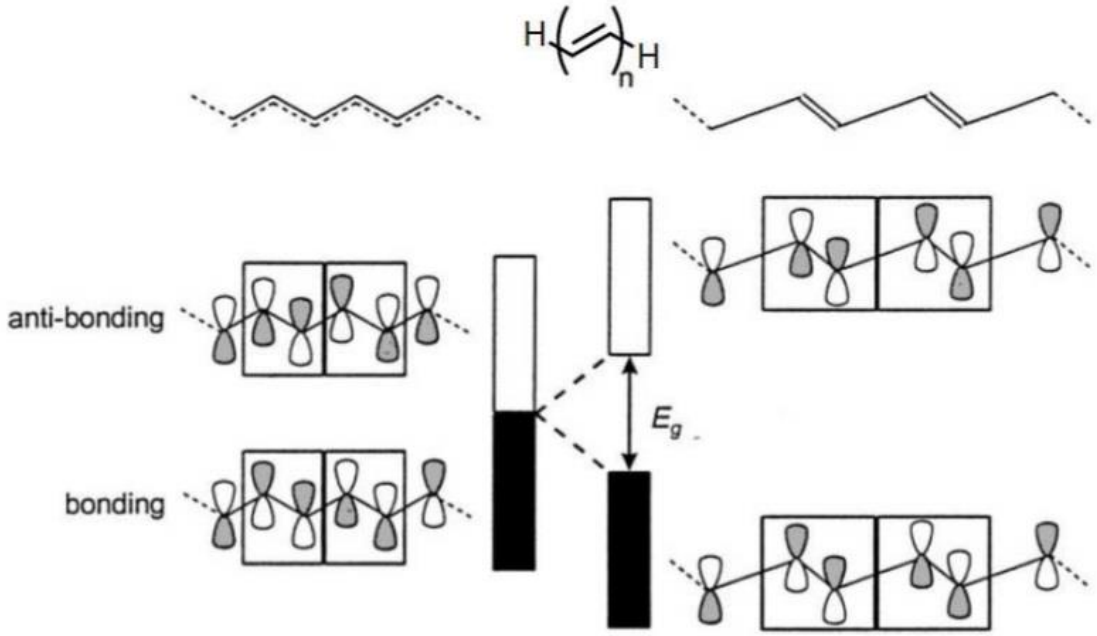

Fig. 2.4 Band gap formation by localization of double bands in polyacetylene [15].

Polyacetylene, as shown in Figure 2.5, has a band gap of around 1.5 eV, while Si and GaAs have band gaps of 1.1 eV and 1.4 eV, respectively [16]. Neutral polyacetylene is not a good semiconductor, though.

While polyacetylene has a significant historical significance, its conjugation can differ significantly from other conjugated polymers by include aromatic bonds or amines in place of carbon doubles. A bit of debate exists in the area as to whether most organic semiconducting polymers, particularly amorphous ones, should be discussed in terms of HOMO and LUMO and some delocalization, or whether a band model is preferable. On the basis of polyacetylene, the conversation can go on.

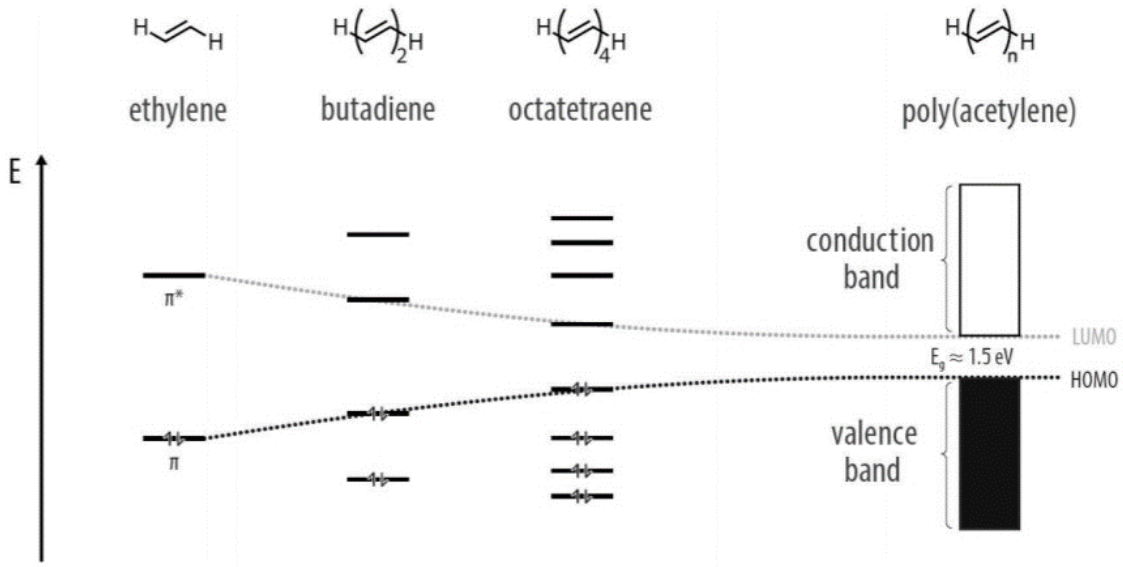

Fig. 2.5 Energy bands formation as the number of polymerizations increases [16].

2.6 Charge generation and transportation within organic semiconductors

From the perspectives of charge creation and charge transport, conjugated polymers' current conduction mechanism differs from that of inorganic semiconductors.

Charge generation

Examining the resonance structures of conjugated molecules helps to explain how charge carriers originate on organic semiconductors. For example, Figure 2.6 illustrates the two geometrically and energetically equivalent resonance forms for polyacetylene, known as the degenerate ground states [17]. As previously established in section 2.2, it is evident that the lower energy ground states are more stable than the greater energy delocalized one, which causes Pierels' distortion of the unstable delocalized one towards the ground states.

Due to lattice flaws, these two ground states can coexist on the same backbone chain with a border separating them. Even with a tiny thermal stimulation, a specific density of lattice defects may exist [9]. Neutral solitons develop spontaneously as a result of the lattice imperfections. For polyacetylene, Figure 2.7a illustrates the lattice defect, also known as the solitonic defect, connected to a domain boundary. From a chemical perspective, neutral solitons are delocalized radicals that are dispersed across seven carbon atoms: Their spin ($s = 1/2$) is equal to their charge ($q = 0$). Since they are chargeless, neutral solitons do not contribute to conduction; however, as shown in Figure 2.7b, they produce an additional energy level in the band gap with limited delocalization.

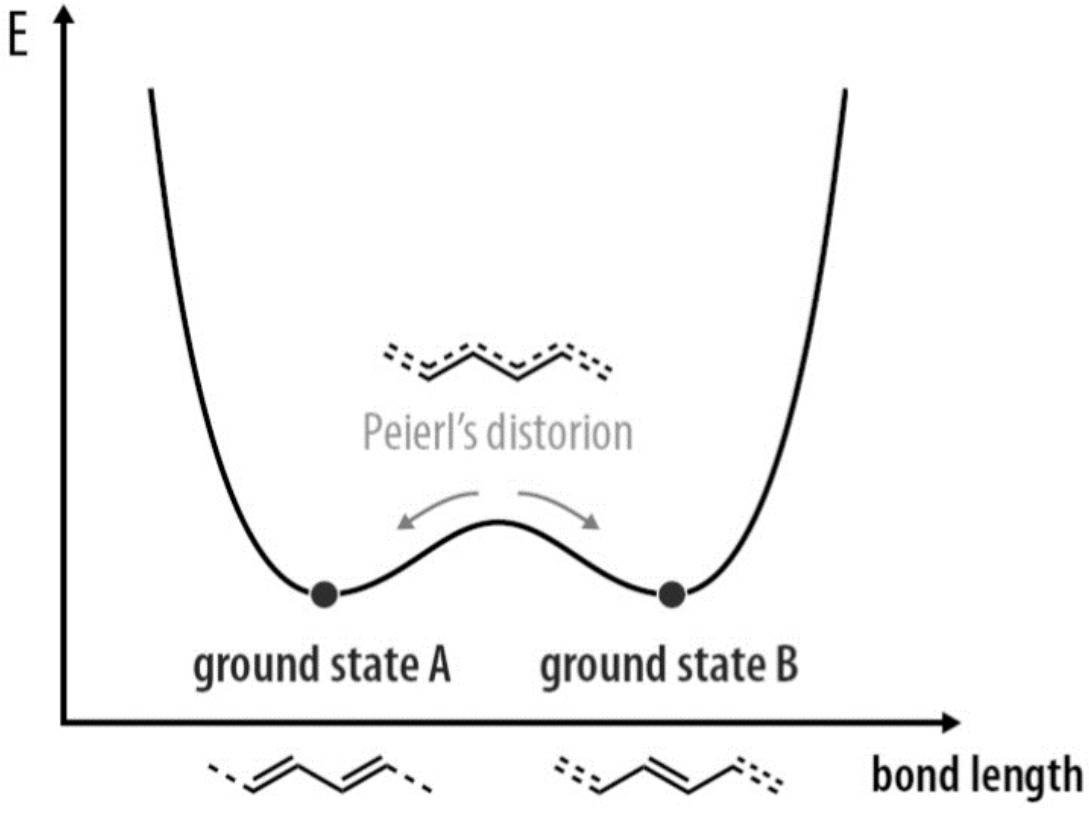

Fig. 2.6 Energy levels for the two ground states of polyacetylene [16].

A poor semiconductor is undoped polyacetylene in its crystalline state. Chemical doping can convert crystalline polyacetylene into semiconducting or even metallic material. As a single electron donor (reductant) or acceptor (oxidant), the dopant does not cause any chemical reactions.

Reductants like Na, K, and Li can accomplish n-type doping, while oxidants like I2, AsF5, and SbF5 can accomplish p-type doping [16]. Chemical doping results in several orders of magnitude increases in conductivity and charge carrier mobility.

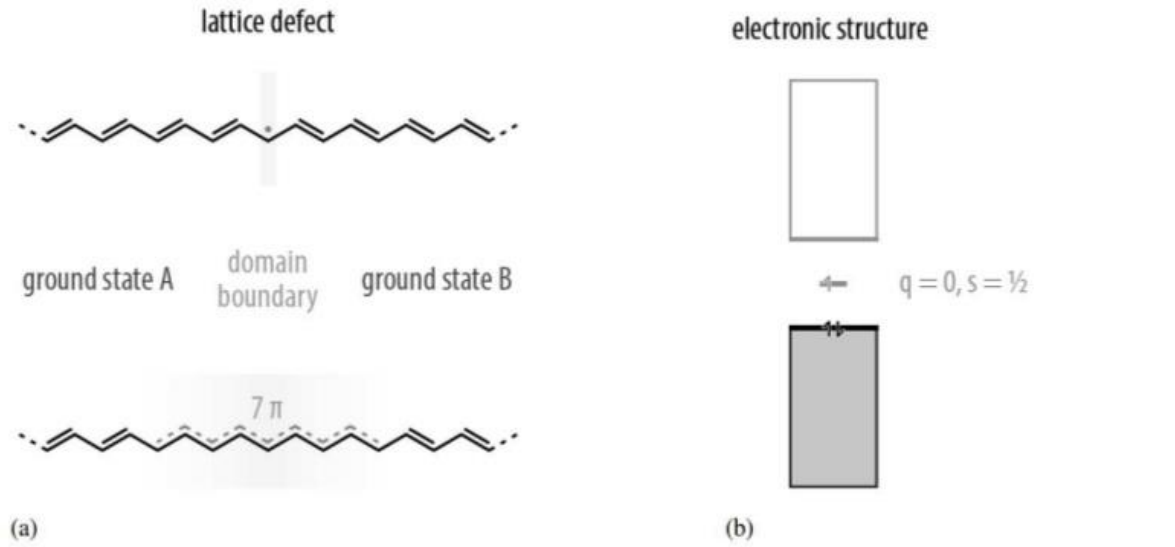

Fig. 2.7 Lattice defect results in (a) neutral soliton formation, and (b) an extra energy level in the band gap of polyacetylene [33].

Positive or negative soliton charge carriers are created by chemical doping of neutral solitons. Figure 2.8 provides a graphical representation of how positive and negative charge carriers develop. The positive and negative solitons have charge (q = +e or -e, respectively), but no spin (s = 0). The positive and negative solitons form isolated charge carriers on an extra energy level in the band gap with limited delocalization, as seen in Figure 2.8. More doping levels initially produce more isolated positive solitons with less delocalization; but, as dopant doses rise, solitanic defect states gradually combine to produce narrow band negative or positive solitons in the band gap. That means polyacetylene becomes a metallic conductor at high doping levels.

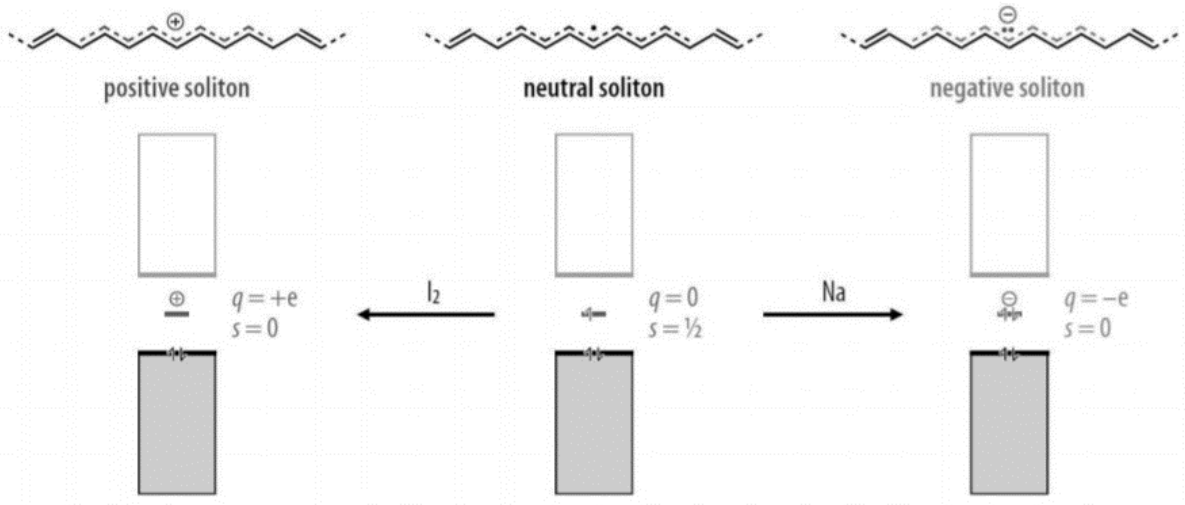

Fig. 2.8 Formation of positive or negative soliton charge carriers [16].

When photons are absorbed by inorganic semiconductors, an electron in the valence band abruptly jumps to the conduction band, creating a free hole in the valence band and a free electron in the conduction band. Due to the screening effect of the surrounding material, a pair of such carriers is not affected by the mutual force of electrostatic attraction. However, the development of a bound state occurs at very low temperatures, when the carriers' kinetic energy is comparatively less than their effective Coulomb attraction. Exciton is generated in such bound situations [18]. Free carriers do not exist in OSCs, in actuality. Excitons in OSCs are essentially the excited states created by an electron-hole pair. There are various forms of excitons that arise from light absorption, including charge transfer excitons (CTE), Wannier-Mott excitons, and Frenkel excitons. The average distance between the hole and the electron essentially determines the classification. Frenkel exciton hold on the same molecule and travel through a lattice as a unit. Compared to the Frenkel exciton, the Wannier-Mott exciton has at least a factor of ten higher carrier separation. Such excitons have relatively high dielectric constants and interaction energies. In organic semiconductors, CTE excitons are the most prevalent. Different lattice constants result in the delocalization of these excitons. In this context, it is pertinent to note that exciton binding energy in organic semiconductors that exhibit stability at room temperature ranges from 100 to 300 meV, while it varies from 1 to 40 meV in inorganic semiconductors [19, 20-22].

2.6.1 Charge Transfer Excitons (CTE) Generation

In this instance, the electron transfer process is initiated by light and moves electrons from the donor element (D) to the acceptor (A). One of the components is taken to the excited state in presence of photon prior to the conduction of electron carriers:

$D+A \Rightarrow D^{*}+A$ (exciton)

$D^{*}+A \Rightarrow D^{+*}+A^{-*}$ (transfer of electron)

State of charge transformation is formed subsequently to transfer of the electron. State of charge transformation is formed subsequently to transfer of the electron. It can be described as the jumping of electrons from D to A to hop around or injection towards an acceptor.

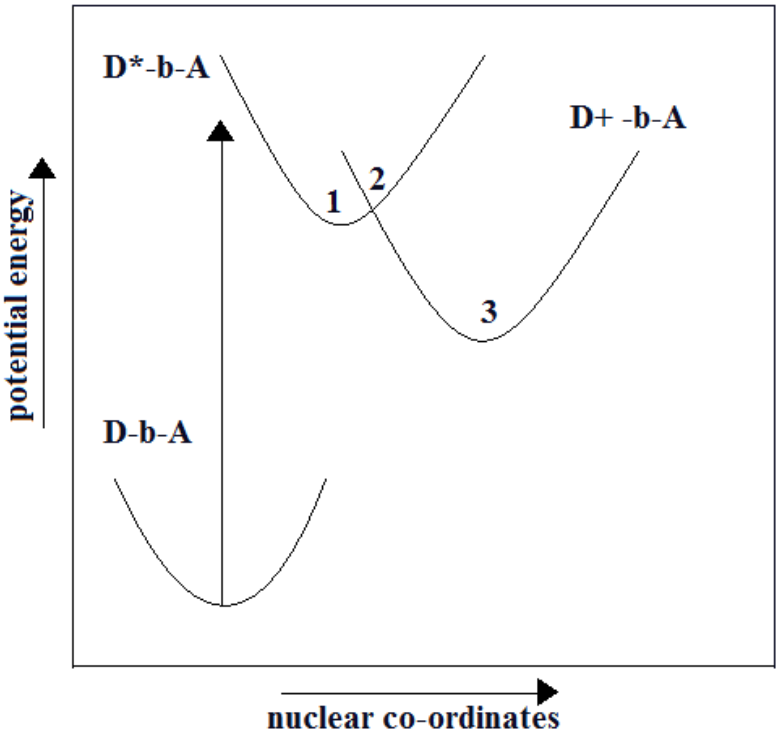

Fig.2.9 Schematic representation of potential energy vs nuclear coordinate relationship where three different positions has been given providing the excited state and charge separation state of a D-A system

An electron transformation state of a system has been explained in Fig. 2.9. which consists of a donor and an acceptor. Three positions of CTE on potential energy graph are represented as ground state (D-b-A), excited state (D^*-b-A) and charge separation state (D+ -b-A), where donor and acceptor are connected by a bridge (b).

2.6.2 Charge Transfer Excitons dissociation

The dissociation of exciton yields free carriers. By combining two organic compounds with varying energy levels, it can be discovered. From a bound exciton state to a less tightly linked CTE, an electron can undergo charge transfer very easily. Pure polymers are a common illustration of this state. After CT, the electron-hole distance increases, causing the binding energy to drop and the charges to dissociate when exposed to external electric fields or thermal activation. The hypothesis of temperature and field assisted CTE dissociation was first explained by Onsager et al., [23], and later on it was modified by Braun et al., [19], and Tachiya et al., [20]. The dissociation barrier at the separation distance between CT is equivalent to the Coulombic binding energy. Generally speaking, the dissociation barrier has a value between 0.1 and 0.5 eV. In this sense, the carrier separation distance in CTE typically falls between 1 and 4 nm [24].

2.6.3 Charge transport

Conjugated polymer charge carrier transport is modelled after extremely disordered systems and usually occurs via hopping mechanisms. The temperature and the thermal vibrations of the molecules affect the hopping transfer, which is dependent on the thermal excitation of the electrons [9]. Their microscopical conductivity is actually dominated by the thermal hopping between limited chains of conjugated polymers. In organic semiconductors, the charge carrier mobility is restricted by this hopping process as well as the movement of positive or negative solitons along the polymer chain. Furthermore, in the stretch direction as opposed to the perpendicular direction, the conductivity of conjugated polymers that are stretch orientated is higher. They have an extremely anisotropic conductivity as a result of these properties [5].

Compared to nondegenerate ground-state polymers, polyacetylene is easier to model as it is a degenerate one. There is no degeneracy in the ground-state energy of the nondegenerate ground-state polymers. Rather, two states with distinct energies are produced when single and double bonds are switched [25]. These nondegenerate ground state energies result in polaron or

bipolaronic states for charged defects instead of solitonic defects [25]. Instead of having a linear backbone chain, the majority of conjugated polymers have a cyclic one that is conjugated to π. Table 2.1 lists a few additional common conjugated polymers.

Table 2.1 Different conjugated polymers [26]

Polymer	Bandgap (eV)	Conductivity (S/cm)
Polyacetylene	1.5	10^3 – 1.7x10^5
Polypyrene	3.1	10^2 – 7.5x10^3
Polythiophene	2.0	10 - 10^3
Para phenylene	3.0	10^2 - 10^3
P-phenylene vinylene	2.5	3 – 5x10^3
polyaniline	3.2	20 - 200

2.7 Carrier Recombination

When an external electric field is present, opposite types of charge carriers in OSc move in the direction of one another through Coulombic interactions. As a result, Coulombic bonds form when the distance between an electron and a hole gets smaller than the capture radius, or rc. The formula for calculating the precise distance at which the Coulombic force equals the thermal energy kBT is $r_c = {e^2}/{(4\pi\epsilon_r k_B T)}$ where ϵ_r is the organic substance's dielectric constant. Recombination is a possibility when electrons and holes have adjacent boundaries. When two such opposite charges belong at the same location, an exciton is produced. A photon of energy is released when the exciton that first appeared decays and undergoes radiative recombination with an electron-hole pair. In the case of organic semiconductors, the energy source might also be non-radiative.

I) Langevin, bimolecular recombination

In certain instances, charge carriers in organic semiconductor blends are confined in material phases, leading to interfacial recombination. The rate of recombination is decreased by such an interfacial state of action. It should be necessary to incorporate an extra factor into the Langevin type recombination rate to account for the interfacial contact area, which usually ranges from 10-1 to 10-3 [27-31]. Charge density dependent mobility can be stated to explain the above-illustrated

fact. Carrier mobility is influenced by charge density, which also affects the carrier density dependence of the recombination rate. Assuming the case of ideal semiconductors where n=p, recombination rate can be expressed as:

$$R = \vartheta \frac{(\mu_e + \mu_h)}{\varepsilon \varepsilon_o} n^2 \qquad (2.3)$$

According to modified Langevin theory, recombination rate applicable to organic semiconductor blends is explained by:

$$R = \vartheta \frac{(\mu_e + \mu_h)}{\varepsilon \varepsilon_o} n^{\lambda+1} \qquad (2.4)$$

It is not easy to predict the prefatory and the order of reaction $(\lambda + 1)$ depends on morphology of the material sample that can be influenced by properties of material as well as conditions of sample preparation.

II) Auger recombination

Recombination of a hole associated with an electron with a third carrier is known as Auger recombination. Recombination of electron-hole opposite type charge carriers releases energy that transfers to a third charge carrier, which causes the carrier to jump higher into the band before returning to the band edge regime. The initial charge pair's energy dissipates as phonons, or thermal heating.

Situated in a defect, a trapped carrier recombines with the counter charge to form a trapped CT state in practice. Any interaction between such trapped CT states and free carriers can result in the Auger process. In this process, all of the recombination energy is fully utilized to match the kinetic energy of the additional free charge carrier. When this kind of recombination occurs close to a surface, photoemission can be seen [32].

2.8 Organic semiconductor Schottky diodes

Molecular electronics can benefit greatly from the unique optical, magnetic, and electrical properties of organic semiconductors. Schottky diodes are semiconductor diodes created when a semiconductor and a metal combine. They bear the name of the German physicist Walter H. Schottky. They switch on quickly and have a little forward voltage drop. When it comes to getting around the drawbacks of pure organic semiconductors, composite materials are essential. In order to maintain high electrical conductivity and other desirable qualities, these materials blend

conducting and insulating polymers to improve mechanical strength. Polyaniline, a p-type semiconductor, and polystyrene are joined to create one such composite system [33].

The active material in organic Schottky diodes is a polycrystalline organic semiconductor layer. A rectifying contact, also known as a Schottky contact, is formed on one side of this layer. Conversely, between the organic semiconductor and the ohmic contact layer, an amorphous doped semiconductor layer serves as a buffer. The modified Schottky equation can be used to fit the observed current-voltage (I-V) characteristics of the polyaniline-polystyrene Schottky diode in a satisfactory manner. The non-linear charts in these examples show rectification behaviour. Furthermore, plots of capacitance versus voltage (C-V) are almost linear in reverse bias [33]. It is possible to compute several junction parameters, including ideality factor and barrier height, using temperature-dependent I-V and C-V data. According to these findings, composite materials outperform pure semiconducting polymers in terms of mechanical strength and diode quality. Microelectronics, which includes transistors and diodes, uses organic Schottky diodes. Scientists are still investigating new materials and manufacturing processes to improve their properties and increase their use in developing technology.

2.9 ZnO nanoparticles in organic devices

ZnO nanoparticles (NPs) have become increasingly important because of their unique chemical and physical characteristics [34]. In flexible electronics, they are among the well-known electron transporting layers (ETLs), particularly in organic solar cells (OSCs) [35]. This is because of their high mobility and transparency, compatibility with large-area fabrication techniques, annealing-free and solution-processable features, etc [36].

Chemical techniques including the mechanochemical process, controlled precipitation, sol–gel, vapour transport, solvothermal, hydrothermal, and emulsion and micro-emulsion environments can all be used to create ZnO NPs. Plant extracts have also been utilized in environmentally friendly ways to synthesize ZnO NPs. Polymer substrates and organic (carboxylic acid, silanes) and inorganic (metal oxides) compounds can be used to modify ZnO NPs. It has been demonstrated that OSCs perform better when ZnO is modified with organic compounds. Zinc oxide (ZnO) possesses a multitude of distinctive chemical and physical characteristics, including high chemical

stability, high electrochemical coupling coefficient, broad range of radiation absorption, and high photostability. These attributes set ZnO apart from other metal oxides and allow for a wide range of applications in various fields. Because zinc is in the second group of the periodic table and oxygen is in the sixth group, ZnO is classified as a group II–VI semiconductor in the field of materials science. Its covalence lies close to the line separating covalent from ionic semiconductors. ZnO is the most preferred multitasking material due to its excellent transparency, high electron mobility, large band gap (3.37 eV), strong room temperature luminescence, high mechanical and thermal stability at room temperature, broad range of radiation absorption, and high photostability. It also has an oversized exciton binding energy (60 meV) [34-36]. It is regarded as a potential material in laser technology, optoelectronic applications, and electronic applications due to its unique optical and electrical properties [36-40]. Zinc Oxide (ZnO) is one of the nano-sized metal oxides that has been extensively studied to potentially benefit from its antimicrobial and antitumor properties [34-36]. Certain cosmetic lotions contain ZnO due to its absorbing and blocking properties [33-35]. ZnO has additional uses in human medicine, including as an astringent (to promote wound healing), a treatment for eczema, hemorrhoids, and excoriation. [36-38] ZnO nanoparticles' distinctive qualities have recently garnered attention. ZnO nanoparticles' wound-healing, antibacterial, antineoplastic, and antigenic qualities make them highly promising for use in veterinary medicine. Zinc oxide (ZnO) materials have been more effective recently due to a multitude of research studies and experimental analyses that have produced nano-structures where each nano-dimension is reduced to generate nanowires, thin films, and other structures for a variety of applications, including defence against intracellular pathogens and brain tumours.

2.9.1 Electronic properties of ZnO nanoparticles

The electronic, optical, and electrochemical properties of zinc oxide (ZnO) nanoparticles are remarkable. Because of its 3.37 eV wide bandgap, ZnO nanoparticles can function at substantially higher voltages, frequencies, and temperatures than traditional semiconductors [37-41]. Several nanostructured ZnO morphologies, such as nanoparticles, nanorods, nanoribbons, and nano shuttles, have been thoroughly studied in terms of their optical, electronic, and structural characteristics [37-41].

Grain boundaries and the semiconducting nature of ZnO nanostructures affect their electrical conductivity [42-43]. Compared to other nanostructures, ZnO nanorods exhibit higher electrical conductivity, whereas ZnO nano shuttles exhibit the lowest electrical conductivity [36-40]. ZnO nanoparticles, ZnO nanorods, ZnO nanoribbons, and ZnO nano shuttles have optical bandgap energies of 3.30, 3.33, 3.39, and 3.36 eV, respectively [37-43]. The morphology and particle size of ZnO nanostructures determine their structural, wettability, optical, and electrical characteristics.

2.9.2 Incorporation of ZnO nanoparticles in organic devices

There are various advantages when using ZnO NPs in organic electronics in conjunction with organic semiconducting materials. ZnO NPs can be utilized in organic solar cells as interlayers for electron transport, which will enhance the stability and efficiency of OSC devices [44].

. ZnO NPs can also be used in conjunction with materials that have smaller energy gaps, like organic polymers, dye sensitizers, and semiconductors with smaller band gaps, to increase their light absorption into the visible region [44]. In order to improve the main layer's adhesion to the substrate and provide nucleation sites for the growth of nanowires, ZnO NPs can also be utilized as a seed layer [45].

We have chosen to use ZnO nanoparticles in our work because of all the aforementioned features. Chapters six and seven provide a detailed discussion of the effects of incorporating ZnO nanoparticles with organic electronic devices based on natural dyes.

2.10 Earlier works on organic semiconductors

Research on organic semiconducting materials has traditionally concentrated on molecules that belong in a crystalline state. It was discovered that molecular crystals that resemble anthracene and naphthalene exhibited semiconducting characteristics [46]. Organic molecules' photosensitive conductivity and anthracene-based electroluminescent devices were first described in the 1960s [47-49]. However, because of their chaotic amorphous structure, which at the time produced poor semiconducting characteristics, organic materials were typically regarded as exotic materials with little potentiality in device application. A few years later, chromophores were used to characterize polymers as side group elements as well as in the polymer chain. Due to their variety in material

usage and environment-safe use, multilayer photosensitive organic semiconductors supplanted amorphous selenium and silicon in the 1970s [50].

Doped polyacetylene, the first polymer with noticeably high conductivity, was first published in 1977 [51]. The doped polymers were initially very unstable in air and extremely challenging to process. The aforementioned materials can still be processed and are stable in nature in new, ungraded generations. For common insulators like silicon, electrical conductivity obtained in this generation varies from 10^{-10} S/cm to 10^{-5} S/cm. Such polymers started to show up in new applications during that time period, including coatings and blends for electromagnetic shielding interference and electrostatic dissipation, conducting layers for optoelectronic devices, and anticorrosion coatings for various metallic surfaces [52]. However, the growing use of organic semiconductors in electronics has been constrained by some fundamental limits. In inorganic crystals, a strong coupling force that acts over a wide range of the constituent atoms drives the delocalization of electronic states and enables the creation of an energy gap between the valence and conduction bands. Executing a photo-excitation or thermal activation process will generate free electrons in the conduction level and living positive holes in the valence band. Bloch function and the k-space dispersion relation of solid-state physics can both be used to describe how these free charges conduct [53].

Intermolecular connections in organic semiconductors are typically covalent, however these contacts are much weaker due to van der Waals and London forces. Therefore, it follows that the transport bands are sufficiently smaller as compared to inorganic materials. As a result, when there is systemic disturbance, energy bands are easily disrupted. Excitations and inherent interactions that are mentioned on the molecular crystals' atoms are therefore more important than the applicability of energy band idea. In essence, organic materials possess - conjugated electrical characteristics created by the overlap of carbon atoms' pz orbitals. Due to this orbital overlap, P-electrons get delocalized, and the energy band gap between the highest-occupied molecular orbital (HOMO) and lowest-unoccupied molecular orbital becomes relatively narrow (LUMO).

The fact that solid state molecules have lower coupling results in the conclusion that the charges in such materials are sufficiently confined. Conduction occurs in a sequence that switches between multiple molecular states, which is remarkably similar to the hopping transport that occurs in various defect states in inorganic semiconductors [54].

Excitons are also created when light is absorbed by organic semiconductors, which do not thermally separate into free carriers at room temperature. Therefore, the generation of stable charge states after photon absorption occurs infrequently; instead, charges develop when excitons are quenched by material impurities. These were the contributing elements to the extremely poor device efficiency.

After some time, Tang et al study's [55] created the donor-acceptor interface (D-A interface), which is generated at the junction of two bilayers of organic materials with differing electro negativities. By dividing the excitons created by the photons' absorption into charge carriers, this difference in electron affinities creates an effective force for the transition of carriers towards excited states.

The development quickens the process of realizing the physics of organic semiconductors for both tiny organic molecules and organic polymers in the late 1980s. The fact prompts (i) the demonstration of improved performance of electroluminescent devices made by multilayer vacuum-sublimated organic dye based thin films at Eastman Kodak (increasing the luminescent efficiency by nearly two orders of magnitude to 1% at nearly 10 volt of operating voltage)[56], (ii) the explanation of the report of conjugated oligomers and organic polythiophene based transistors[57-58], (iii) discovery of optoelectronic device from conjugated polymers at Cambridge University [59], (iv) hetero-structure based efficient solar cell [60]. Recently, in 2000s, Nobel prize has been won by Heeger-Mcdiarmid-Shirakawa for their remarkable work on development and application of organic semiconductors.

2.11 Natural dyes in organic electronics

Recently, a thorough investigation was conducted on the optoelectronic characteristics of natural dyes derived from beetroot, red cabbage, walnut leaves, and henna [61]. Study results showed that the henna dye had minimum values for all three of these properties, while the red cabbage dye had maximum values for refractive index, dielectric constant, and optical conductivity. The transition type between the bonding and antibonding molecular energy levels was identified as the direct allowed transition of the dyes' optical absorption [62].

The research progress on natural dyes over the past ten years is summarized in another review article [62]. Organic light-emitting diodes, dye-sensitized solar cells, and organic field-effect transistors are just a few of the applications for natural dyes that are highlighted in the article [62].

In summary, organic electronics has demonstrated a great deal of promise for natural dyes. These are affordable, easily obtainable, and environmentally friendly. Improvements in efficiency and sustainability in electronic devices could result from more research in this field. The experimental research work of the thesis consists of three natural herbal dye-based organic semiconducting materials such as turmeric dye, indigo dye and beetroot dye.

2.12 Conclusion

An extensive overview of OSCs is given in this chapter. There has been discussion of previous important works on theoretical and experimental research based on OSCs. The chemical characteristics of these semiconductors have received attention. An example of how their bonds form in various small organic molecules has been presented. The electronic structure of OSCs has subsequently been shown. These materials can be divided into three categories based on the levels of disorder produced by their amorphous nature: highly ordered systems, slightly disordered systems, and highly disordered systems. This chapter has purposefully included a brief discussion of these systems. The recombination process and exciton generation in OSCs have been discussed in the following section. In the current discussion, a pertinent comparison between two distinct types of recombination processes—Langevin recombination and Auger recombination—has been obtained. Once more, we have covered the electrical and optoelectronic properties of zinc oxide nanoparticles. The following chapter will provide a detailed theoretical interpretation of the charge transport modelling in the Schottky diode based on organic semiconductors.

2.13 References

1. Streetman BG, Banerjee S. Solid state electronic devices. New Jersey: Prentice hall; 2000 Apr.
2. Sun Y, Liu Y, Zhu D. Advances in organic field-effect transistors. Journal of materials Chemistry. 2005;15(1):53-65.
3. Strobl GR, Strobl GR. The physics of polymers. Berlin: Springer; 1997 Aug.
4. Shirakawa H, Louis EJ, MacDiarmid AG, Chiang CK, Heeger AJ. Synthesis of electrically conducting organic polymers: halogen derivatives of polyacetylene, (CH) x. Journal of the Chemical Society, Chemical Communications. 1977(16):578-80.
5. Heeger AJ, MacDiarmid AG, Shirakawa H. The Nobel Prize in chemistry, 2000: conductive polymers. Stockholm, Sweden: Royal Swedish Academy of Sciences. 2000 Oct:1-6.
6. Burroughes JH, Bradley DD, Brown AR, Marks RN, Mackay K, Friend RH, Burns PL, Holmes AB. Light-emitting diodes based on conjugated polymers. nature. 1990 ;347(6293):539-41.
7. Günes S, Neugebauer H, Sariciftci NS. Conjugated polymer-based organic solar cells. Chemical reviews. 2007 Apr 11;107(4):1324-38.
8. Bao Z, Locklin J, editors. Organic field-effect transistors. CRC press; 2018 Oct 3.
9. Kymissis I. Organic field effect transistors: theory, fabrication and characterization. Springer Science & Business Media; 2008 Dec 25.
10. Rani V, Santhanam KS. Polycarbazole-based electrochemical transistor. Journal of Solid State Electrochemistry. 1998 Mar;2:99-101.
11. Mabeck JT, Malliaras GG. Chemical and biological sensors based on organic thin-film transistors. Analytical and bioanalytical chemistry. 2006 Jan;384:343-53.
12. Goetz SM, Erlen CM, Grothe H, Wolf B, Lugli P, Scarpa G. Organic field-effect transistors for biosensing applications. Organic Electronics. 2009 Jul 1;10(4):573-80.
13. Seres I, Stepanov S, Mansurova S, Grabar A. Non-steady-state photoelectromotive force effect in photorefractive Sn 2 P 2 S 6 crystals. JOSA B. 2000 Dec 1;17(12):1986-91.
14. Gather MC, Mansurova S, Meerholz K. Determining the photoelectric parameters of an organic photoconductor by the photoelectromotive-force technique. Physical Review B—Condensed Matter and Materials Physics. 2007 Apr 15;75(16):165203.
15. Van Mullekom HA, Vekemans JA, Havinga EE, Meijer EW. Developments in the chemistry and band gap engineering of donor–acceptor substituted conjugated polymers. Materials Science and Engineering: R: Reports. 2001 Feb 1;32(1):1-40.

16. Özen B, Candau N, Temiz C, Grozema FC, Tirani FF, Scopelliti R, Chenal JM, Plummer CJ, Frauenrath H. Engineering polymers with improved charge transport properties from bithiophene-containing polyamides. Journal of Materials Chemistry C. 2020;8(18):6281-92.

17. Hudson BS, Allis DG. Bond alternation in infinite periodic polyacetylene: Dynamical treatment of the anharmonic potential. Journal of Molecular Structure. 2013 Jan; 1032:78-82.

18. Śliwińska E, Mansurova S, Hartwig U, Buse K, Meerholz K. Effect of co-sensitization in new hybrid photo-refractive materials based on PVK polymer matrix and inorganic LiNbO 3 nano-crystals. Applied Physics B. 2009 Jun; 95:519-24.

19. Braun CL. Electric field assisted dissociation of charge transfer states as a mechanism of photocarrier production. The Journal of chemical physics. 1984 May 1;80(9):4157-61.

20. Tachiya M. Kinetics of quenching of luminescent probes in micellar systems. II. The Journal of Chemical Physics. 1982 Jan 1;76(1):340-8.

21. Basu PK, Bhattacharya K. Alloy scattering limited mobility of two-dimensional electron gas in quaternary alloy semiconductors. Journal of applied physics. 1986 Feb 1;59(3):992-4.

22. Shapiro FR, Adler D. Equilibrium transport in amorphous semiconductors. Journal of non-crystalline solids. 1985 Nov 1;74(2-3):189-94.

23. Onsager L. Initial recombination of ions. Physical Review. 1938 Oct 15;54(8):554.

24. Efros AL, Shklovskii BI. Coulomb interaction in disordered systems with localized electronic states. InModern Problems in Condensed Matter Sciences 1985 Jan 1 (Vol. 10, pp. 409-482).

25. J. Hwang, D.B. Tanner, I. Schwendeman, and J.R. Reynolds. Optical properties of nondegenerate ground-state polymers: Three dioxythiophene-based conjugated polymers. Physical Review B, 67(11):115205, 2003.

26. Anderson C, Davidson E. Conducting polymers. Physics 141A–Introduction to Solid-State Physics. 2013 Apr 23.

27. Juška G, Arlauskas K, Stuchlik J, Österbacka R. Non-Langevin bimolecular recombination in low-mobility materials. Journal of non-crystalline solids. 2006 Jun 15;352(9-20):1167-71.

28. Deibel C, Baumann A, Dyakonov V. Polaron recombination in pristine and annealed bulk heterojunction solar cells. Applied Physics Letters. 2008 Oct 20;93(16).

29. Clarke TM, Jamieson FC, Durrant JR. Transient absorption studies of bimolecular recombination dynamics in polythiophene/fullerene blend films. The Journal of Physical Chemistry C. 2009 Dec 10;113(49):20934-41.
30. Koster LJ, Kemerink M, Wienk MM, Maturová K, Janssen RA. Quantifying bimolecular recombination losses in organic bulk heterojunction solar cells. Advanced Materials. 2011 Apr 12;23(14):1670-+.
31. Deibel C, Wagenpfahl A, Dyakonov V. Origin of reduced polaron recombination in organic semiconductor devices. Physical Review B. 2009 Aug 7;80(7):075203.
32. Mandoc MM, Kooistra FB, Hummelen JC, De Boer B, Blom PW. Effect of traps on the performance of bulk heterojunction organic solar cells. Applied Physics Letters. 2007 Dec 24;91(26).
33. Gupta RK, Singh RA. Junction properties of Schottky diode based on composite organic semiconductors: polyaniline-polystyrene system. Journal of Polymer Research. 2005 Jan;11: 269- 73.
34. Liu C, Xiao C, Li W. Zinc oxide nanoparticles as electron transporting interlayer in organic solar cells. Journal of Materials Chemistry C. 2021;9(40):14093-114.
35. Khairnar N, Kwon H, Park S, Lee H, Park J. Tailoring the Size and Shape of ZnO Nanoparticles for Enhanced Performance of OLED Device. Nanomaterials. 2023 Oct 24;13(21):2816.
36. Van Ngo G, Margaillan A, Villain S, Leroux C, Bressy C. Synthesis of ZnO nanoparticles with tunable size and surface hydroxylation. Journal of nanoparticle research. 2013 Jan;15:1-5.
37. Roy VA, Djurišić AB, Chan WK, Gao J, Lui HF, Surya C. Luminescent and structural properties of ZnO nanorods prepared under different conditions. Applied physics letters. 2003 Jul 7;83(1):141-3.
38. Chen QH, Zhang WG. Continuous preparation of decorated nano zinc oxide organic sols with intense luminescence. Journal of non-crystalline solids. 2007 Mar 15;353(4):374-8.
39. Allen MW, Alkaisi MM, Durbin SM. Metal Schottky diodes on Zn-polar and O-polar bulk ZnO. Applied physics letters. 2006 Sep 4;89(10).

40. Middya S, Layek A, Dey A, Ray PP. Morphological impact of ZnO nanoparticle on MEHPPV: ZnO based hybrid solar cell. Journal of Materials Science: Materials in Electronics. 2013 Nov;24:4621-9.

41. Chen Y, Bagnall DM, Koh HJ, Park KT, Hiraga K, Zhu Z, Yao T. Plasma assisted molecular beam epitaxy of ZnO on c-plane sapphire: Growth and characterization. Journal of Applied Physics. 1998 Oct 1;84(7):3912-8.

42. Zhang J, Sun L, Yin J, Su H, Liao C, Yan C. Control of ZnO morphology via a simple solution route. Chemistry of Materials. 2002 Oct 21;14(10):4172-7.

43. Ahmad AA, Alsaad AM, Aljarrah IA, Al-Bataineh QM, Telfah AD. Optical, electronic, and structural properties of different nanostructured ZnO morphologies. The European Physical Journal Plus. 2022 Jun 30;137(6):752.

44. Liu C, Xiao C, Li W. Zinc oxide nanoparticles as electron transporting interlayer in organic solar cells. Journal of Materials Chemistry C. 2021;9(40):14093-114.

45. Gartner M, Stroescu H, Mitrea D, Nicolescu M. Various applications of ZnO thin films obtained by chemical routes in the last decade. Molecules. 2023 Jun 9;28(12):4674.

46. Kao KC, Hwang W. Electrical transport in solids, with particular reference to orgainc semiconductors. Pergamon; Oxford 1981.

47. LeBlanc Jr OH. Hole and electron drift mobilities in anthracene. The Journal of Chemical Physics. 1960 Aug 1;33(2):626.

48. Kepler R. Charge carrier production and mobility in anthracene crystals. Physical Review. 1960 Aug 15;119(4):1226.

49. Pope M, Kallmann HP, Magnante P. Electroluminescence in organic crystals. The Journal of Chemical Physics. 1963 Apr 15;38(8):2042-3.

50. Pai DM, Springett BE. Physics of electrophotography. Reviews of Modern Physics. 1993 Jan 1;65(1):163.

51. Chiang CK, Fincher Jr CR, Park YW, Heeger AJ, Shirakawa H, Louis EJ, Gau SC, MacDiarmid AG. Electrical conductivity in doped polyacetylene. Physical review letters. 1977 Oct 24;39(17):1098.

52. Epstein AJ. Electrically conducting polymers: science and technology. MRS Bulletin. 1997 Jun;22(6):16-23.
53. Ashcroft NW. Solid State Physics (HR&W) Google Scholar NW Ashcroft and ND Mermin 1979. Solid State Physics. 1976; 1:2.
54. Baranovski S, editor. Charge transport in disordered solids with applications in electronics. John Wiley & Sons; 2006 Aug 14.
55. Tang CW. Two-layer organic photovoltaic cell. Applied physics letters. 1986 Jan 13;48(2):183-5.
56. Tang CW, VanSlyke SA. Organic electroluminescent diodes. Applied physics letters. 1987 Sep 21;51(12):913-5.
57. Koezuka H, Tsumura A, Ando T. Field-effect transistor with polythiophene thin film. Synthetic Metals. 1987 Feb 1;18(1-3):699-704.
58. Horowitz G. Organic field-effect transistors. Advanced materials. 1998 Mar;10(5):365-77.
59. Burroughes JH, Bradley DD, Brown AR, Marks RN, Mackay K, Friend RH, Burns PL, Holmes AB. Light-emitting diodes based on conjugated polymers. nature.1990 Oct;347(6293):539-41.
60. Garnier F, Horowitz G, Peng X, Fichou D. An all-organic" soft" thin film transistor with very high carrier mobility. Advanced Materials. 1990 Dec;2(12):592-4.
61. Peshawa O. Amin, Fahmi F. Muhammadsharif, Salah Raza Saeed & Khaulah Sulaiman. (2022). A Study on the Optoelectronic Parameters of Natural Dyes Extracted from Beetroot, Cabbage, Walnut, and Henna for Potential Applications in Organic Electronics. Journal of Fluorescence, 32(1), 203–213.
62. Zhang, X., Li, Y., & Li, Y. (2022). Insight into the Progress on Natural Dyes in Organic Electronics. Molecules, 27(10), 3291.

Chapter 3

Electrical Characteristics of Turmeric dye-based organic device and the effect of light and temperature

3.1 Introduction

The objective of our work is to study the charge transport mechanism through the natural dye-based organic Schottky diodes. For this we have selected few organic natural dyes such as turmeric, beetroot and indigo. In the previous chapter a review on charge transport mechanism through some organic polymers has been done. In this present chapter we will present the semiconducting behaviour of turmeric dye and the effect of temperature and light on Al/Turmeric/Cu device. Turmeric, a common spice and medicinal herb, provides a sustainable and eco-friendly source for semiconductor materials. Researchers appreciate its renewable nature and low environmental impact. The chemical formula of turmeric dye is $C_{21}H_{20}O_6$. Turmeric dye, unlike certain synthetic dyes, is non-toxic, making it safer for both fabricating processes and possible applications. Turmeric dye provides very easy surface modification, increasing its applicability in device fabrication. Its biocompatibility opens the way for electronic and optoelectronic applications.

Recently organic polymers are drawing considerable attention to the researchers for its promising opto-electronics properties. Organic materials have such advantages over inorganic materials which we have discussed in first chapter [1-19]. The natural herbal dyes have potential to play a role as photosensitizer and also possess some excellent film forming properties. The donor-acceptor (D-A) type chromophores with low band gap are particularly of interest. The band gap levels and other optoelectronic properties of the chromophores can be easily tuned. Since naturally occurring curcumin behaves as a donor-acceptor-donor (D-A-D) chromophore [20], turmeric(curcumin) based natural dye has been introduced in the present work for the formation Al/Turmeric/Cu device. The advantages of choosing curcumin as barrier are the followings: (i) it is known that thin dielectric between two metal layers forms a parallel plate capacitor of high capacitance with large time constant (TC). It means a small value of maximum operating frequency while applying in communication system. This is not good enough for acceptance in the device of high-speed communication. But curcumin has small dielectric constant k [21] which reduces the capacitance of the device, (ii) the electroluminescent peak emission for curcumin occurs at wavelength 612 nm and (iii) in comparison to other chromophores this is less expansive, compatible and naturally available non-toxic dye [22]. The main focus of this experiment is whether this device behaves as a superior diode with acceptable rectifying characteristics or not.

In this present work it is found that these dye-based device behaves like a diode. The I-V characteristics of the diode are determined to find diode asymmetry which is simply defined as the ratio of forward current to reverse current (I_F/I_R).

Schottky barrier diodes are very important devices in modern electronics and semiconductor studies because of its high current density and low forward voltage drop. These diodes show fast response due to current flow mainly by majority carriers. The I-V characteristics of Schottky diodes are depend on the nature of the metal / organic semiconductor junction. In practice it is found that these Schottky diodes do not behave as ideal diode due to the effect of series resistance (R_s), formation of barrier height, insulating layer between metal and metal interface states etc. One of the important parameters is the series resistance for which the characteristics of Schottky diodes to be non-ideal [23- 25]. Present work demonstrates the metal-insulator-metal Schottky diode using natural dye (turmeric), where two different metals having different work function has been chosen as front and counter electrodes. There is a variety of factors on which the current transport mechanism in these devices depends such as, fabrication parameters of semiconductors, formation of insulator layer, device temperature and bias voltage, etc.

The detail fabrication and characterization of Al/Turmeric/Cu diode is presented here in this work. Outcome of the experiment shows excellent result to improve the rectification ratio of the device. Observation represents that our achieved rectification ratio (asymmetry) is 30 at the 4V bias voltage which indicates enormous improvement over the previous highest reported rectification ratio 10 at 3 V for a double insulator layer MIIM device [19]. Observation also leads to conclude that the series resistance of the device decreases with temperature. From the calculated values of nonlinearity, sensitivity and energy gap between HOMO and LUMO of curcumin molecule, the device has a great acceptance in optoelectronics application.

3.2 Materials and methods

The detail fabrication and characterization of Al/Turmeric/Cu diode is carried out in step by step and described in the following subsection for better understanding as follows.

3.2.1 Materials

Fig.3.1 shows the pictorial representation of raw herbal turmeric and the Al/Turmeric/Cu device. Turmeric (Curcumalonga) is rhizomatous herbaceous perennial plant of the ginger family Zingiberacuae [26]. It is native to Southeast Asia, and requires temperatures between 20 and 30 °C and a considerable amount of annual rainfall to thrive. The main organic compound in turmeric is curcumin. This is yellow colour pigment present in turmeric plant roots. In the present work natural curcumin dye was extracted from turmeric plant root, which has been bought from local market.

(a) Turmeric

(b) Turmeric paste

(c) Al/Turmeric/Cu

(d) Turmeric solution

Fig.3.1 Pictorial representation of Al/Turmeric/Cu raw herbal Turmeric

Turmeric consists of 60-70% carbohydrates, 6-10% water 6-8% protein and rest of other materials. Its phytochemical components include diarylheptanoids, demethoxycurcumin and bisdemethoxycurcumin, germacrone, atlantone and zingiberene and other materials. Its chemical structure has been shown in Fig.3.2.

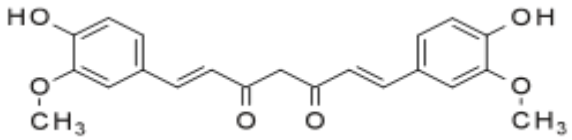

Curcumin Keto form

Fig. 3.2 Pictorial representation of chemical structure of turmeric

3.2.2 Preparation of the dye solution

We have purchased raw turmeric root shown in Fig. 1(a). Here used methanol (99.9%) was purchased from Changshuhongshu fine chemical co ltd. After cleaning and washing the paste of turmeric was prepared as shown in Fig. 1(b). Here we have used methanol-based solution (22gm raw turmeric and 180 ml methanol) of turmeric. The solution was stirred for half an hour at room temperature.

3.2.3 Fabrication of the diode

The aluminium and copper substrates were cleaned for 10 minutes using distilled water in ultrasonic cleaner and after drying, the substrates were etched with HF and H_2O (1:10) to remove the native oxide from the substrate. And the film was coated on aluminium substrate using a spin coater with angular rotation of 1000 rpm at room temperature. The copper was formed on turmeric film through a shadow mask in the vacuum system at 1002 mbar. Finally, the diode was fabricated (shown in Fig. 3.1c) and the fabricated device was kept at 50 ^{0}C for 1 hour to let the moisture in the film evaporate. Here we fabricate two different diodes for I-V and temperature dependent I-V. These two Al/ Turmeric/ Cu devices are of contact area 4 mm^2 and 2.2 mm^2. For these two experiments the used dye layers are of different thicknesses (42μm and 84 μm) and thickness of

the Al electrode is .05mm. Firstly, ampere-volt measurements were held in dark. Then we have used a 100w bulb and a convex lens of focal length 20 cm to illuminate the sample and effect of light on the I-V characteristics was observed.

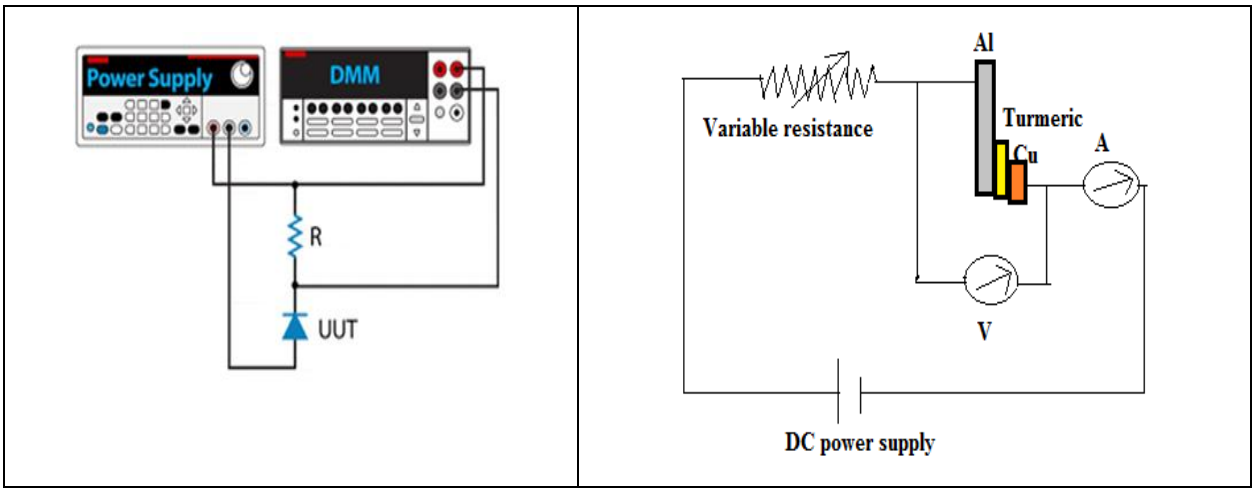

Fig.3.3 experimental arrangement and circuit diagram for electrical characterization of turmeric dye-based device.

3.3 Results and discussion

The experimental arrangement and circuit diagram for electrical characterization of turmeric dye-based device is shown in Fig. 3.3. It works in such a way that when a current is passed through these two layers of metal, the electrons get induced to quantum mechanically tunnel from one piece to other piece of metal passing through the thin insulator placed between them at very low voltage. When electrodes with different barrier heights as well as different work functions (4.26 eV and 5.10 eV for Al and Cu respectively) are used, an internal electric field will build up resulting from a built-in voltage V_{bi}, which equals to the difference in work function of the electrodes. So, when voltage is applied across the metal insulator metal diode, electrons preferentially make a tunnel in one particular direction over the other, therefore resulting in the formation of a diode [27]. Fig.3. 4(a) and 3.4(b) shows the current voltage characteristics of the Al/Turmeric/Cu device for resistance R=0 and R=1 KΩ respectively, performed at room temperature. These characteristics indicate a non-linear, asymmetric behaviour with high rectification ratio. If this device is

considered as metal-insulator-metal (MIM) tunnel diode, a quantum mechanical tunnelling action takes place. Quantum mechanical tunnelling depends on the metal structure and a small area of the metal surface induces a low tunnelling voltage with higher tunnelling current [28]. If the surface area of the two metals is different, tunnelling-voltage is to be different and much more asymmetric graph will be obtained. Due to the reason mentioned above, two metals (Aluminium and copper) of different work function with different surface area have been used, which are described by figure 3.4(c). A thin turmeric layer is deposited between aluminium and copper plates. The area of contact in this experiment is 4 mm^2. The flow of electron occurs from one metal to another through the insulating layer (turmeric) by the field-effect tunnelling. This tunnelling probability is to be controlled by the contact area of the metals and the bias voltage. In this device at very low temperature current conduction mechanism is dominant by quantum tunnelling. The energy band diagram depends on work function of metals (4.20, 5.10), electron affinity of curcumin (1.9 – 2.4 eV) [29] and the band gap of curcumin (2.6 eV). The energy band diagram of Al/ Turmeric/ Cu at zero bias is shown in figure 3.4c. For a negative bias, shape of the energy band diagram alters and it is shown in figure 3.4d. From figure 3.4(d) it is shown that electrons in Cu may tunnel into the vacant states of Al. For very small thickness of turmeric layer there is an occurrence of quantum tunnelling of electron through it. This tunnelling probability depends on the applied voltage. In this figure 3.4d the applied voltage is slightly greater than the barrier height at the junction of Al and turmeric. When this bias voltage is increased, there is a decrease in width of the insulating layer near the Fermi level. So, there is an increase in tunnel current due to the decrease in tunnel distance. When a positive voltage is applied to the device same phenomena arises. In this case tunnelling occurs from Al to Cu. Here for a voltage above the barrier height, the current also increases with the decrease in tunnelling distance. So, work function difference is the main reason for the asymmetric behaviour of the I-V characteristic for Al/Turmeric/Cu device [30].

In this device current conduction occurs either by quantum tunnelling or by Schottky emission. We know that for any organic material current conduction is governed by other different mechanism. For turmeric the band alignment for insulating and semiconducting turmeric is shown in Fig. 3.14. Since the band offset is very small so copper forms ohmic contact. For MIM diode tunnelling current should be directly proportional to the bias voltage for bias voltages less than barrier height and should increase exponentially with voltages when the bias becomes comparable to the barrier height. For this work 1.85 eV barrier heights along Al/Turmeric contact and there is

ohmic behaviour at Cu/Turmeric contact. In presence of a series resistance of 1kΩ the device behaves like a MIM diode and the I-V characteristics shown in Fig. 3.4(b) is a typical MIM I-V characteristics. But Fig. 3.4(a) shows Schottky diode I-V characteristics of an Al/n-type semiconductor for the device structure which is similar with a band bending shown in Fig. 3.4(c).

In the present device, current conduction mechanism occurs due to quantum tunnelling and thermionic emission. At very low temperature (below 170 K), when turmeric (curcumin) behaves like an insulator then quantum tunnelling dominant over thermionic emission. Here the tunnelling occurs between two dissimilar work function metals Al (4.20) and Cu (5.10) separated by turmeric layer. In current conduction mechanism electrons face off non-identical barriers ($\varphi_1$and φ_2) because of the work function difference between Al and Cu. A voltage was applied to Al and Cu was grounded for biasing the device. In the presence of 1 kΩ resistance in series and temperature below 190K in this device, there is a domination of direct tunnelling (DT) for low forward and low reverse bias, where the applied bias is less than the barrier height. On the other hand, for high forward and high reverse bias that means when the bias voltage is greater than the barrier height then the current conduction is dominant by Fowler-Nordheim tunnelling (FNT) [31]. But the temperature dependent I-V shown in Fig. 10 shows that thermionic emission is dominant over quantum tunnelling in current conduction mechanism of this device. Fig. 3.4(a) and Fig. 3.10 demonstrate Schottky diode I-V characteristics of Al/Turmeric/Cu device at room temperature and above.

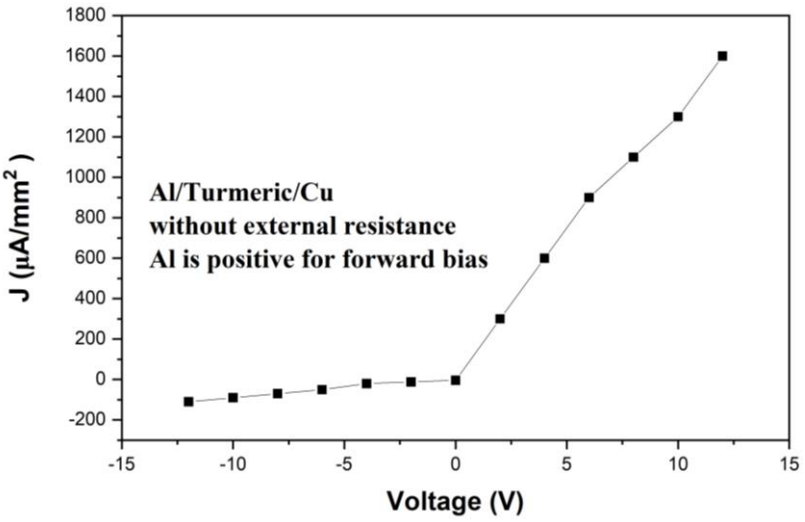

Fig. 3.4 (a) Current density vs Voltage for R = 0 Ω

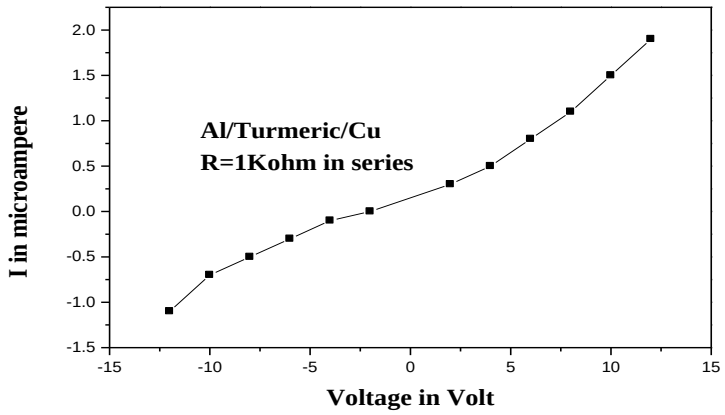

Fig. 3.4 (b) Current vs Voltage for R=1 kΩ

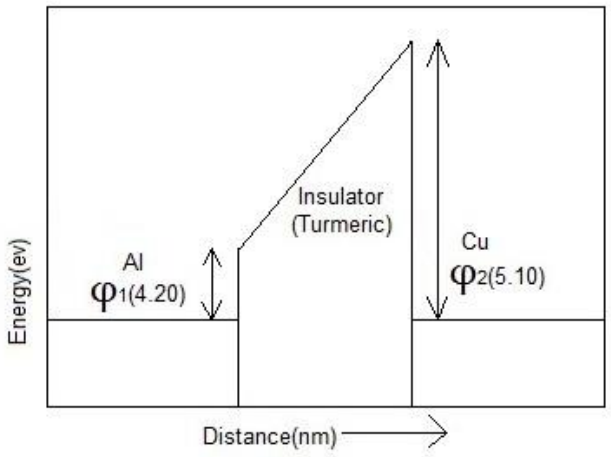

Fig. 3.4(c) Energy band diagram of Al/ Turmeric/ Cu diode at zero bias where we assume the Fermi levels of the Al and Cu have same height.

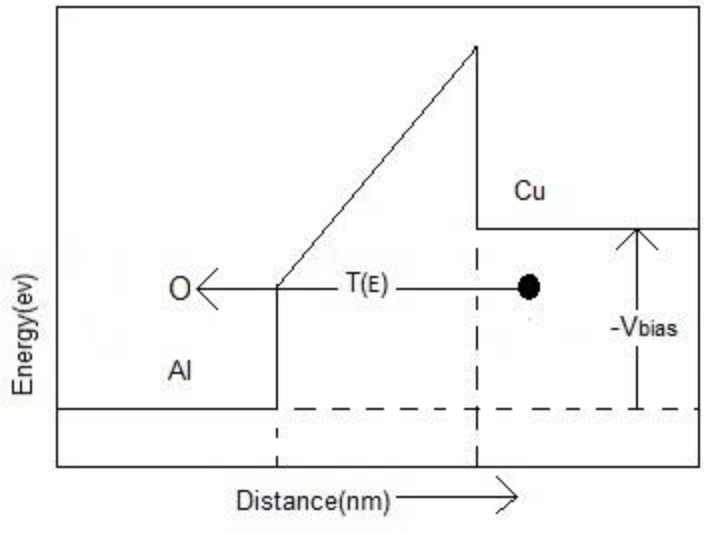

Fig. 3.4(d) Energy band diagram of Al/ turmeric/ Cu at reverse bias.

Figure 3.4(a) shows that I-V characteristics are non-linear and asymmetric with very low turn on voltage (below 1V). This non-linear asymmetric behaviour can be explained with the junction resistance and interface states of junction. Due to different injection direction the energy barrier of this device is asymmetric. The barrier varies with bias voltage due to the injection of electrons from curcumin, on the other hand when electrons injected from cathode (Cu), the barrier height remains constant. When a positive voltage applied, the Al/Curcumin barrier will decrease and electron will transport through the junction. When negative voltage applied, electron transportation is controlled by Cu/curcumin barrier. If the turmeric (curcumin) behaves like organic semiconductor then the depletion layer at the junction is to be decreased at forward bias and increased at reverse bias. As a result, the ampere-volt (I-V) characteristic is to be non-linear and asymmetric. So, the device then behaves like a Schottky diode, and the current of the device is obtained due to thermionic emission and it is given by Equation (3.1) and (3.2) [32]:

$$I = I_o[\exp\left(-\frac{q(v-IR_s}{nkT}\right)] \qquad (3.1)$$

Where, I_0 is the reverse saturation current and given as Equation 2:

$$I_o = AA^*T^2 \exp\left(\frac{-q\phi}{kT}\right) \quad (3.2)$$

Where, A is contact area of the device,

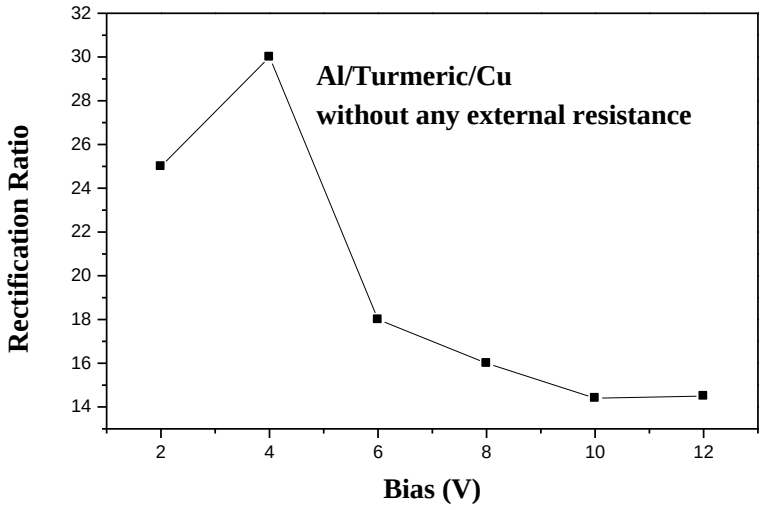

Fig. 3.5 Plot of Rectification Ratio (RR) vs Voltage for R=0 ohm

The reverse saturation current is derived from the straight-line intercept of ln (I) at zero bias voltage. To evaluate the rectification behaviour of the device, the I-V characteristics was measured under ambient condition shown in Fig. 3.4a and Fig. 3.4b, and asymmetry, nonlinearity and sensitivity of the device are extracted from this I-V. The characteristic shows the rectifying property of the device with non-linear manner. The rectification ratio (RR) is determined from the ratio of the forward current to the reverse current at a certain applied voltage. In this experiment we observed that the rectification ratio varies with applied voltage. For this Al/Turmeric/Cu junction device the maximum value of Rectification Ratio was found to be 30 at 4 V. Fig.3.5. shows the variation of Rectification Ratio (RR) with applied voltage (V). Ideality factor (n) is the most important parameter of the diode calculated by using the following Equation (3.3) [33]:

$$n = \frac{q}{kT}\left(\frac{dV}{dlnI}\right) \quad (3.3)$$

Where V is the applied voltage, T is the temperature in Kelvin. The value of ideality factor for an ideal diode is to be 1. For a real Schottky diode the value of ideality factor is greater than 1. In this experiment the value of ideality factor is found to be about 6.56. It is quite normal to have high value of ideality factor of herbal and organic devices because of their disordered amorphous nature. This greater value of ideality factor might be explained from the recombination of electrons and holes in the depletion region and it is also associated with Fermi-level pinning at the interface region. In this device thickness of the dye layer is greater in comparison with normal Schottky diode. The greater thickness of the curcumin layer leads to a huge recombination of electrons and holes. So, the probable reasons of high value of ideality factor of the device are that potential drop in the interfacial layer and the presence of excess current and a high recombination current through the interfacial states between metal curcumin layers [34]. The ln(I) vs V characteristic is linear at low forward bias, but at higher forward voltages the characteristic becomes non-linear. This deviation from the linearity occurs due to the effect of series resistance. The complex behavior of non-ideal diodes arises due to the occurrence of various conduction mechanisms [34]. For such non-ideal diodes, the following modified Schottky equation as given Equation (3.4) can be used [35]:

$$I = I_{01}\left[\exp\left(\frac{qV-IR_s}{n_1kT}\right)-1\right] + I_{02}\left[\exp\left(\frac{qV-IR_s}{n_2kT}\right)-1\right] + \frac{V-IR_s}{R_{sh}} \qquad (3.4)$$

Where, R_s is the series resistance and R_{sh} is the shunt resistance. Fig. 3.6 shows the variation of junction resistance ($R_J = dV/dI$) with applied voltage (V). The non-linear behaviour of the current-voltage (I-V) characteristic for this device can be achieved by the variation of junction resistance. At certain positive bias the junction resistance reduces to a minimum value. This value of the junction resistance is called series resistance (R_s). On the contrary, with a certain negative voltage the junction resistance increases to a maximum value. This value of the junction resistance is called shunt resistance (R_{sh}). It is observed for this device the Values R_s and the R_{sh} are found 8 KΩ and 100 KΩ respectively.

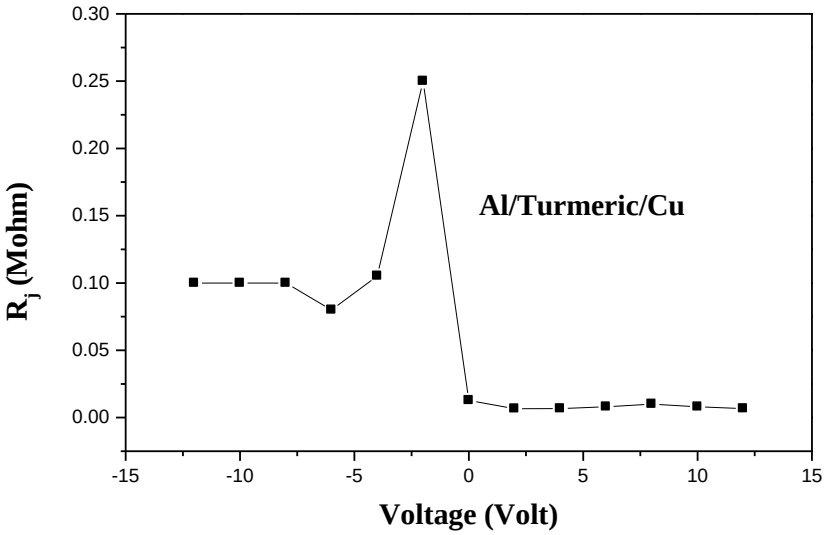

Fig. 3.6 Plot of junction resistance of Al/Turmeric/Cu

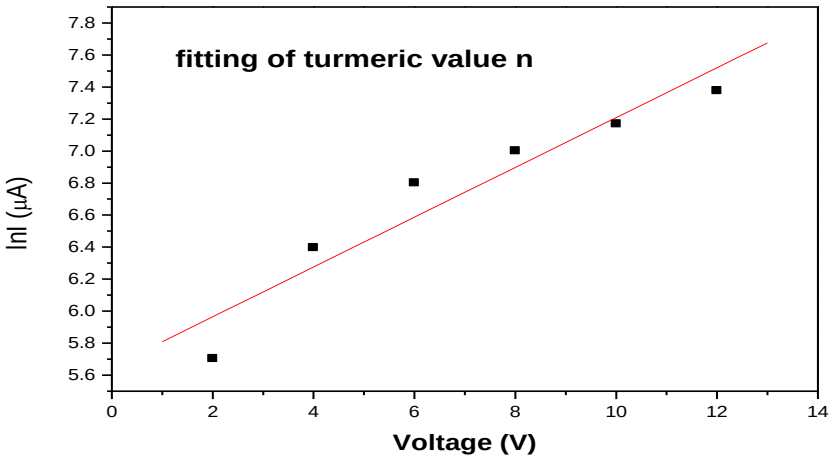

Fig.3.7 Linear fitting of lnI for Al/Turmeric/Cu

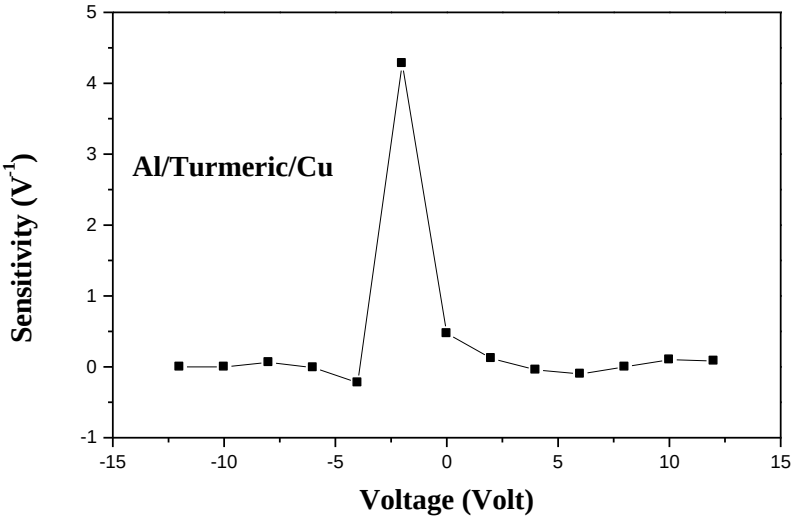

Fig.3. 8 Sensitivity vs Voltage for Al/Turmeric/Cu

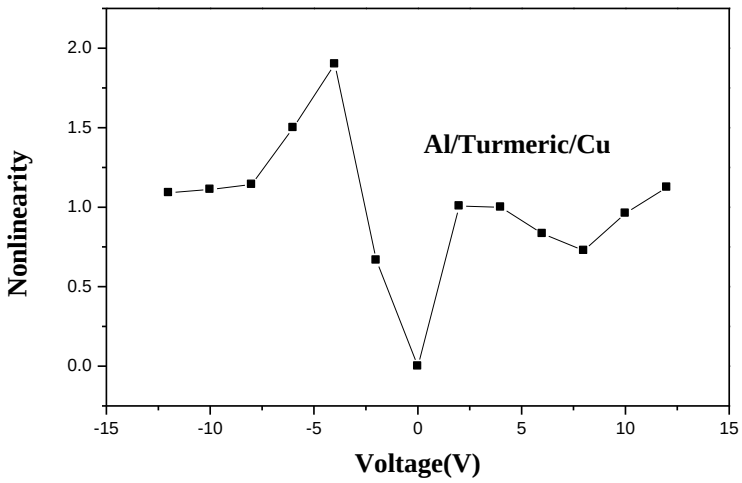

Fig. 3.9 Device nonlinearity factor for Al/Turmeric/Cu

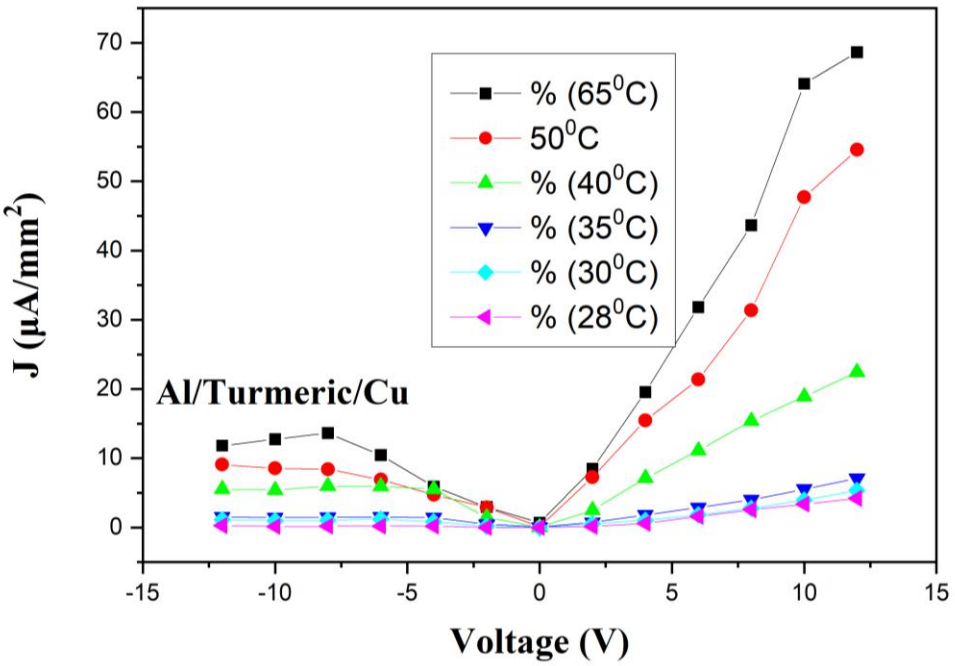

Fig. 3.10 Experimental temperature dependence current-voltage (I-V) of Al/Turmeric/Cu

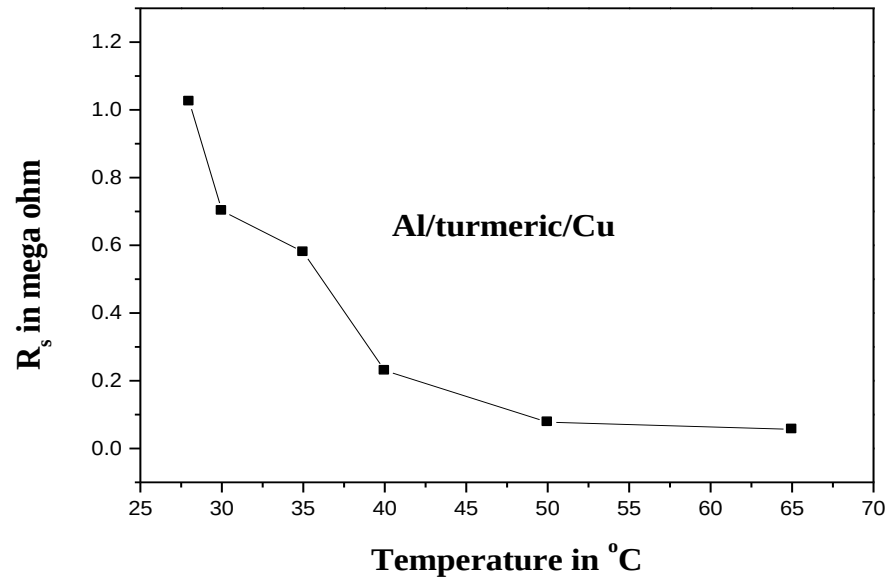

Fig. 3.11 Temperature dependence of series resistance (R_s) of Al/Turmeric/Cu

The sensitivity vs voltage graph for this device is shown in Fig.3.8. The maximum sensitivity was found 4.3 V^{-1} at -2 V. The sensitivity is the measure of rectified dc voltage or current with respect to the input power. We can see from Figure 6 that the slope of the junction resistance (R_j) at -2V is steeper. Due to this rapid resistance change there is a maximum nonlinearity in current is 1.9 shown in Figure 3.9. Because of this there is the maximum sensitivity 4.3 V^{-1} at -2V. The maximum sensitivity was found 0.1V^{-1} under an applied bias 5V and 4.3 V^{-1} at -2 V. The variation of nonlinearity factor for the above device is shown in Fig.3.9. The diode's non-linearity is given by,$(\frac{dI}{dV})\frac{V}{I}$; Where, dI, dV, I and V are variations in current, variation in voltage, current and voltage respectively. Nonlinearity is a measure of deviation of the I-V characteristics of an electrical device from Ohmic I-V characteristics, which means deviation of the device performance from the linear behavior. From fig. 3.9, it is observed that the nonlinearity is maximum at very low bias voltage and its maximum value is 1.9, which quantitatively benchmarks the capability of a diode working as a rectifier.

It is observed that the I-V characteristics vary from diode to diode. At first, we fabricate the device for I-V characteristics and we have done the experiment. Then after one month we fabricate another device and we have done the experiment for temperature dependent I-V. For these two I-V we have used two different Al/ Turmeric/ Cu devices with different contact area 4mm^2, 2.2 mm^2 and of different thickness. Because of this there is a change in current in two different I-V characteristics. The temperature dependent current – voltage (I-V) measurements were made over the temperature range of 28 ^oC – 65 ^oC. From Fig.3.10 we observed that, the I-V characteristics changes very much with temperature for Al/Turmeric/Cu device. This shows that in our device thermionic emission is dominant over quantum tunnelling. The values of series resistance have been changed from 0.056 MΩ (at 65 ^oC) to 1.1 MΩ (at 28 ^oC). When the temperature is below 190 K, turmeric behaves like an insulator and the device is like a MIM diode. At room temperature and above, when thermal energy of electron is greater than the band gap of curcumin then turmeric behaves like a semiconductor and the device is a Schottky diode. If we consider turmeric as n-type semiconductor then the Schottky junction formed between Al and turmeric. Before the contact formation the Fermi level of turmeric is higher than Al, but after the formation of contact the Fermi levels must line up at equilibrium that means there is a conduction of electron from the conduction band of the turmeric to empty energy states above the Fermi level of Al. Due to this motion of electrons there is positive charges on the turmeric side and electrons on the Al side, which forms an electric field directed

from turmeric to Al. After the formation of Al-Turmeric junction electrons are not only conducted from the surface of turmeric but also from a certain depth. Because of this there is a formation of depletion region at the Al/Turmeric junction. Since the depletion region extends within a certain depth in the turmeric so there is a bending of the energy bands on the turmeric side and the energy band bends up continuing from turmeric to Al [36] shown in Fig. 3.14. Band bending for p-type conductivity of turmeric shown in Fig. 3.14(c) (this band bending will be upward at Al/Turmeric interface for n-type conductivity).

When temperature of the device increases, thermal energy of the electrons increases and the depletion layer decreases. As a result, current increases and the series resistance decreases with temperature. Variation of series resistance changes with temperature shown in Fig.11, which reveals that Series resistance (R_s) decreases with increase in temperature. Current transport across the metal semiconductor junction is a temperature activated process, because of these electrons at low temperatures are able to surmount the lower barriers and current transport will be dominated by current flowing through the paths of lower Schottky barrier height with a large ideality factor. At room temperature the barrier height increases with temperature and bias voltage [37, 38]. The temperature dependent current-voltage (I-V) characteristics are indicating the dominance of quantum tunnelling mechanism at low temperature and the dominance of thermionic emission mechanism at higher temperature. From quantum mechanical calculation using Gaussian 03W package and density functional theory (DFT) [39], it is observed that two oxygen atoms are responsible for push-pull effect through π electron delocalization in curcumin molecule. In curcumin atom there is a single pair of oxygen in hydroxyl group, which pushing the aryl residual electron into π conjugated system. So, the electron is pulled out to one of the carbonyl groups. There is a difference in electronegativity and oxygen hybridization in C-O and C=O. The calculated value of energy difference between HOMO and LUMO is 2.95 eV (at 420 nm) [20]. Which shows, it might behave as an organic semiconductor and has great possibility of using as an organic light emitting diode? On a semi-logarithmic scale, the forward-bias I-V characteristics are linear at low bias voltages, but there is a deviation from linearity due to the effect of series resistance, the interfacial insulator layer and the interface states when the applied voltage is sufficiently large. Main problem of this device (diode) is that current decreases with time. This occurs because of the space charges at the junction. If we use some impurity (or electrolyte) with the turmeric (curcumin) layer which can trap the electrons and may resolved this problem.

3.3.1 Absorption spectra of curcumin

Perkin-Elmer Lambda 25 UV-V spectrometer is used to measure the absorption spectra of curcumin as a solution in pure methanol, shown in Fig. 3.12. The value of energy gap between HOMO and LUMO levels of curcumin is 2.95 eV (at 420 nm), which is calculated from absorption spectra of curcumin [20]. The HOMO and LUMO levels are shown in Fig. 3.13. This energy gap is less than 5 eV and the temperature variation of series resistance shows that curcumin might behave like a semiconductor and the Al / Turmeric / Cu device is a surface type Schottky diode which is much better than organic Schottky diodes with high ideality factor. There are different number of mechanisms for current conduction. If the temperature is below 190K turmeric (curcumin) is insulator then there is only Quantum Tunnelling but in this temperature range (25^0C-65^0C) Richardson-Schottky emission (thermionic emission through Schottky junction in presence of electric field) dominant over Quantum Tunnelling and Poole-Frenkle emission, which we have observed in the next chapter.

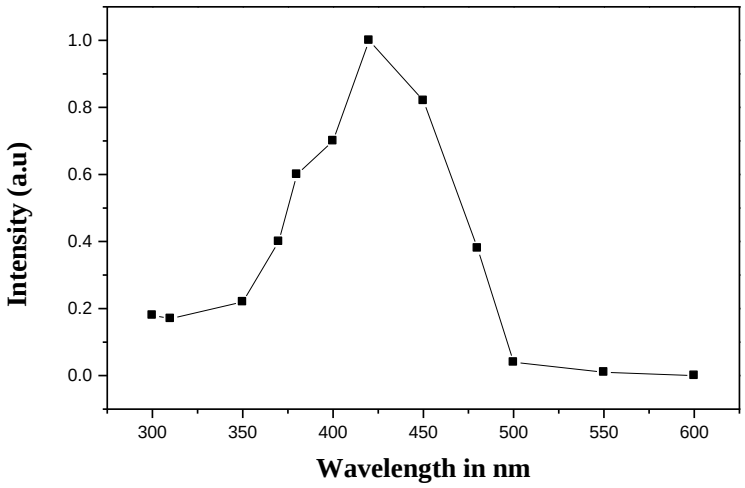

Fig. 3.12 represents the absorption spectra of curcumin

But the problem of this device is the stability, load current decreases with time. At the moment of photo excitation, the curcumin dye emits the electron which travel through the film by diffusion into the conduction band of metal and hole is generated by photon excitations on the molecule. Since the HOMO of dye is separated from all other energy levels of the device, there is no energy channel for the hole to diffuse into electrode, causes current decrease with time. To reduce this problem authors suggest using an electrolyte. In that case the holes will be filled

up by electrons from electrolyte ions, will help to conduct current between cathode and the dye molecule. Another problem of this device is its trap energy, which we discussed in detail in the next chapter [40].

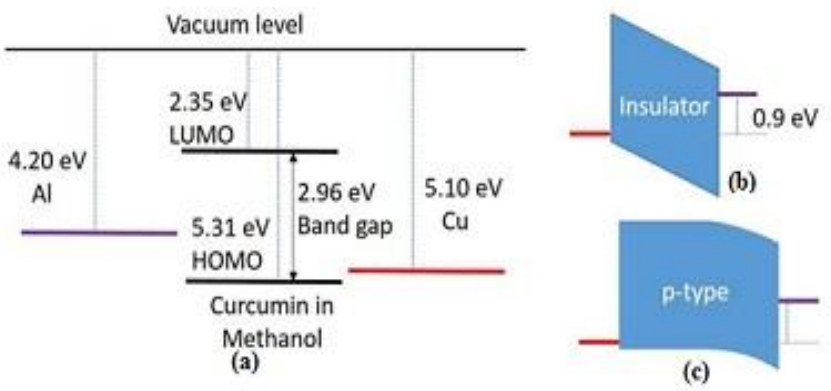

Fig. 3.13 (a) Energy band alignment for turmeric (curcumin) in methanol with respect to vacuum, **(b)** insulating behaviour of turmeric for a temperature below 190K and **(c)** band bending for p-type conductivity of turmeric (this band bending will be upward at Al/ Turmeric interface for n-type conductivity).

3.4 Conclusions

The electronic parameters of Al/Turmeric/Cu surface type Schottky diode have been evaluated in this chapter by current-voltage method at room temperature. Also, the electronics properties of Al/Turmeric/Cu device have been investigated by temperature dependent current-voltage (I-V) measurements at different temperature using another diode. The average values of ideality factor, series resistance and shunt resistance have been observed to be about 6.562, 8 kΩ and 105 kΩ, respectively, from forward bias current-voltage characteristics. High value of Rectification Ratio as found to be maximum 30 at 4 V indicates that this junction has potential to be used as a good rectifier. maximum sensitivity was found $0.1V^{-1}$ under an applied bias 5V and $4.3V^{-1}$ at -2V. The interesting result obtained in this present work is that the series resistance decreases with temperature and current increases with temperature. At $65^{o}CR_s$ is 56 kΩ and at $28^{o}CR_s$ is 1.06 MΩ and the energy difference between HOMO and LUMO is 2.95 eV (at 420 nm). These findings indicate that turmeric behaves like a semiconductor and has a potential to be used as organic semiconductor diode. Turmeric contains diarylheptanoids and phenolic compounds. These molecules contribute to its semiconducting behaviour. Also, it is suggesting that this diode can be used as a good rectifier in electronics.

3.5 References

1. Klauk H (Ed.) (2006), Organic Eletronics: Materials, Manufacturing and Applications 2006, Wiley-VCH, Weinheim. Print ISBN 9783527312641.

2. Klauk H (Ed.) (2006) Organic Eletronics: Materials, Manufacturing and Applications 2006, Wiley-VCH, Weinheim. Print ISBN 9783527640218.

3. Barbec CJ, Sariciftci NS, Hummelen JC (2001) Plasticsolar cells. Adv. Funct, Mater.11: 15-26.

4. Kawano K, Sakai J,Yahiro M, Adachi C (2009) Effect of solvent on fabrication of active layersin organic solar cells based on poly (3-hexylthiophene) and fullerene derivatives. Solar EnergyMaterials and Solar Cells 93: 514-518.

5. Yu G, Jeeger AJ, Charge separation and photovoltaic conversion in polymer composites with internal donor / acceptor heterojunctions. Journal of Applied Physics78

6. Feron K, Belcher WJ, Fell CJ, Dastoor PC (2012) Organic solar cells: understanding the role offorster resonance energy transfer. International Journal of Molecular Sciences 13: 17019-17047.

7. Benanti TI, Venkataraaman D (2006) organic solar cells: an overview focusing on active layermorphology. Photosynth Research 87:73-81.

8. Haldar A, Maity S, Manik NB (2008) Effect of back electrode on photovoltaic properties of crystal-violet-dye-doped solid-state thin film. lonics14: 427-432.

9. Thompson BC, Frechet JMJ (2008) Ploymer-fullerence composite solar cells. Angewandt Chemie International Edition 47: 58-77.

10. Elumalai NK, Saha A, Vijila C, Rajan Jose R, Zhang Jie Z, Ramakrishna S (2013) Enhancingthe stability of polymer solar cells by improving the conductivity of the nanostructured MoO_3hole transport layer. Physical Chemistry Chemical Physics15: 6831-6841.

11. Alimardani N, Conley JF Jr (2014) Enhancing metal-insulator-insulator-metal tunnel diodes via defect enhanced direct tunneling J. Appl, phys. 105: 082902.

12. Alimardani N, Conley JF Jr (2013) Step tunneling enhanced asymmetry in asymmetric electrode metal-insulator-metal tunnel diodes.Applied Physics Letters102: 143501. doi: 10.1063/1.4799964

13. Maraghechi P, Foroughi-Abari A, CadienK, Elezzabi AY (2011) Enhanced rectifying response from metal-insulator-metal junctions. Applied Physics Letters99: 253503

14. Grover S, Moddel G (2012) Engineering the current voltage characteristics of metal-insulator-metal diodes using double insulator tunnel barriers. Solid state electron67: 94-99.

15. Aydinoglu F, Alhazmi M, Cui B, Ramahi OM, Irannejad M, Brzezinski A, Yavuz M (2014) Higher performance metal-insulator-metal diodes using multiple insulator layers. Austin Journal of Nanomedicine&Nanotechnology1(1): 1004

16. Maraghechi P, Foroughi-Abari A, CadienK, Elezzabi AY (2012) Observation of reson at tunneling phenomenon in metal-insulator-insulator-insulator-metal electron tunnel devices.Applied Physics Letters100:113503.

17. Gaddala MN, Abdei-Rahman M, Shamim A (2014) Design, optimization and fabrication of a 28.3 THz nano-rectenna for infrared detection and rectification. Scientific Report4 (1): 1-9.

18. Grover S,Moddel G (2011) Applicability of metal/insulator/metal (MIM) diodes to solar rectennas. IEEE Journal of Photovoltaics1(1): 78-83.

19. Weerakkody AD, SedghiN,MitrovicIZ,Zalinge HV, Noureddine IN, Hall S, Wrench JS, Chalker PR, Phillips LJ, TreharneR, Durose K (2015) Enhance low voltage nonlinearity in resonant tunneling metal-insulator-insulator-metal nanostructures. Microelectronic Engineering 147: 298-301.

20. Rad MNS, Sharbati MT, S. Behrouz S, A.R. Nekoei AR (2015) Fabrication of non-doped red organic light emitting diode using naturally occurring Curcumin as donor-acceptor-donor (D-A-D) emitting layer with very low turn-on voltage. Iranian Journal of Science & Technology 39A3: 297-304

21. Dakhel AA, Cassidy S, Jasim KE, Henari FZ. Synthesis and characterisation of curcumin–M (M= B, Fe and Cu) films grown on p-Si substrate for dielectric applications. Microelectronics Reliability. 2015 Feb 1;55(2):367-73.

22. Sharbati MT, Rad MNS, Behrouz S et al. (2011) fabrication and electrical characterization of red organic light emitting diodes based on acceptor-donor-acceptor (ADA) using novel conjugated isatin Schiff bases. Journal of Luminescence 131: 553-558.

23. Tataroglu A, Altindal S (2008) Analysis of interface states and series resistance of MIS Schottky diodes. Microelectronic Engineering 85(1): 233-237.

24. Nicollian EH, Goetzberger A (1965) MOS conductance technique for measuring surface state parameters. Applied Physics Letters 7: 216, https://doi.org/10.1063/1.1754385

25. Aydin SBK, Yildiz DE, Cavus HK and Sahingoz R (2014) ALD TiO2 thin film as dielectric for Al/p-Si Schottky diode. Bulletin of Materials Science 37: 1563-1568.

26. Priyadarsini KI (2014) The chemistry of curcumin: from extraction to therapeutic agent. Molecules19 (12): 20091-112. Doi: 10.3390/molecules 191220091. PMID 25470276.

27. Bruyn PD, Van Rest AHP, Wetzelaer GAH, Leeuw DMD, Blom PWM (2013) Physical Review Letters PRL 111:186801(2013).

28. Shin JH, Jaehan Im, Choi JW et al. (2016) Jae Eun Jang carbon 102: 172-180

29. Hayder MA, Musa KM, Hussein AM (2018) Theoretical study of the electronic properties of the curcumin molecule: using density functional theory. Journal of university of Babylon, Pureand Applied Sciences, Vol. (26): No.(5)

30. Eliasson BJ (2001) Metal-Insulator-Metal diodes For Solar Energy Conversion a thesis submitted to the graduate School of the University of Colorado, doctor of Philosophy, Department of electrical and computer engineering.

31. Cowell EW, Muir SW, Keszler DA, Wager JF (2013) Journal of Applied Physics 114: (21), 213703

32. Rhoderick EH, Williams RH (1988) *Metal-Semiconductor Contacts*, Clarendon Press, Oxford,

33. Rhoderick EH (1978) *Metal Semiconductors Contacts*, Oxford University Press.

34. Quan DT, Habib H (1993) solid state electron. 1993,36,339. DOI 10.1016/0038-1101(93) 90085-5

35. Ranuarez JC, Sanchez FJG, Ortiz-conde A (1999) Procedure for determining diode parameters at very low forward voltage. Solid-State Electronics 43(12): 2129-2133.

36. Kasap SO (2001) Principle of Electronic Materials and devices. Mcgraw-Hill (Tx) (2001) ISBN 10:0072393424/ ISBN 13:9780072393422

37. Naik SS, Reddy VR (2012) Temperature dependency and current transport mechanism of Pd/V/n-type In Pschottky rectifiers. Advanced Materials Letters (3): 188-196

38. Karatas S, Altindal S, Turnt A, Ozmen A (2003) Applied Surface Science 2003, 217, 250.

39. Frish MJ et al. (2003) Gaussian 03, Revision B.05, Gaussian, Inc., Pittsburgh PA.

40. Chakrabarty K, Das AK, Mandal R, Mandal DK (2020) Investigation on the trap signature in Organic semiconductor turmeric film through current-voltage analysis. Transactions of Tianjin University volume 26, pages 265-272

Chapter 4

The current transport mechanism of Al/Beetroot/Cu used as an organic semiconductor Schottky diode is superior than natural dye-based thin film devices

4.1 Introduction

In the previous chapter we have discussed the semiconducting behaviour of turmeric dye and fabrication and characterization of turmeric dye-based device. We also measure the electrical parameters analysing the I-V characteristics of that device. The main focus of this chapter is to observe the semiconducting behaviour of beetroot dye and a detailed study on charge transport mechanism through beetroot dye-based electronic device. For this we have used beetroot dye as insulating layer to fabricate an organic thin film device. Use of a suitable insulating or semiconducting layer possesses the utmost importance in thin film electronic or optoelectronic devices. For both quantum tunnelling and thermionic emission, the current conduction mechanism depends on the properties of the insulating or semiconducting layer. The quantum tunnelling depends on the work function of the two constituent metals, the electron affinity and band gap of the insulator component [1-17]. The dielectric constant of this type of film is extremely low which can be utilised in MIM and Schottky devices [17]. In addition, we found the dielectric constant of beetroot (k = 2.8) to be low, which could be extremely useful for a high-speed communication system [18]. In our knowledge some previously reported rectification parameter like asymmetry 10 at 3 V for Cr/Al_2O_3/ HFO_2/Cr [19] and 18 at 0.35 V for Ta_2O_5/Al_2O_3 and Nb_2O_5/Al_2O_3 bi-layer MIIM devices [20].

In addition, we found that the ideality factor for p-Si/TiO_2/Al schottky diode is 8.9 [21] and 42.9 for 5,14-dihydro-5,7,12,14-tetraazapentacene doped Schottky [22]. The value of n in organic Schottky diodes has been reported to range from 2 to 11 to our knowledge [23-28]. For the first time, we have reported the electrical properties of a herbal dye-based organic thin film device that behaves as a MIM at temperatures below 140 K and as a Schottky diode at room temperature in this study. In our fabricated device the maximum asymmetry is 17.6 at 0.85 V and the ideality factor is 4.5, which secures the device as a promising candidate as an organic Schottky diode in rectifying application. The device exhibits a more impressive performance than the previously reported organic Schottky diodes. In this paper we also fabricate Al/TiO_2/Cu surface type Schottky diode for a comparative study between this and organic dye based organic diodes. The main aim of this study is to verify the semiconducting behaviour of beetroot dye molecules. ii) Quantum tunnelling and trap-assisted current conduction observed in this Al/Beetroot/Cu device. We also found that SE and GD may also be effective. iv) Determination of the insulating temperature of this device. Finally, we compared different natural dye-based thin film diodes and found that Al/beetroot/Cu has significantly superior electrical characteristics than our previously published Al/indigo/Cu device.

4.2 Materials and methods

In this work we have used red beetroot dye active layer. Here we have also used ethanol (99.9%) and polyvinyl alcohol (PVA). We have purchased PVA from Loba Chemie Pvt. Ltd. and ethanol obtained from Changshu Hongsheng Fine Chemical Co,.Ltd. Here used substrate is FTO coated glass of resistivity 15 Ωcm^{-2}. We have purchased raw beetroot then cleaned with distilled water and rinsed with ethanol. In a clean beaker 35 mL beetroot juice is taken and 15 mL ethanol is mixed with it. This mixture is stirred for 30 min at room temperature in a magnetic stirrer. Beetroot dye was recrystallized twice in ethanol before being combined with PVA. Here molecular weight of the used PVA is 1,15,000. In a cleaned beaker 20 mL distilled water is taken and 4 g of PVA is added with it and the mixture stirred with a magnetic stirrer for half an hour at 70^0 C to form a gel like transparent viscous PVA solution. 6 mL beet root-ethanol solution has been mixed with this PVA solution. Here we have used PVA as an inert blinder to stable the dye film.

To fabricate the Al/Beetroot/Cu organic Schottky diode, we have used Al (4.20 eV) and Cu (5.10 eV) as two electrodes. As a consequence, there is high work function difference between two electrodes. Here the substrate FTO glass was chemically cleaned by acetone. Then native oxide of Al wafer was removed in HF: H_2O (1:10) solution and finally the wafer is rinsed in deionised water for one minute. The Cu layer was deposited as base electrode using thermal evaporation process. The dye (Beetroot) solution is coated onto Cu using a spin coater at 2000 rpm and then the dried at 50^0 C for one hour to let the moisture. Here beetroot dye thin film of 50 μm was deposited. Thickness of the Al electrode is about 0.005 mm. Then the beetroot dye solution spin-coated on the Al, and finally these two electrodes are sandwiched to form Al/Beetroot/Cu diode. At last, this Al/Beetroot/Cu device has been dried for 10 hours before characterization. The experimental circuit shown in Fig. 4.1.

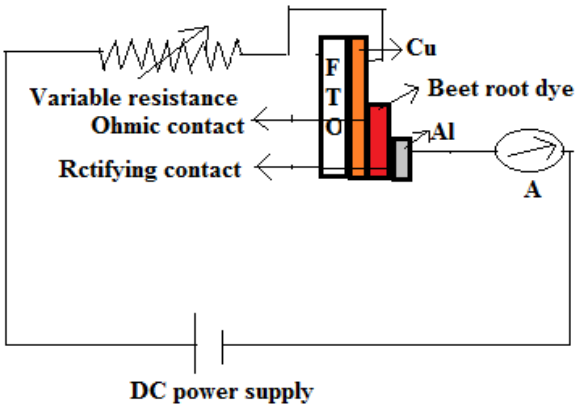

Fig. 4.1. Schematic circuit representation of the experiment with sandwiched configuration of Al/ Beetroot/ Cu thin film device.

4.3 Results and discussion

4.3.1 Current transport and rectifying Mechanism of Al/Beetroot/Cu device

Fig. 4.2 shows the I-V characteristics of Al/Beetroot/Cu thin film device. It is depicted from the I-V that, the device exhibits a rectifying behaviour with a suitable non-linear characteristic, for two metals of different work function. When we use two metals of equal work function as electrodes then the I-V is linear in nature. These two opposite behaviours might be explained by the current conduction mechanism of the device. In this experiment the current conduction mechanism through the Al/Beetroot/Cu device may be explained with the help of the quantum tunnelling, thermionic emission and Poole-Frenkle emission theory.

From Fig. 4.3 it is observed that f_{ASYM} increases with increasing biases and reaching a maximum value of 17.6 at0.85 V, then decreases with increasing bias. The tunnelling current (I) exponentially varies with the forward bias voltage V, as previously described in the literature [29]. In this experiment we also observed the exponentially varying I-V characteristics. So, electron flux of tunnelling current will change with the change in polarity, when an alternating voltage field is applied on the Al/Beetroot/Cu device in presence of an external bias voltage [30]. In presence of forward bias, if an alternating voltage is applied to the device, then more electrons are tunnelling from the positive biased Al to the negative biased Cu. So, there is a direct current formed in the device output. From the exponential I-V characteristics of the device, we may say that rectifying characteristics of the diode is to be more efficient at higher voltages. Since there is a work function difference between Al and Cu electrodes, because of this an asymmetric slope of the I-V characteristics is achieved even when

no biased is applied to the junction [31]. In this diode there is a higher barrier height for the electron, when tunnelling occurs from the metal of high work function (Cu) to the metal of low work function (Al) than the reverse way. So, there is a direct current flows from the metal of low work function to the metal of high work function [32].

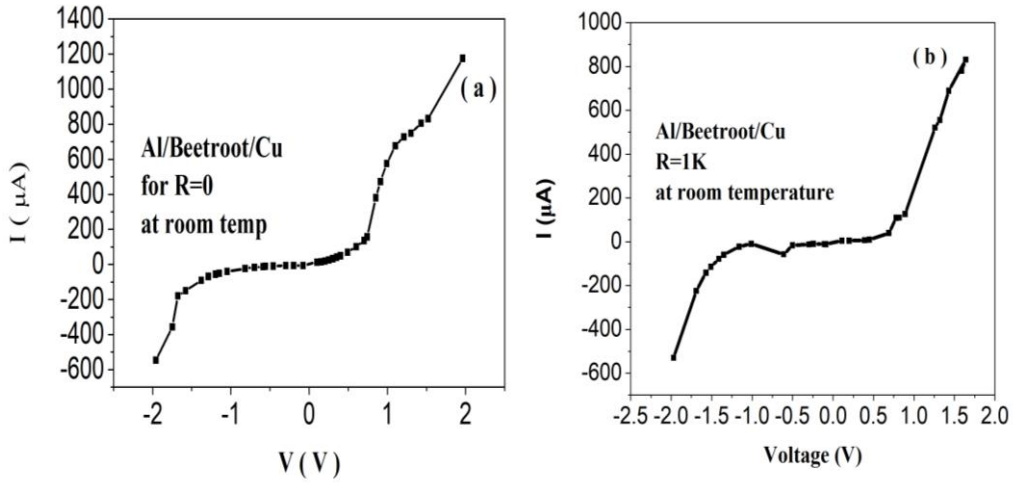

Fig. 4.2. Represents the I-V characteristics of the Al/ Beetroot/Cu device

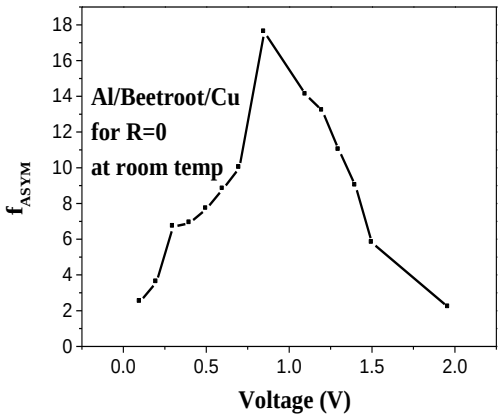

Fig. 4.3 Variation of asymmetry for Al/Beetroot/Cu

4.3.2 Thermionic emission and electrical characterization

The current conduction process might be explained using thermionic emission theory since the device behaves like a Schottky diode at room temperature and above. According to this theory, the current in Schotky diodes can be expressed as [33]

$$I = I_o \exp\{q(V - IR_S) / nkT\} \quad (4.1)$$

Where I_0 is the reverse saturation current and can be expressed as

$$I_o = AA^*T^2 \exp(-q\phi / kT) \quad (4.2)$$

Where V is the applied voltage, A is the effective junction area of the diode, A* is the Richardson constant, ϕ is the barrier height at zero bias, k is Boltzman constant and T is the operation temperature in Kelvin scale. We have calculated the ideality factor n from the slope of the linear region of the forward bias lnI-V plot using the relation:

$$n = \frac{q}{kT}\left(\frac{dV}{d\ln I}\right) \quad (4.3)$$

Slope of the line in lnI-V plot described in Fig. 4.4(a) is determined and imposing this value in equation 3 we found n = 9.5. This value is higher than any ideal Schottky diode, which delineates that the charge transportation mechanism can't be explained by thermionic emission only. To study the charge transportation mechanism this device we have drawn the LogI-LogV characteristics in the forward bias of the device at room temperature, shown in Fig. 4.4(b). From the LogI-LogV characteristics we observed that there was, three distinct regions. The bias voltage V < 0.25 represents region – I, where the slope is very close to 1 and the current varies almost linearly. So, the region is ohmic, and the quantum tunnelling is dominant over thermionic emission for charge transport mechanism. The bias voltage lying between 0.25V to 0.85V represents region- II, where the slope is larger than 2 and current varies exponentially. In this region charge transportation primarily depends on trap charge limited current with recombination tunnelling [34-36]. Bias voltage V > 0.85 represents region-III, where the slope value is less than 2 and the maximum charge transportation occurring due to space charge limited current (SCLC) [37].

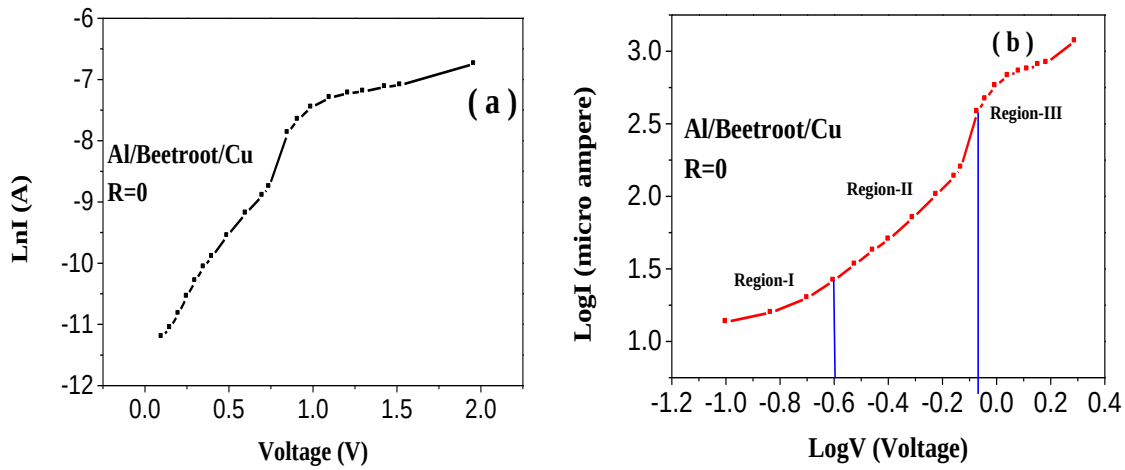

Fig. 4.4(a) Forward bias LogI-V characteristics and **4(b)** Forward bias LogI-LogV

The reverse saturation current for Al/Beetroot/Cu diode is 10.86 μA, determined from semi lnI-V graph. The value of zero bias barrier height for Al/Beetroot/Cu Schottky diode is 0.5 eV. From lnI-V characteristics demonstrated in Fig. 4.4(a), we found that at low forward bias the curve is linear, but at higher voltages the device characteristics deviates from linear behaviour. This non-linear behaviour is due to the presence of R_s, the effect of interface traps distribution and the semiconducting behaviour of the dye [38]. For a greater effect of series resistance Rs, the curve of the non-linear region of forward bias I-V will be large [38]. The variation of junction resistance R_j with the bias voltage shown in Fig. 4.6. From this curve we found that the value of Rs is 1.46 KΩ. Again, we have determined the electronic parameters of this device using Cheung and Cheung method. According to this method we have calculated series resistance, n and ϕ by the given equations

$$dV/dlnI = n(kT/q) + IR_S \qquad (4.4)$$

$$\text{and } H(I) = V - (nkT/q)\ln(I/AA^{*}T^{2}) = IR_S + n\phi \qquad (4.5)$$

The values of n and R_s are found from the graph dV/dlnI vs I shown in Fig. 4.5(b). Using this graph we have found that n = 4.5 and R_s = 1.10 KΩ. Again, using equation 4.5 measured value of ϕ and R_S is 0.75 eV and 1.087 KΩ. Table 4.1 demonstrates that the measured values of series resistances in three distinct approaches are quite near to each other, however the values of ideality factors differ. The existence of high R_s and high interface state density is demonstrated by this disparity.

4.3.3 Temperature dependent I-V

Fig. 4.7 shows the temperature dependent I-V of Al /Beetroot /Cu. There is a more shift in I-V characteristics at high voltages but a decrease in temperature. In Fig. 4.7 all the I-V characteristics shows a non-linear temperature dependence. Which shows an increasing conductivity with increasing temperature. The experimental values of n, φ and R_s for natural dye-based Al /Beetroot /Cu Schottky diode are displayed in Table 4.2.

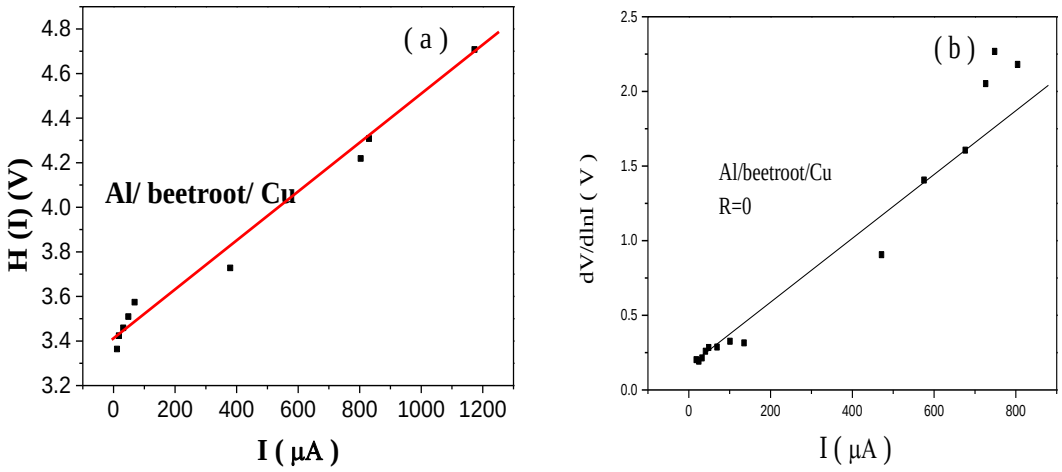

Fig . 4.5. (a) H (I) vs I plot of Al/ beetroot/ Cu at room temperature and (b) shows dV/dlnI vs I plot

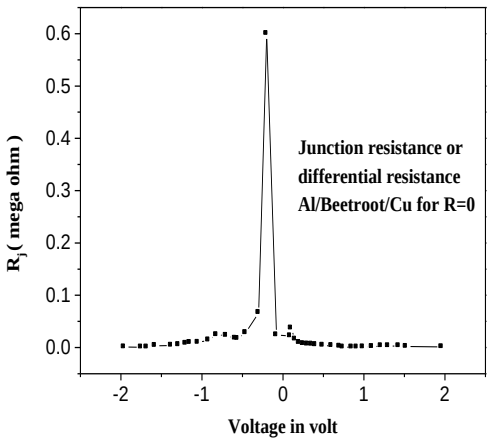

Fig. 4.6 Variation of R_j with voltage.

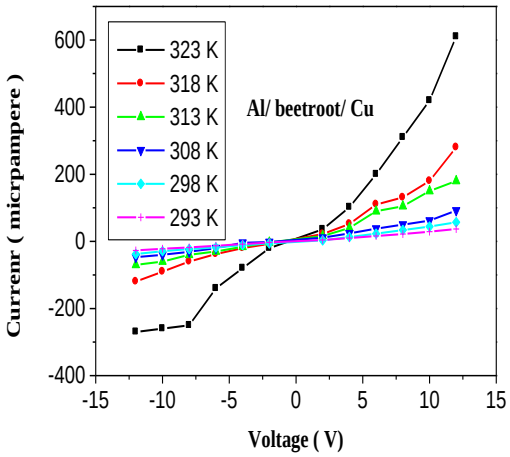

Fig. 4.7 Temperature dependent I-V characteristics of Al/ Beetroot/ Cu.

Table 4.1 The calculated electrical parameters of Al/Beetroot/Cu in two different methods.

Method	Barrier height(ϕ)	Series Resistance(Rs)	Ideality factor(n)
I-V Experimental	0.73 eV	1.46 KΩ	9.5
dV/dlnI vs I		1.10 KΩ	4.5
H (I) vs I	0.751 eV	1.087 KΩ	

Table 4.2 Temperature dependent electrical parameters of Al /Beetroot /Cu.

Temperature (K)	Barrier height(ϕ) eV	Series Resistance (Rs) KΩ	Ideality factor(n) from I-V
293	0.22	333	15.1
298	0.25	173	12.1
308	0.41	80	9.1
313	0.57	45	8.7
318	0.61	27	8.4
323	0.72	10.53	7.1

Here we found that n, ϕ, and Rs all have a strong temperature dependency, where n decreases with increasing temperature but ϕ increases. The series resistance also decreases with increasing temperatures. From this temperature dependency, we may say that in this device, the current transportation will be mostly dependent on the flow of charge through the lower barrier height and a larger ideality factor due to the temperature activated process [40]. Due to increasing temperature and bias voltages, the barrier height will be increased and, due to the high temperature, a large number of electrons will have gained sufficient energy to overcome the higher barrier heights. In this device, the presence of the beetroot (natural dye) affects the current conduction through the electrode-organic layer junction.

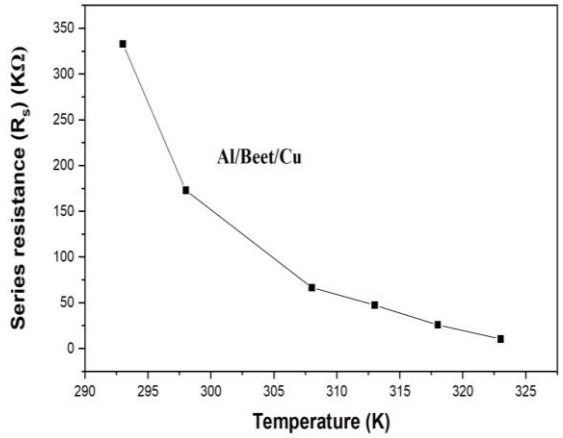

Fig. 4.8 Temperature dependence of R_s.

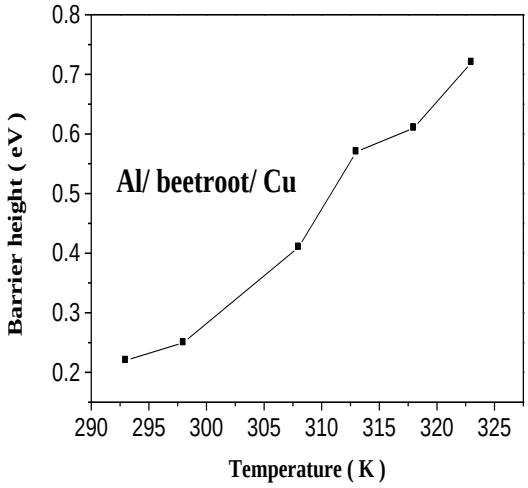

Fig. 4.9 Temperature dependence of ϕ.

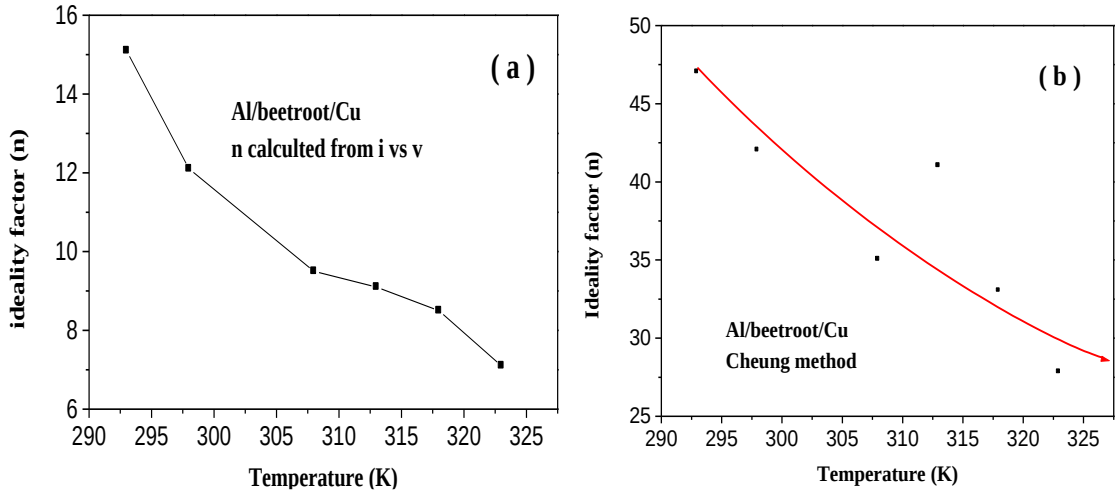

Fig.4.10 Temperature dependence of ideality factor of Al/ Beetroot/ Cu.

4.3.4 Semiconducting behaviour of beet root (Betanin)

The characteristic absorption spectra of betanin were measured in reference with ethanol, using Shimazu UV-2400 Pc series spectrometers across a wavelength range 200-800 nm [41]. Betanin was extracted from beetroot, then it is used for absorption spectra. The peak absorbance for the beet root was observed at 535 nm shown in Fig. 4.11. The band gap between HOMO and LUMO energy levels was calculated from absorption spectra is 2.31 eV [42]. Again, the band gap value of betanin was verified by DFT (density function theory) simulation using Gaussian 09. From DFT simulations we found the energy levels of the molecular orbital,

charge distributions on the molecule and dipole moment of the molecule. The band gap between HOMO and LUMO of betanin was found from DFT simulation is 2.1 eV [43]. Temperature varying, I-V shows that current increases with temp means, increase in conductivity with increasing temperature. Once more we observed that R_s decreases with increasing temperature in Fig. 8., and temperature variation of n and φ in Fig. 9-10 shows that the dye (red beet root) behaves like a semiconductor. The energy band gap is 2.1 eV, which is less than the band gap of TiO_2 (3.2 eV) and the presence of conjugated covalent bond in the molecular structure of betanin confirms the beetroot dye molecule behaves like a semiconductor. Moreover, we observed that for a Schottky diode the φ vs 1/n graph is linear in nature [44]. In Fig. 4.12(a) the graph shows a linear relation between φ and 1/n which confirms the device is a Schottky diode [44].

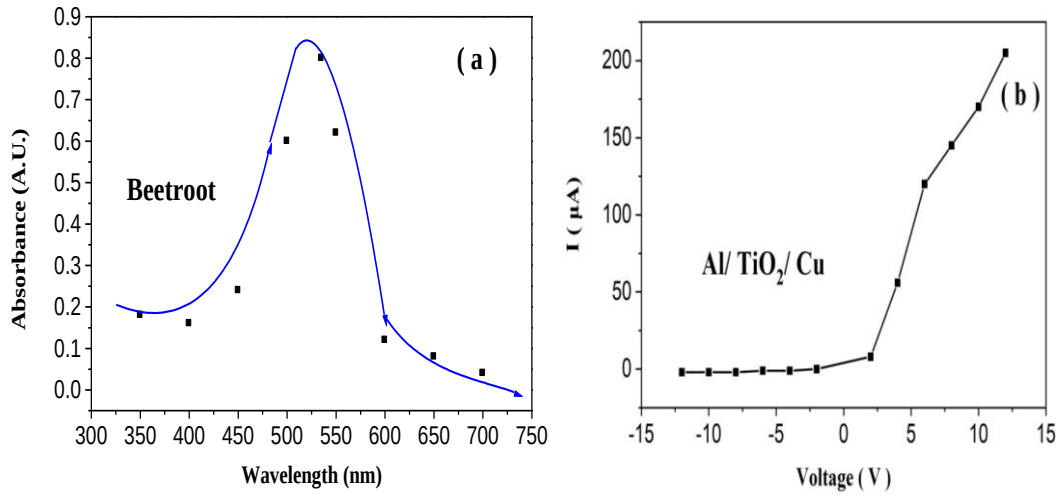

Fig. 4.11 (a) Absorption spectrum of beetroot and (b) dark I-V of Al/ TiO_2/ Cu

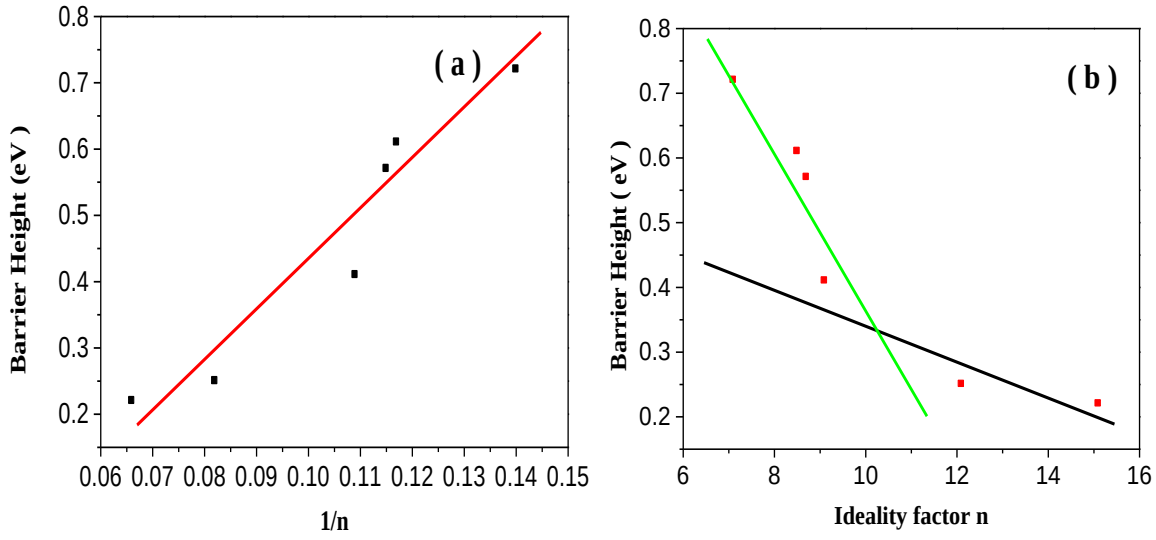

Fig. 4.12 (a) Represents ϕ vs 1/n and **(b)** plot of ϕ vs n for the Al/beetroot/Cu junction.

4.3.5 Comparative study

Table 3 shows a comparative study between previously reported some Schottky diodes and our fabricated diode. We observed that the values of n, R_s and ϕ are comparable with some previously reported Schottky diode, even better n and R_s values than organic Schottky, Al/L5 HZ-doped Schottky and p-si/TiO_2/Al Schottky. From table 3 we have conducted a comparative study between our fabricated three natural dye base Schottky diodes. We have got the electrical parameters of Al/Indigo/Cu and Al/Turmeric/Cu our previous work [45]. According to the comparison analysis, when we use beetroot dye instead of indigo dye, the values of n and R_s drop from 11.65 to 4.5 and 430 KΩ to 1.1 KΩ, respectively. From this comparison table it is noted that Al/Beetroot/Cu has the lowest ideality factor and series resistance. In our knowledge the indigo molecule is asymmetric and the dipole moment is 0.0053 D, which is very negligible. On the other hand, the dipole moment of curcumin and betanin molecules are 5.7D and 8.689D respectively [46]. Due to negligible magnetic moment of indigo, there is a weak interaction with electrodes and charge transfer rate is slow. But for curcumin and betanin, there is a significant value of dipole moment indicating strong interaction with electrodes and charge transfer rate is high. Because of this current density is higher and series resistance is lower for Al/Beetroot/Cu. Therefore, we have got better electrical parameters for Al/Beetroot/Cu than any other natural dye based organic Schottky diodes.

Table 4.3 Comparison of proposed Al/Beetroot/Cu diode with some previously reported Schottky diodes and natural dye based Schottky

Schottky	n	R_s	Φ (eV)	I_0 (μA)
Organic Schottky [23-28]	2-11			
Al/L5 HZ-doped Schottky [22]	42.9, 18.8, 20	$3x10^6$, $2x10^7$, $1.2x10^7$Ω	0.78, 0.81, 0.75	
Au/DNA/ITO [46]	1.4 to 8.9	0.12 MΩ to 1.6 MΩ		
p-si/TiO_2/Al [21]	8.9			
Al/Indigo/Cu	11.65	0.43 MΩ	0.8	0.69
Al/Turmeric/Cu	6.56	8 KΩ	0.738	8
Al/Beetroot/Cu [this work]	4.5	1.1 KΩ	0.732	10.13
Al/TiO_2/Cu [this work]	3.75	198 K Ω	0.76	3.04

4.3.6 Schottky emission (SE) and Poole-Frenkle emission (PFE)

From figure 2(a) and 2(b) we observed that the reverse current characteristics of Al/Beetroot/Cu are unsaturated. The reverse current of the all the herbal dye based thin film diodes increase with increasing reverse bias. In this paper we investigate the current conduction mechanism in the reverse bias of Al/Beetroot/Cu, Al/Turmeric/cu, Al/Indigo/Cu and Al/TiO_2/Cu diodes using Poole-Frenkle emission (PFE) and Schottky emission (SE) models. We know the reverse current in PFE model is given by

$$I_R = I_o \exp(\beta_{PF} V^{1/2} / kTd^{1/2}) \qquad (4.6)$$

and the current dominant by Schottky lowering is given by

$$I_R = AA^*T^2 I_o \exp(-\phi / kT)\exp(\beta_{SE} V^{1/2} / kTd^{1/2}) \text{ [47, 48]} \qquad (4.7)$$

where β_{PF} and β_{SE} are PFE and SE field lowering coefficients respectively. The theoretical value of β_{PF} and β_{SE} is to be determined by the relation

$$\beta_{PF} = 2\beta_{SE} = (q^3/\pi\varepsilon_0\varepsilon_r)^{1/2} \qquad (4.8)$$

Using this equation the theoretical values and experimental values β for all the natural dye based thin film diodes are shown in table 4. We observed from the table 4 that the values for Al/Beetroot/Cu are $\beta_{PF} = 4.5x10^{-5}$ $eVm^{1/2}V^{-1/2}$ and $\beta_{SE} = 2.25x10^{-5}$ $eVm^{1/2}V^{-1/2}$. The experimental value of β is determined from the slope of the plot of ln (I_R) vs $V_R^{1/2}$ shown in

Fig. 4.13(a). The experimental value of β for Al/Beetroot/Cu is $3.07x10^{-5}$. Here we observed that the experimentally calculated value of β for Al/Beetroot/Cu is closer to the theoretical value of β_{SE}, which concludes that Schottky emission is more dominant over PFE in the reverse bias. From the table 4.5. we observed that for Al/Turmeric/Cu SE is more dominated over PFE among all the diodes and we also observed that for Al/Indigo/Cu the value of β is away from both the values of β_{PF} and β_{SE}, so in this diode SE and PFE both of this mechanism have similar contribution in reverse current conduction. Fig. 4.13(b) depicts the ln (I_R) vs $V_R^{1/2}$ for Al/Beetroot/Cu at various temperatures, which are not perfectly linear due to the high ideality factor of organic devices with high series resistance, interface states, and trap energy. From table 4.5. we observed that at high temperature the value of β for Al/Beetroot/Cu is closer to β_{SE}. Which confirms at high temperature SE dominant PFE, where the carriers absorb thermal energy and then emitted over the potential barrier at Al/beetroot junction. Because of this we observed that the 'n' values decrease with increasing temperature. At very low temperature in reverse bias PFE dominant SE due to donor-like trap, and thermal de-trapping of a carrier from bulk layer to conduction band. Because of this, it is entitled bulk limited conduction current [49, 50]. In this bulk limited region current transportation is due to the defect states. We present the ϕ vs. n graph in Fig. 4.12(b). In this diagram, there are two different linear zones with varying slopes. This study demonstrates the existence of two different current conduction processes corresponding to two different temperature ranges. This also suggests that the Gaussian distribution model could be useful [51-54].

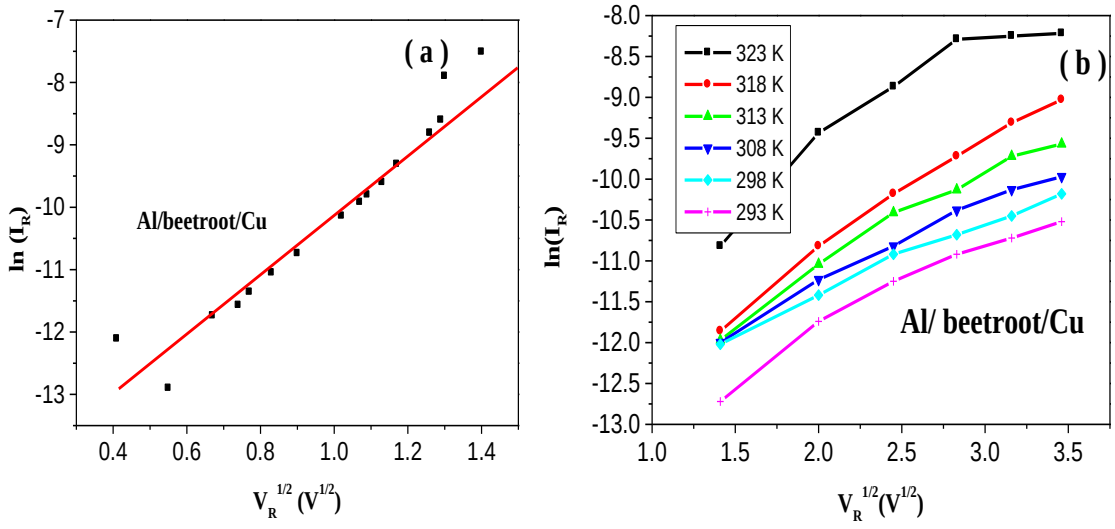

Fig. 4.13 (a) Plot of ln(I_R) vs $V_R^{1/2}$ for Al/Beetroot/Cu thin film diode at room temperature **(b)** Plot of ln(I_R) vs $V_R^{1/2}$ for Al/beetroot/Cu thin film diode at different temperatures

Table 4.4 Represents the comparison of theoretical and experimental value of β for three natural dye based thin film diode.

Thin film diode	Experimental β ($eVm^{1/2} V^{-1/2}$)	Theoretical β_{SE} ($eVm^{1/2} V^{-1/2}$)	Theoretical β_{PFE} ($eVm^{1/2} V^{-1/2}$)
Al/Beetroot/Cu	$3.069x10^{-5}$	$2.25x10^{-5}$	$4.5x10^{-5}$
Al/Indigo/Cu	$0.45x10^{-5}$	$1.825x10^{-5}$	$3.65x10^{-5}$
Al/Turmeric/Cu	$0.52x10^{-5}$	$0.514x10^{-5}$	$1.013x10^{-5}$

Table 4.5 Represents temperature dependence of β for Al/Beetroot/Cu

Temperature (K)	293	298	308	313	318	323
β ($eVm^{1/2} V^{-1/2}$)	$0.59x10^{-5}$	$0.53x10^{-5}$	$0.65x10^{-5}$	$0.71x10^{-5}$	$0.78x10^{-5}$	$0.89x10^{-5}$

4.3.7 Insulating behaviour of the organic semiconductors

To adequately explain the insulating behaviour of the organic semiconductors, we have properly introduced a theoretical analysis. In this study we carefully consider a temperature called insulating temperature and symbolise as T_i (K) such that, below this temperature any organic semiconductor material behaves like an insulator and above this temperature the material is a semiconductor. We think this insulating temperature (T_i) is proportional with energy band gap (E_g) of the material that means

$$T_i \propto E_g \qquad (4.9)$$

Using this equation, we have measured the insulating temperatures for Al/Turmeric/Cu, Al/Indigo/Cu and Al/Beetroot/Cu diodes.

To measure these temperatures, we have used V_2O_5 and Ge as references. We found that V_2O_5 shows insulating behaviour at 150 K [50] and we theoretically predict this temperature for Ge

is 38 K. Using these two references the calculated insulating temperatures (T_i) are shown in table 6. This table shows the measured insulating temperatures with respect to two references are extremely close to each other, which confirms our theoretical assumption. We observed that conductivity of the diodes decreases with decreasing temperature and below a certain temperature the diodes shows insulating behaviour. The corresponding temperatures for Al/Turmeric/Cu, Al/Indigo/Cu and Al/Beetroot/Cu diodes are 170 K, 144 K and 133 K respectively. When temperature is below 133 K this device shows insulating behaviour. Hence, we can say that, when temperature of the device is low enough then thermal energy of electrons is extremely small, these low energy electrons can travel from Al to Cu through beetroot dye by quantum tunnelling and the limited amount of current is due to the quantum tunnelling only, but for a high enough temperature thermal energy of electrons is high enough then current conduction mechanism depends on both the process of the quantum tunnelling and thermionic emission. Fig. 4.14 shows the variation of conductance with applied bias. This nearly parabolic behaviour of conductivity of the device confirms there is quantum tunnelling mechanism takes an important role with thermionic emission in this device.

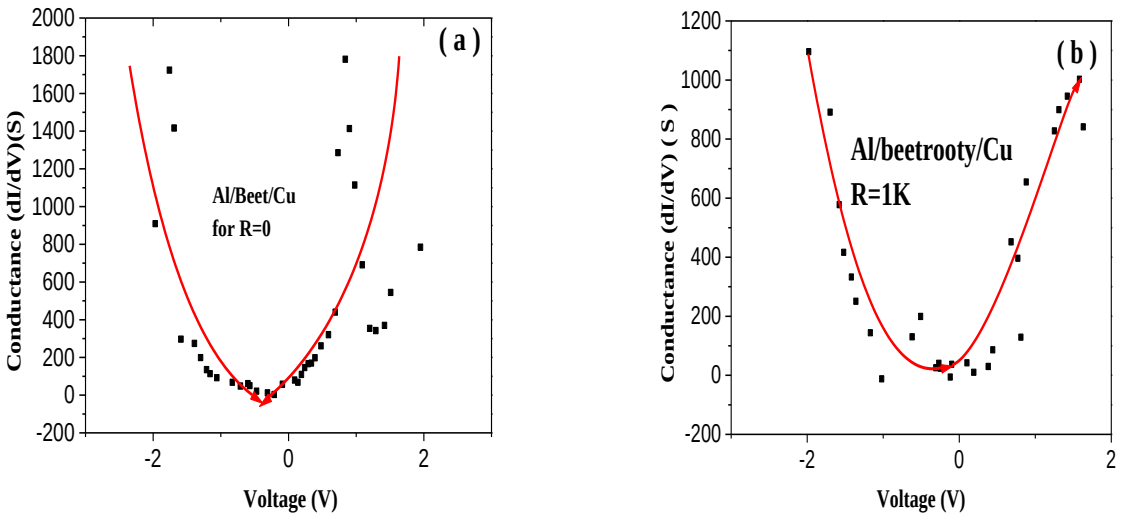

Fig.4.14 Represents the variation of conductivity with bias voltage.

Table 4.6 Represents the insulating temperatures (T_i) for natural dye based organic semiconductors

Reference	Curcumin (Turmeric 2.95 eV)	Indigo (2.5 eV)	Betanin (Beetroot 2.3 eV)
Measured T_i w.r.t V_2O_5 (2.6 eV)	170.2 K	144.2 k	132.7 K
Measured T_i w.r.t Ge (0.67 eV)	167.3 K	141.8 K	130.45 K

4.3.8 Trap energy

G(V) vs V characteristics have been used to analyse the trap assisted current conduction. Here is the equation

$$G(V) = (d \log I)/(d \log V) \qquad (4.10)$$

Above the built-in voltage, G(V) forms a strong peak to present the change from exponentially growing current flow to comparably slower power law dependency. Trap filling states are depicted by the peak in the diagram. As a result, the G(V) vs V plot in Fig. 4.15 focuses on the trap signature, making it very simple to understand the nature of the traps. In trap-free devices, the function G(V) should decline monotonically, however in the aforementioned plot, there is a notable amount of distortion at various voltage regimes, indicating the presence of trapping states in the device. We have calculated trap energy from the ln I - ln V plot of Al/Beetroot/Cu diode which shown in Fig. 4.16. The trap charge concentration N_t can be expressed as

$$N_t(\varepsilon) = N_0 exp[-\varepsilon / kT] \qquad (4.11)$$

where ε is depth of traps below conduction band mobility edge and T_c is the temperature of trap distribution (i.e., $T_c = E_c / k$, where E_c is the characteristic trap energy). $m = T_c / T$, where T is the room temperature. We have calculated the trap energy using the equation which can be expressed as [56]

$$E_c = mkT \qquad (4.12)$$

Trap energy E_c can be measured from the value of m, which can be estimated from ln I- ln V plot of Al/Beetroot/Cu organic Schottky diode. When beetroot dye is substituted for indigo dye, the values of E_c and ϕ drop from 0.073 eV to 0.021 eV and 0.87 eV to 0.732 eV, respectively. The values of E_c and ϕ of some metal-organic semiconductor junction Schottky

diodes are shown in table 4.7. From this table we observed that the values of R_s, E_c and ϕ for Al/Beetroot/Cu show promising results in compared to our previously reported organic dye-based diodes [45, 57-60]. When we use beetroot dye then there is a significant reduction in R_s, E_c and ϕ. So, our fabricated Al/Beetroot/Cu organic device possess vast possibilities in optoelectronic application.

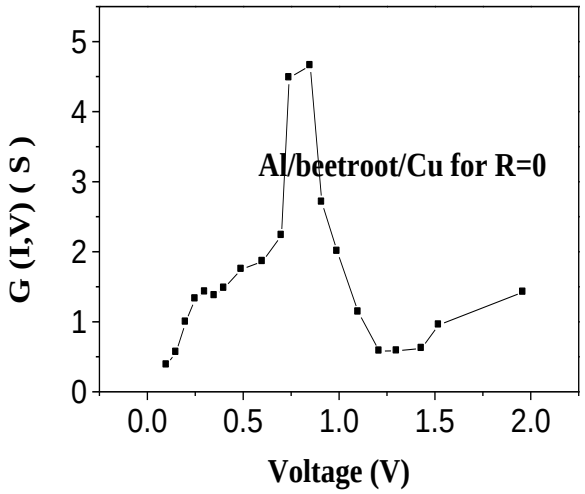

Fig. 4.15. G(V) vs V plot of Al/Beetroot/Cu.

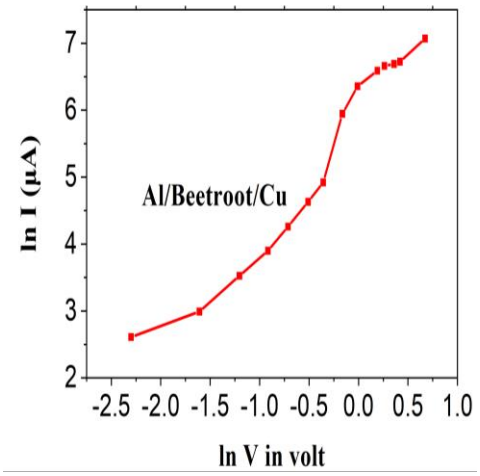

Fig. 4.16. ln I-ln V plot of Al/Beetroot/Cu.

Table 4.7 Values of trap energy and barrier height for different dyes used in organic Schottky device.

Device and used dye	Trap energy (E_c) in eV	Barrier height from I-V in eV	Series resistance (s) in kΩ
ITO/CV/Al [52]	0.044	0.80	
ITO/CV/Al-M [52]	0.034	0.77	
Al/Turmeric/Cu [53]	0.028	0.825	
Al/Indigo/Cu[45]	0.073	0.87	127
ITO/RB/Al-M [55]	0.086	0.95	202
ITO/MR/Al-M[55]	0.076	0.99	439
Al/Beetroot/Cu [this work]	0.021	0.732	1.1 and 1.46

Conclusions

The electronic properties of the Al/Beetroot/Cu device have been investigated in the temperature range of 293-323K by means of current-voltage (I-V) measurement. The average experimental values of ideality factor, series resistance, and ϕ have been calculated to be about 4.5, 1.10 K, and 0.73 eV, respectively, from forward bias current-voltage characteristics. Also in this study, we used Cheung's functions to calculate n and R_s of an Al/Beetroot/Cu device, and the values are in good agreement with each other. The fascinating result obtained in this work is that the series resistance decreases with the increase in temperature, and ϕ increases with temperature. The band gap of the betanin molecule present in beetroot is 2.1 eV. These findings indicate that the betanin molecule is a semiconductor with a band gap lower than TiO_2, and the linear behaviour of the vs 1/n graph confirms the device is a Schottky diode. Moreover, we found that the reverse leakage current is dominated by SE over PFE, and from the temperature dependent I-V, the values of β are noticeably closer to β_{SE} than β_{PFE}. At 140 K, the dye behaves like an insulator and the quantum tunnelling effect dominates over the thermionic emission. On the other hand, at room temperature, the dye behaves like a semiconductor and thermionic emission dominates quantum tunnelling. As a result, at room temperature and higher, the device could be a Schottky diode. The G(V) vs V plot was used to explain the existence of the dye's trapping effect. There is a significant reduction in R_s, E_c, and ϕ that has been gained in the use of beetroot dye over some previously reported organic dyes. As a result, we may conclude that Al/Beetroot/Cu exhibits significantly better electrical properties than herbal dye-based organic diodes.

4.5 References

1. Maeda T, Takagi S, Ohnishi T, Lippmaa M. Sulfur passivation of Ge (0 0 1) surfaces and its effects on Schottky barrier contact. Materials science in semiconductor processing. 2006 Aug 1;9(4-5):706-10.
2. Aydoğan Ş, Çınar K, Asıl H, Coşkun C, Türüt A. Electrical characterization of Au/n-ZnO Schottky contacts on n-Si. Journal of Alloys and Compounds.2009May12;476(1-2):913-8.
3. Shah M,. Sayyad M.H,. Karimov Kh.S , Tahir M.M. Optoel. Adv. Mater. Rapid Comm. OAM-RC 3 (2009) 831.
4. Shah M, Sayyad MH, Karimov KS, Maroof-Tahir M. Investigation of the electrical properties of a surface-type Al/NiPc/Ag Schottky diode using I–V and C–V characteristics. Physica B: Condensed Matter. 2010 Feb 15;405(4):1188-92.
5. Aydoğan Ş, İncekara Ü, Deniz AR, Türüt A. Extraction of electronic parameters of Schottky diode based on organic Orcein. Microelectronic Engineering. 2010Dec 1;87(12):2525-30.
6. Park JS, Lee BR, Lee JM, Kim JS, Kim SO, Song MH. Efficient hybrid organic-inorganic light emitting diodes with self-assembled dipole molecule deposited metal oxides. Applied Physics Letters. 2010 Jun 14;96(24).
7. Güllü Ö, Asubay S, Biber M, Kiliçoglu T, Türüt AB. Electrical properties of safranine T/p-Si organic/inorganic semiconductor devices. The European Physical Journal-Applied Physics. 2010 Apr;50(1):10401.
8. Yakuphanoglu F. Determination of electronic properties of Al/p-Si/composite organic semiconductor (MIOS) junction barrier by current–voltage and capacitance–voltage methods. Synthetic metals. 2008 Feb 1;158(3-4):108-12.
9. Shah M, Karimov KS, Ahmad Z, Sayyad MH. Electrical characteristics of A1/CNT/NiPc/PEPC/Ag surface-type cell. Chinese Physics Letters. 2010 Oct 1;27(10):106102.
10. Okur S, Yakuphanoglu F, Ozsoz M, Kadayifcilar PK. Electrical and interface properties of Au/DNA/n-Si organic-on-inorganic structures. Microelectronic engineering. 2009 Nov 1;86(11):2305-11.
11. Shah M, Sayyad MH, Karimov KS, Wahab F. Electrical characterization of the ITO/NiPc/PEDOT: PSS junction diode. Journal of Physics D: Applied Physics. 2010 Sep 21;43(40):405104.
12. Yakuphanoglu F. Controlling of silicon–insulator–metal junction by organic semiconductor polymer thin film. Synthetic metals. 2010 Jul 1;160(13-14):1551-5.

13. Yakuphanoglu F. Photovoltaic properties of the organic–inorganic photodiode based on polymer and fullerene blend for optical sensors. Sensors and Actuators A: Physical. 2008 Feb 15;141(2):383-9.
14. Yakuphanoglu F, Kandaz M, Senkal BF. Inorganic–organic photodiodes based on polyaniline doped boric acid and polyaniline doped boric acid: nickel (II) phthalocyanine composite. Sensors and Actuators A: Physical. 2009 Aug 3;153(2):191-6.
15. Rad S, Sharbati MT, Behrouz S, Nekoei AR. Fabrication of non-doped red organic light emitting diode using naturally occurring Curcumin as a donor-acceptor-donor (DAD) emitting layer with very low turn-on voltage. Iranian Journal of Science. 2015 Sep 6;39(3):297-304.
16. Bouzidi A, Yahia IS, El-Sadek MS. Novel and highly stable indigo (CI Vat Blue I) organic semiconductor dye: Crystal structure, optically diffused reflectance and the electrical conductivity/dielectric behaviors. Dyes and Pigments. 2017 Nov 1;146:66-72.
17. Dakhel AA, Cassidy S, Jasim KE, Henari FZ. Synthesis and characterisation of curcumin–M (M= B, Fe and Cu) films grown on p-Si substrate for dielectric applications. Microelectronics Reliability. 2015 Feb 1;55(2):367-73.
18. Usha P, Kumar S. Study on dielectric properties of fresh vegetables and jamun. InIOP Conference Series: Materials Science and Engineering 2017 Aug 1 (Vol. 225, No. 1, p. 012287). IOP Publishing.
19. Maraghechi A. Foroughi-Abari, K. Cadien, and AY Elezzabi. Appl. Phys. Lett. 2012;100:113503.
20. Weerakkody AD, Sedghi N, Mitrovic IZ, Van Zalinge H, Noureddine IN, Hall S, Wrench JS, Chalker PR, Phillips LJ, Treharne R, Durose K. Enhanced low voltage nonlinearity in resonant tunneling metal–insulator–insulator–metal nanostructures. Microelectronic Engineering. 2015 Nov 1;147:298-301.
21. Taşdemir İH, Vural Ö, Dökme İ. Electrical characteristics of p-Si/TiO2/Al and p-Si/TiO2-Zr/Al Schottky devices. Philosophical Magazine. 2016 Jun 2;96(16):1684-93.
22. Olyaee HG, Foot PJ, Montgomery V. Electrical properties and I–V characteristics of 5, 14-dihydro-5, 7, 12, 14-tetraazapentacene doped Schottky barrier diode. Journal of Theoretical and Applied Physics. 2015 Dec;9:315-9.
23. Kanicki J. METAL-POLYACETYLENE SCHOTTKY BARRIER DIODES. Molecular crystals and liquid crystals. 1983 Mar 1.
24. Grant PM, Tani T, Gill WD, Krounbi M, Clarke TC. Properties of metal/polyacetylene Schottky barriers. Journal of Applied Physics. 1981 Feb 1;52(2):869-72.

25. Turut A, Köleli F. Semiconductive polymer-based Schottky diode. Journal of applied physics. 1992 Jul 15;72(2):818-9.
26. Nazarova IB, Krinichnyi VI, Goldenberg LM. Schottky diodes based on poly (p-phenylene) and poly (1, 4-dipyrrolobenzene). Synthetic metals. 1993 Feb 1;53(3):399-402.
27. Misra SC, Chandra S. Electronic applications of semiconducting polymers. J.Chem.33A (1994) 583.
28. Chen SA, Fang Y, Lee HT. Polyacrylic acid-doped polyaniline as p-type semiconductor in Schottky barrier electronic device. Synthetic metals. 1993 Apr 12;57(1):4082-6.
29. Fowler RH, Nordheim L. Electron emission in intense electric fields. Proceedings of the Royal Society of London. Series A, Containing Papers of a Mathematical and Physical Character. 1928 May 1;119(781):173-81.
30. Slovick BA, Bean JA, Krenz PM, Boreman GD. Directional control of infrared antenna-coupled tunnel diodes. Optics express. 2010 Sep 27;18(20):20960-7.
31. Bareib M, Tiwari BN, Hochmeister A, Jegert G, Zschieschang U, Klauk H, Fabel B, Scarpa G, Koblmuller G, Bernstein GH, Porod W. Nano antenna array for terahertz detection. IEEE Transactions on Microwave Theory and Techniques. 2011 Jul 21;59(10):2751-7.
32. Bareiß M, Ante F, Kälblein D, Jegert G, Jirauschek C, Scarpa G, Fabel B, Nelson EM, Timp G, Zschieschang U, Klauk H. High-yield transfer printing of metal–insulator–metal nanodiodes. ACS nano. 2012 Mar 27;6(3):2853-9.
33. Rhoderick E H, Metal-semiconductors contacts. Oxford University Press, Oxford (1978).
34. Koteeswara Reddy N, Ahsanulhaq Q, Kim JH, Hahn YB. Behavior of n-ZnO nanorods/p-Si heterojunction devices at higher temperatures. Applied Physics Letters. 2008 Jan 28;92(4).
35. Klason P, Nur O, Willander M. Electrical characteristics and stability of gold and palladium Schottky contacts on ZnO nanorods. Nanotechnology. 2008 Oct 29;19(47):475202.
36. Kim DC, Han WS, Cho HK, Kong BH, Kim HS. Multidimensional ZnO light-emitting diode structures grown by metal organic chemical vapor deposition on p-Si. Applied Physics Letters. 2007 Dec 3;91(23).
37. Tataroglu AD, Buyukbas Ulusan A, Altındal Ş, Azizian-Kalandaragh YA. A compare study on electrical properties of MS diodes with and without CoFe 2 O 4-PVP interlayer. Journal of Inorganic and Organometallic Polymers and Materials. 2021 Apr;31:1668-75.
38. Aydoğan Ş, Sağlam M, Türüt A. Some electrical properties of polyaniline/p-Si/Al structure at 300 K and 77 K temperatures. Microelectronic Engineering. 2008 Feb 1;85(2):278-83.

39. Turut A, Saglam M, Efeoglu H, Yalcin N, Yildirim M, Abay B. Interpreting the nonideal reverse bias CV characteristics and importance of the dependence of Schottky barrier height on applied voltage. Physica B: Condensed Matter. 1995 Jan 2;205(1):41-50.
40. Schmitsdorf, R.F., Kampen, T.U. and Mönch, W., 1997. Explanation of the linear correlation between barrier heights and ideality factors of real metal-semiconductor contacts by laterally nonuniform Schottky barriers. *Journal of Vacuum Science & Technology B: Microelectronics and Nanometer Structures Processing, Measurement, and Phenomena*, *15*(4), pp.1221-1226.
41. Sreeja S, Pesala B. Co-sensitization aided efficiency enhancement in betanin–chlorophyll solar cell. Materials for Renewable and Sustainable Energy. 2018 Nov;7(4):25.
42. Calogero G, Bartolotta A, Di Marco G, Di Carlo A, Bonaccorso F. Vegetable-based dye-sensitized solar cells. Chemical Society Reviews. 2015;44(10):3244-94.
43. Sreeja S, Pesala B. Co-sensitization aided efficiency enhancement in betanin–chlorophyll solar cell. Materials for Renewable and Sustainable Energy. 2018 Nov;7(4):25.
44. Mao LF. Physical origin of the temperature-dependent open-circuit voltage in solar cells. Applied Physics A. 2020 Jan;126(1):42.
45. Das AK, Mandal R, chakrabarty K, Mandal DK. IJIKC ISSN 7 (2019) 2454-2415.
46. Sreeja S, Pesala B. Performance enhancement of betanin solar cells co-sensitized with indigo and lawsone: A Comparative Study. ACS omega. 2019 Nov 11;4(19):18023.
47. Kumar AA, Reddy VR, Janardhanam V, Yang HD, Yun HJ, Choi CJ. Electrical properties of Pt/n-type Ge Schottky contact with PEDOT: PSS interlayer. Journal of alloys and compounds. 2013 Feb 5;549:18-21.
48. Reddy VR, Manjunath V, Janardhanam V, Kil YH, Choi CJ. Electrical properties and current transport mechanisms of the Au/n-GaN Schottky structure with solution-processed high-k BaTiO3 interlayer. J. Electron. Mater. 2014 Sep 1;43(9):3499-507.
49. Rhoderick EH, Williams RH. Metal-semiconductor contacts. Oxford: Clarendon press; 1988 Sep.
50. Sze SM. Semiconductor Device Development in the 1970s and 1980s-A perspective. In1980 International Electron Devices Meeting 1980 Dec 8 (pp. 7-12). IEEE.
51. Arslan E, Badali Y, Aalizadeh M, Altındal Ş, Özbay E. Current transport properties of (Au/Ni)/HfAlO3/n-Si metal–insulator–semiconductor junction. Journal of Physics and Chemistry of Solids. 2021 Jan 1;148:109758.

52. Eroğlu A, Demirezen S, Azizian-Kalandaragh Y, Altındal Ş. A comparative study on the electrical properties and conduction mechanisms of Au/n-Si Schottky diodes with/without an organic interlayer. Journal of Materials Science: Materials in Electronics. 2020 Sep;31:14466-77.
53. Altındal Yerişkin S, Balbaşı M, Demirezen S. Temperature and voltage dependence of barrier height and ideality factor in Au/0.07 graphene-doped PVA/n-Si structures. Indian Journal of Physics. 2017 Apr;91:421-30.
54. Buyukbas-Ulusan A, Altındal-Yerişkin S, Tataroğlu AD. Forward and reverse bias current–voltage (I–V) characteristics in the metal–ferroelectric–semiconductor (Au/SrTiO3/n-Si) structures at room temperature. Journal of Materials Science: Materials in Electronics. 2018 Oct;29(19):16740-6.
55. Mahato S, Biswas D, Gerling LG, Voz C, Puigdollers J. Analysis of temperature dependent current-voltage and capacitance-voltage characteristics of an Au/V2O5/n-Si Schottky diode. AIP Advances. 2017 Aug 1;7(8).
56. Haldar A, Maity S, Manik NB. Effect of back electrode on photovoltaic properties of crystal-violet-dye-doped solid-state thin film. Ionics. 2008 Sep;14:427-32.
57. Sen S, Manik NB. Effect of back electrode on trap energy and interfacial barrier height of crystal violet dye-based organic device. Bulletin of Materials Science. 2020 Dec;43(1):60.
58. Chakraborty K, Das AK, Mandal R, Mandal DK, Transactions of Tianjin University 26 (2020) 265.
59. Chakraborty K, Das A, Mandal R, Mondal DK. Interpretation of trap-assisted conduction with estimation of electrical parameters of thin indigo film-based semiconducting device. Bulletin of Materials Science. 2021 Jun;44(2):92.
60. Chakraborty K, Chakraborty S, Manik NB. Effect of single walled carbon nanotubes on series resistance of Rose Bengal and Methyl Red dye-based organic photovoltaic device. Journal of Semiconductors. 2018 Sep 1;39(9):094001.

Chapter 5

A natural dye-based Schottky diode with observed quantum tunnelling and determined trap density, mobility, and excellent sensitivity and non-linearity

5.1 Introduction

The fundamentals of organic semiconductors and devices made using organic semiconductor diodes based on natural dyes were covered in the earlier chapters. The electrical characteristics of various MIM and Schottky diodes have been covered in [1-23]. The semiconducting behaviour of beetroot dye molecules and the charge transportation mechanism via a Schottky diode based on beetroot dye were covered in chapter 4. Excellent rectification parameters, such as asymmetry and sensitivity, are essential for any diode. We are aware of the highest reported rectification parameters such as, sensitivity 2.5A/W and asymmetry 10 at 3V for $Cr/Al_2O_3/HFO_2/Cr$ [24] and asymmetry 18 at 0.35V for Ta_2O_5/Al_2O_3 and Nb_2O_5/Al_2O_3 bi-layer MIIM devices [25]. Again, we know that for $Al/Al_2O_3/Ag$ MIM diode the rectification parameters are: sensitivity (f_{SENS})= 18 A/W, nonlinearity =12.5 and asymmetry (f_{ASYM})= 1.2 [26]. An essential factor in determining how well a MIM diode performs rectification is its sensitivity. Sensitivity is the diode's ability to detect weak signals. Any diode must have great sensitivity in order to correct high frequencies with tiny amplitudes without the use of an external voltage. Many studies have been conducted on MIM diodes with different metal work functions in an effort to create devices with higher sensitivity and nonlinearity at low turn-on voltage. The majority of the MIM diodes that have been previously described have lesser sensitivity and higher zero bias resistance. Therefore, additional research was necessary to improve the sensitivity with low zero bias resistance.

Here we have fabricated a natural dye based thin film diode where Al_2O_3 has been replaced by natural dye layer (betanin, curcumin and indigo) and Ag has been replaced by Cu. Under the same ambient conditions, we have fabricated another ($Al/TiO_2/Cu$) diode, and we have compared the rectifying parameters between these two diodes. We know that TiO_2 is the mostly used active layer for MIM and Schottky diode. This work compares all of the natural dye based Schottky diodes in order to experimentally confirm the observation of quantum tunnelling through the current conduction mechanism of a series of natural dye based Schottky diodes. For a single layer Al/Beet/Cu diode, we have found a superior low bias asymmetry of 18 at 0.85 V and the highest sensitivity of 25.7 A/W at 0.7 V, making the diode a good choice for high-speed optoelectronic use. Poisson's equation was used in this investigation to quantify the trap density, carrier density, and mobility of the active layer (beetroot dye). Again, we suggested a natural dye-based one-dimensional organic semiconductor Schottky diode. As shown in Fig. 14, a natural dye-based organic semiconductor in this configuration is covered by an oxide layer and only partially exposed at the one-dimensional edge.

5.2 Materials and Methods

For the experimental study of the natural dye based organic thin film, the following procedures have done to prepare the Al/Beet/Cu thin film diode.

5.2.1 Material

In this experiment, the insulating layer was made of TiO_2 and red beetroot paste. Actually, this crimson beetroot is the plant's taproot. Additionally, 99.9% pure ethanol and polyvinyl alcohol were employed here (PVA). We acquired ethanol from Changshu Hongsheng Fine Chemical Co,.Ltd. and PVA from Loba Chemie Pvt. Ltd. Here, the substrate is FTO-coated glass with a resistivity of 15 cm^{-2}, and the two electrodes are Al and Cu.

5.2.2 Preparation of the dye solution

We purchased raw beetroot root, cleaned it in distilled water, pilled and diced it and then rinsed it in ethanol. The ethanol-based beetroot root solution was made using 15ml of ethanol and 35ml of beetroot root juice. The primary component of red beetroot is betanin, whose chemical composition and IUPAC nomenclature [27-29] are depicted in Fig. 5.1. The solution was left at room temperature for 30 minutes on a magnetic stirrer. PVA was combined with twice-recrystallized beet root dye made from ethanol. The PVA utilized here has a molecular weight of 1,15,000 units. Initially, 20 ml of distilled water was added to 4 g of PVA in a beaker, and the mixture was stirred with a magnetic stirrer for 30 minutes at 700 C to create a thick, translucent gel-like PVA solution. This PVA solution has been combined with 6 ml of beet root-ethanol solution. Here PVA has been used as an inert blinder which has been stable the dye film.

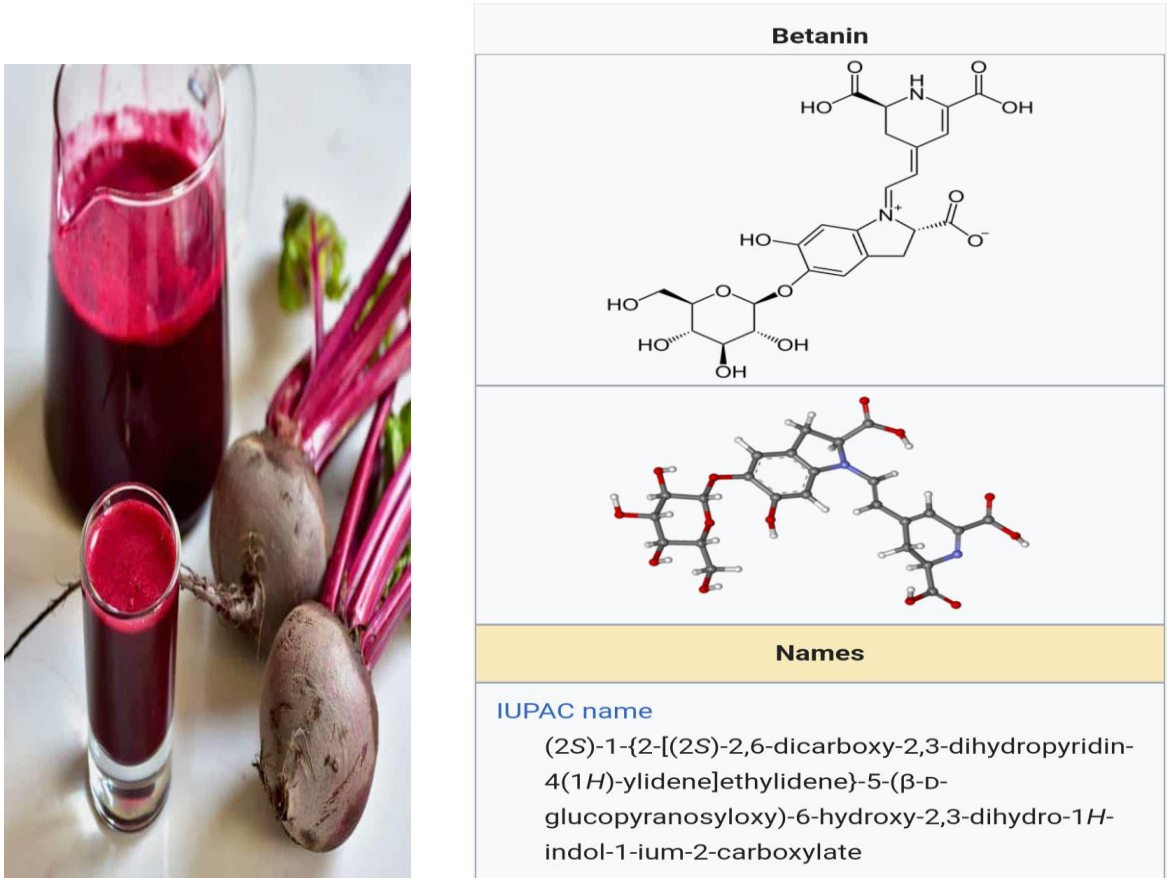

Fig. 5.1 Beetroot juice and chemical structure of betanin with its IUPAC name.

5.2.3 Fabrication of the device

The fabrication process is same to that used by A.K. Das et al. to produce Al, Beetroot, and Copper [1]. We select Al (4.20 eV) and Cu (5.10 eV) for the fabrication of the organic dye-based thin film diodes, resulting in a significant work function difference between the electrodes. In this investigation, the film developed on the FTO-coated glass was an insulating layer made of beetroot paste. The glass substrate was chemically cleaned with acetone prior to film development. Al and Cu wafers were treated in deionized water for a minute after being treated with HF: H_2O (1:10) solution to remove the oxide coatings from their surfaces. The thin film was produced, spun-coated onto a Cu substrate at 2000 rpm, and then dried for an hour at 50 ^{0}C to remove any remaining moisture. A 50 μm thin layer of beetroot root dye was applied here. The TiO_2 layer is roughly 50 μm thick, while the Al electrode is about 0.055 mm thick. Al is spin-coated with the same thin film, followed by the sandwiching of these two electrodes to create an Al/Beetroot/Cu diode. This Al/beet root/Cu gadget has now finished its 10-hour drying process. In the similar way Al/indigo/ Cu, Al/Turmeric/Cu and Al/ TiO_2/ Cu surface type Schottky diodes were fabricated and the experimental circuit shown in Fig. 5.2.

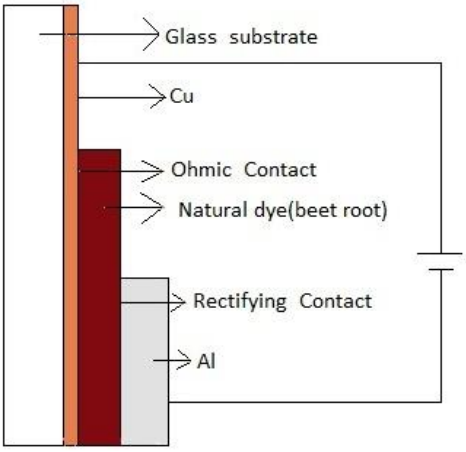

Fig. 5.2 Schematic representation of sandwich configuration of Al/ Beet root/ Cu thin film device

5.3 Results and discussion

5.3.1 Rectifying mechanism

Now we want to determine the rectifying characteristics of the natural dye-based Al/Beet/Cu diode and for this the I-V characteristics is derived and presented in Fig. 5.3. The I-V characteristic shows a strong rectifying behaviour. The f_{ASYM} increases with increasing bias, reaching a maximum value of 17.6 at 0.85 V, and then falls with increasing bias, as seen in Fig. 5.4.

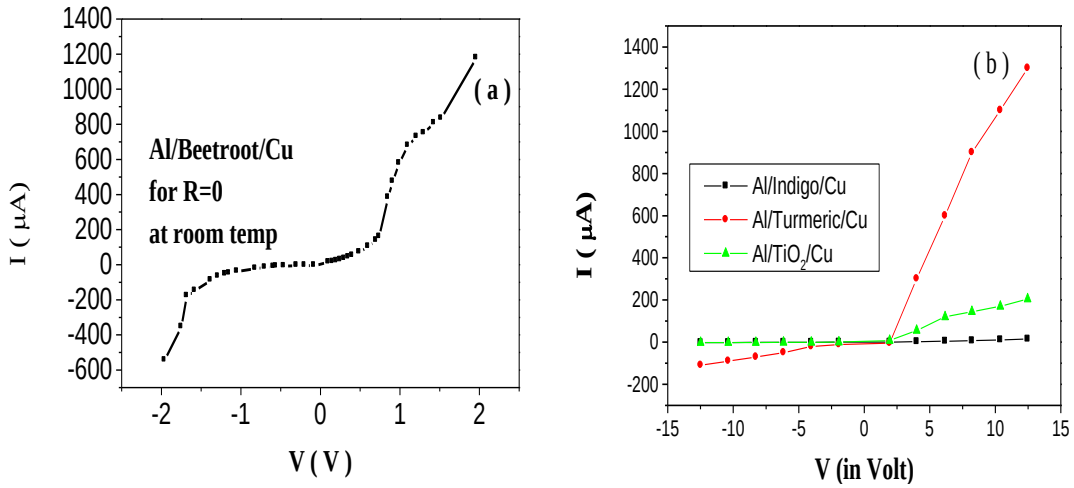

Fig. 5.3 (a) I-V characteristic of Al/Beet/Cu, adapted from A.K.Das et al [1] (b) I-V characteristics of another three MIM diodes

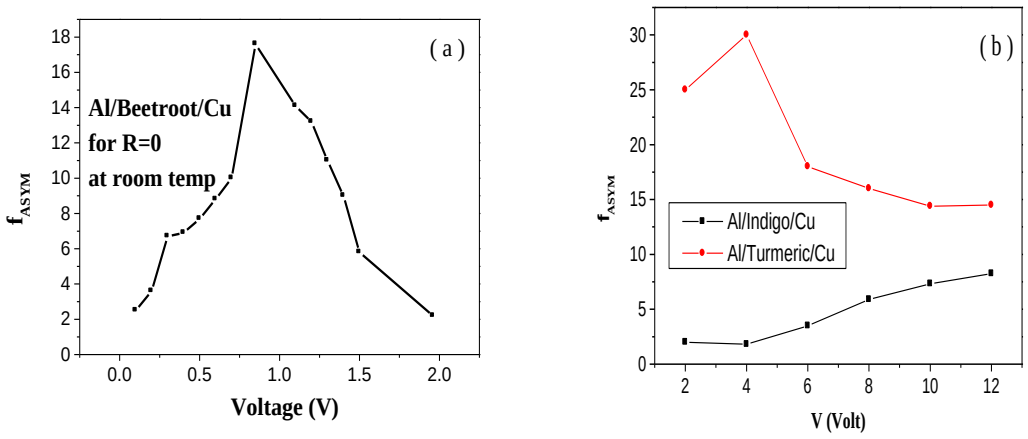

Fig. 5.4 (a) Device asymmetry with respect to bias voltage, adapted from A.K.Das et al [1]. (b) Asymmetry of indigo and turmeric based MIM diode.

Strong rectification behaviour is depicted in Fig. 5.3 and is defined by $f_{ASYM} = I_F/I_R$. Fig. 5.4 demonstrates that f_{ASYM} rises with rising biases, reaches a maximum value of 17.6 at 0.85 V, and subsequently falls with rising bias. We are aware that the forward bias voltage (V) and the tunnelling current (I) vary exponentially [30]. We also saw the same type of I-V characteristics in this MIM diode. So, when an AC voltage is given to the described device under an external bias, we may claim that the electron flux of the tunnelling current is to be modified with the change in polarity [31]. More electrons tunnel from the positively biased Al to the negatively biased Cu when a constant voltage is supplied to Al with respect to Cu and an alternating voltage is applied simultaneously. Hence, the Al/Beet/Cu MIM diode output has a DC voltage produced. The device's I-V relationship is exponential, which makes the rectifying ability of the diode more effective at higher voltages. We employed two metals (Al and Cu) with different work functions as electrodes in this device, and as a result, the I-V characteristics exhibit an asymmetric slope even though there is no bias applied to the diode [32]. In this diode, the barrier height for electrons is larger when tunnelling occurs from the metal of high work function (Cu) to the metal of low work function (Al), as opposed to the other way around. Direct current consequently flows from a metal with a low work function to a metal with a high work function [33].

5.3.2 Figure of Merits of the reported diode

Fig. 5.5 shows that the variation of differential resistance of the diode with respect to applied input bias. With the increasing applied bias, the differential resistance decreases. It is found that the maximum value of the resistance at zero bias is 23.3kΩ.

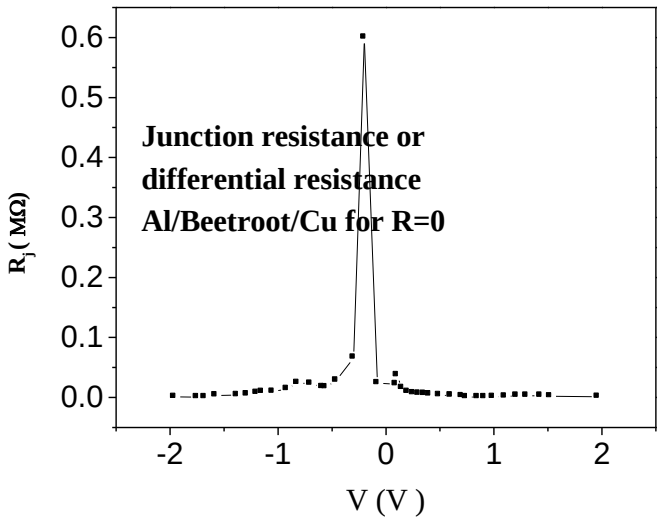

Fig. 5.5 Variation of R_j with applied bias [1].

For a better use of MIM diode in rectenna application, the zero-bias resistance of the MIM diode must be small or of the order of the resistance of the antenna [34]. For Al/Beet/Cu the calculated zero bias resistance is 23.3kΩ, which is smaller than previously reported $Al/Al_2O_3/Ag$ and $Al/Al_2O_3/Pt$ MIM diodes [26]. Fig. 5.8 shows the variation of conductance with bias voltage, which exhibits the higher value of forward bias as compared to the reverse bias. So, we may say that the natural dye based thin film behaves like a diode. We know that nonlinearity and sensitivity are two important parameters for any MIM diode. The mathematical representation of nonlinearity is given in equation (5.1) as follows;

$$f_{NL} = \frac{\frac{dI}{dV}}{\frac{I}{V}} \qquad (5.1)$$

So, the nonlinearity factor is defined as the ratio of dynamic to the static conductance. The sensitivity represents the relationship between the input ac signals with the output rectified current and is given in equation (5.2) as follows;

$$f_{SENS} = \frac{\frac{d^2I}{dV^2}}{\frac{dI}{dV}} \qquad (5.2)$$

In rectenna applications this sensitivity also known as responsivity or curvature coefficient which is defined by the ratio between outputs rectified voltage in response to the input power. This responsivity is given as in equation (5.3);

$$f_{RES} = f_{SENS}/2 \qquad (5.3)$$

Fig. 5.6 shows the variation of sensitivity (responsivity) and its maximum value is 25.1 A/W at 0.7V, and zero bias sensitivity is 5.47. The variation of nonlinearity with bias voltage is shown in Fig. 5.7. which shows that the maximum nonlinearity is 5.998 at 0.74 V. Again we observed that in reverse bias the maximum sensitivity is 19.38 at -1.58V and maximum nonlinearity is 13.35 at -1.68V, this is due to the sharp change in current in that region which we observed from the I vs V plot shown in Fig. 5.3.We know that for an ideal MIM diode, f_{NL}> 3 and f_{SENS}> 7 A/W [35, 36].Therefore, all the values of figure of merits (FOMS) of this device (Al/Beet/Cu) shows that this present device has a great potential as a rectifier and in rectenna application. Moreover, the FOMS may vary from device to device.

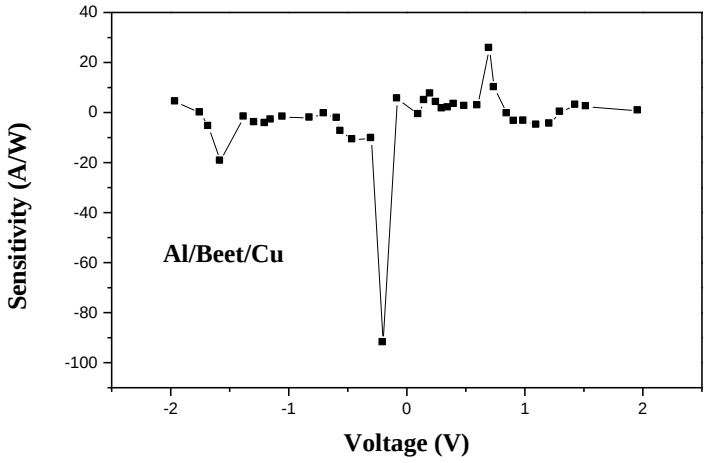

Fig. 5.6 Device sensitivity for Al/Beet/Cu MIM diode

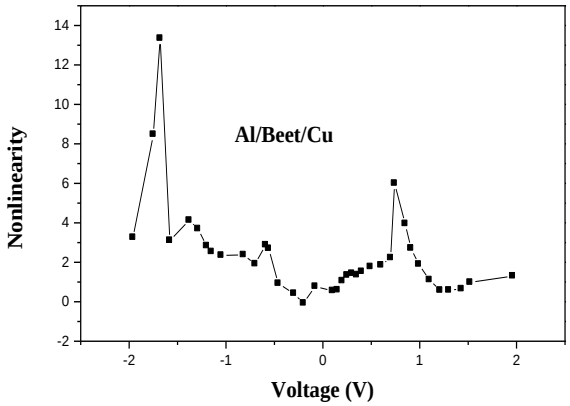

Fig. 5.7 Device nonlinearity factor for Al/Beet/Cu MIM diode

5.3.4 Quantum Tunnelling

Fig. 5.8 shows the variation of conductance with bias voltage, which exhibits a parabolic behaviour of conductivity of the device. This parabolic conductivity behaviour of the Al/Beet/Cu device proves that the quantum tunnelling process plays a significant part in the current conduction mechanism. Additionally, an asymmetry in this parabolic curve is seen. The dissimilarity in work functions between Al and Cu electrodes is what causes this imbalance in parabolic conductance. Therefore, all the natural dye-based Schottky diodes is to be forward biased if the voltage applied to the Al with the lower work function is greater than the voltage applied to the Cu with the higher work function.

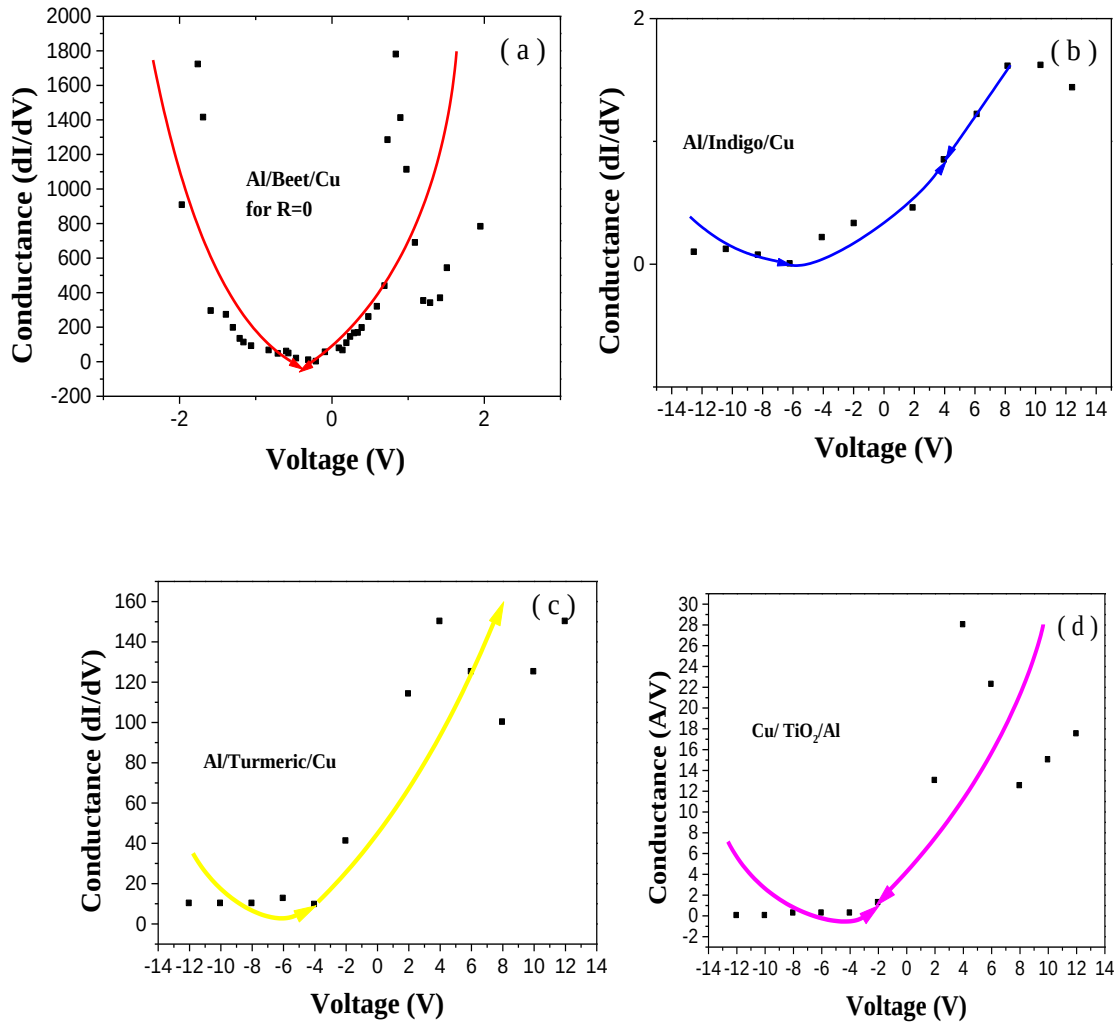

Fig. 5.8 Device conductance for the MIM diodes (a)Al/Beet/Cu, (b) Al/Indigo/Cu (c) Al/Turmeric/Cu and (d) Al/TiO_2/Cu.

From Fig. 5.8 we observed that the conductivity is higher in forward bias region than reversed bias region of all the Schottky diodes, which is due to the work function difference between Al and Cu. According to Brinkman et al., the dI/dV vs V (conductance vs V) plot will be a parabola for quantum tunnelling in MIM diode [37]. Therefore, it was proven by the parabolic behaviour of the dI/dV versus V plot that all-natural dye-based Schottky diodes may be affected in some way by the quantum tunnelling phenomena.

Fig. 5.9 shows the energy band diagram of the reported device. The device consists with a dye (beetroot) layer of very small thickness surrounded by two metals (Al, Cu). In current conduction there arises a barrier due to the band gap of betanin molecule present in the beetroot layer. Metal bands are filled up to Fermi energy.

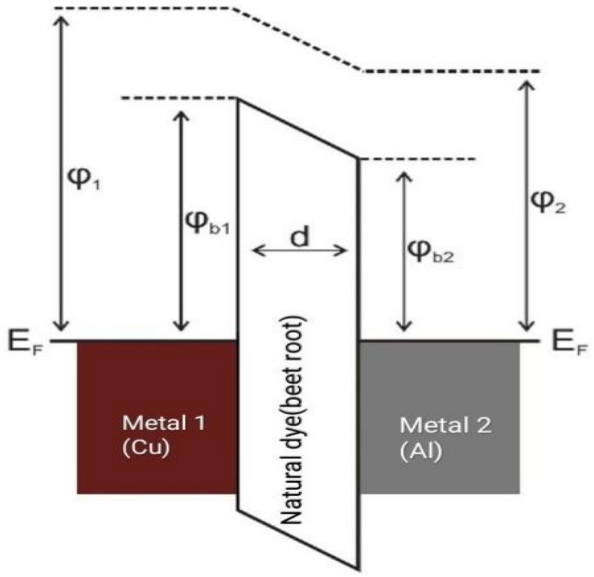

Fig. 5.9 Represents the energy band diagram of Al/ Beet/ Cu device

The barrier heights (ϕ_{b1}, ϕ_{b2}) at junctions are depends on the work functions of used electrodes (Cu=5.10 eV, Al=4.20 eV) and the work function of betanin present in the insulating layer. Here the current conduction depends on quantum tunnelling and this tunnelling current depends on the motion of electrons and holes. It is due to the high barrier height for holes causes' motion of electrons as well as the tunnelling current. In quantum tunnelling if the barrier width is thin enough then the electronic wave can penetrate the barrier with large enough amplitude. In MIM diode with two same metals as electrodes the tunnelling current is to be determined by Simmons theory [38]. In this device tunnelling appears between two different work function metals Al and Cu separated by natural dye paste layer. Fig 5.9 shows the energy band diagram of the Al/Beet/Cu device in different bias voltages. There are non-identical barriers (ϕ_{b1}, ϕ_{b2})

arise to the conduction of electron in this device, due to the difference in work functions between Cu and Al. So, barrier height difference ($\Delta\phi = \phi_{b1} - \phi_{b2}$) arises at zero bias which is shown in Fig. 5.9.

5.3.5 Comparative study

Now we discuss a comparative study between three natural dye-based MIM diodes and Al/TiO_2/Cu, which are prepared in same ambient condition. From Fig. 5.4 we observed that for beetroot and turmeric, asymmetry is maximum at low voltage and then it decreases with bias voltages, but for indigo and TiO_2asymmetry is an increasing function of bias. This can be explained from the I-V characteristics of all the natural dye based MIM diodes shown in Fig. 5.3, where we observed that the reverse current of Al/Beet/Cu, Al/Turmeric/Cu diodes increase with reverse bias but for Al/Indigo/Cu there is a saturated reverse current. Because of this we have found two different types of asymmetry plot. The FOMs of the diodes are shown in Table. 1. We have seen from that table, the current density, sensitivity and all other FOMs of Al/Beet/Cu are comparatively better than other two natural dye-based diodes. This is due to the higher dipole moment of betanin (8.69D) in comparison with indigo (0.0053D) and curcumin (4.854 D) [1,39]. Because of this there is a strong interaction between betanin molecule with the electrodes, which causes a large value of carrier conduction rate. If we use beetroot instead of TiO_2, rectification behaviour observed again, and current is much higher compared to the diode with TiO_2. This is because of the band gap of betanin is 2.1eV, which is smaller than band gap of TiO_2 (3.3eV). So, there is a significant thermionic emission with the quantum tunnelling in current conduction mechanism of Al/Beet/Cu based Schottky diode.

Table 5.1 FOMs comparison between natural dye-based diodes with Al/TiO_2/Cu

diode	I (μA) at 2V	f_{ASYM}	f_{NL}	f_{SENS} (A/W)	Zero bias resistance
Al/Indigo/Cu	0.6	Increases with bias	3	0.4	2.57MΩ
Al/Turmeric/Cu	300	30	1.9	4.3	12.8kΩ
Al/Beet/Cu	1180	17.6	5.998	25.7	23.26kΩ
Al/TiO_2/Cu	8	Increases with bias		0.4	436kΩ

The literature for the Al/Beetroot/Cu structure is lacking, though. In order to compare our findings with those kinds of literature, we gathered some other MIM structures that are relevant. Table.2 represents the comparison between Al/Beet/Cu and previously reported some MIM diodes. This table shows that Al/Beet/Cu diode exhibits maximum nonlinearity and maximum sensitivity with smaller zero bias resistance than Al-Al_2O_3-Ag. This may occur due to the high value of work function difference between Al and Cu, and high value of dipole moment (8.689D) of betanin molecule present in the beetroot. From Fig. 5.6 and Fig. 5.7, we observed that the maximum sensitivity and zero bias resistance of Al/Beet/Cu diode are 25.7A/W and 23.26kΩ, which is much better than previously reported Al-Al_2O_3-Ag MIM diode with highest sensitivity 18A/W with zero bias resistance 27KΩ [26]. Therefore, from the comparative study we may conclude that this MIM diode has a great potential in energy harvesting rectifier application.

Table 5.2 Comparison of Al/Beet/Cu MIM diode with previously reported MIM diodes.

Work	MIM diode	Zero bias resistance (Ω)	Max Sensitivity (A/W)
Pashang Esfandiari (2005) [40]	Al-Al_2O_3-Al, Ni-NiO-Pt	In mega ohms	-1.4, -13
Jffrey A. Bean(2009) [41]	Al/Al_2O_3/Pt	312 M	4.8
Mohamed Abdel-Rahman(2018)[42]	V-V_2O_5-Al	20 K	-8.52
Zia, M. F(2015)[43]	V/V_2O_5/V	13.4K	2.35
M. N. Gadalla (2014)[37]	Au/CuO/Cu	505	6
Martino Aldrigo et al.(2018)[44]	Au/HfO_2/Pt	405	6.58
Kapil Bhatt et al.(2019)[26]	Al/Al_2O_3/Ag	27K	18
Present Work	Al/Beet/Cu	23K	25.7

5.3.6 Determination of N_t and n_o for Al/Beet/Cu

From the examination of the I-V curve, the charge transport pathways through the beetroot layer may be inferred. Fig. 5.9 depicts the variation of log (I) with log (V) for the Al/beetroot/Cu diode. Voltage dependency is first shown in the characteristic, then power law dependence in higher voltage regions. This behaviour fits with the space charge-limited current theory (SCLC). The ohmic, SCLC, trap filling limit, and trap-free SCLC regimes are the four primary zones that might manifest in double-logarithmic characteristic, as shown in Fig. 5.10.

Applying the following equations [45-46], the traps density, carriers' density, and mobility of the active layer (beetroot dye) were determined from Fig. 5.10. We used the Poisson equation to get the density of the trap N_t. Therefore, it is simple to determine the trap concentration N_t.

$$N_t = 2\,\varepsilon\varepsilon_0 V_{FL} / qd^2 \qquad (5.5)$$

A trap density of about 1.25×10^9 cm^{-3} was obtained for V_{FL} = 1.14 V and d = 5μm

The following expression can be used to determine the carriers' number, n_0:

$$n_0 = 9\varepsilon\varepsilon_0 V_{ohm} / 8qd^2 \qquad (5.6)$$

For V_{ohm} = 0.3 V a density of carriers was found in the order of 1.8×10^9 cm−3.

Finally, the mobility was determined from the experimental characteristic in region IV and presented in the following equation:

$$Jscl = 9\varepsilon\varepsilon_0 \mu V^2 / 8d^3 \qquad (5.7)$$

As shown in Fig. 10, for V = 1.8 V, I = 800 $\times 10^{-6}$ A/cm^2 which gives a mobility of about 124.54 $cm^2 v^{-1} s^{-1}$.

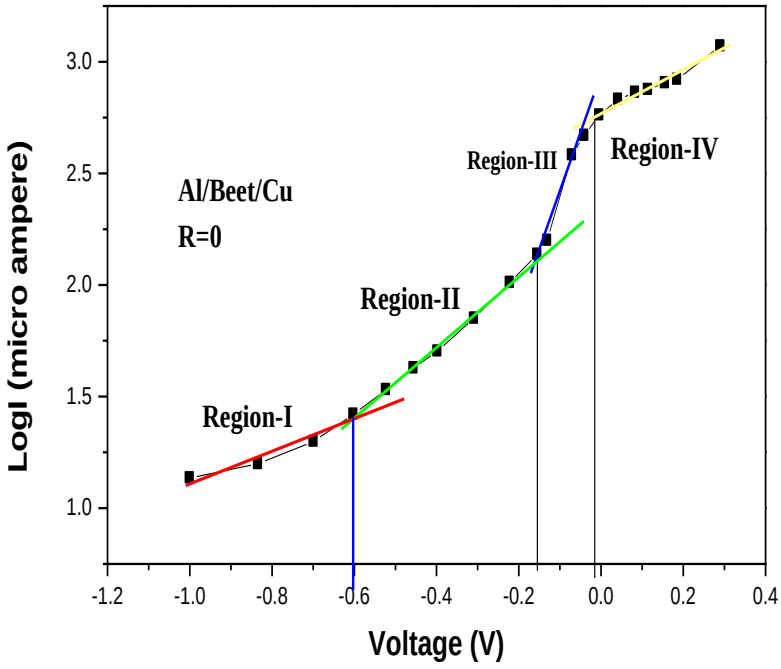

Fig. 5.10. Forward bias LogI-LogV (experimental)

5.3.7 Simulation study to verify the experimental result

Without introducing additional defects, we have modeled the J-V parameters of the Al/Beet/Cu device in this article. Fig. 5.11(a) displays the J-V characteristics of this device. It has properties similar to those of a Schottky diode and is in strong agreement with our experimental findings. We calculate the device's series resistance using the R_j-V figure in Fig. 5.11(b). The experimental value of 1.10 K and the simulated value of R_s are extremely similar. The device's threshold voltage is 0.70 V and the measured value of is 0.69 eV. According to the temperature-dependent J vs. V. plot in Fig. 5.12, the device's insulating temperature is close to 140 K, which is quite close to the theoretical value of 133 measured by A K Das et al [1]. The electrical characteristics derived from the experimental and simulated results are compared in Table 3, which demonstrates that they are reasonably close to one another.

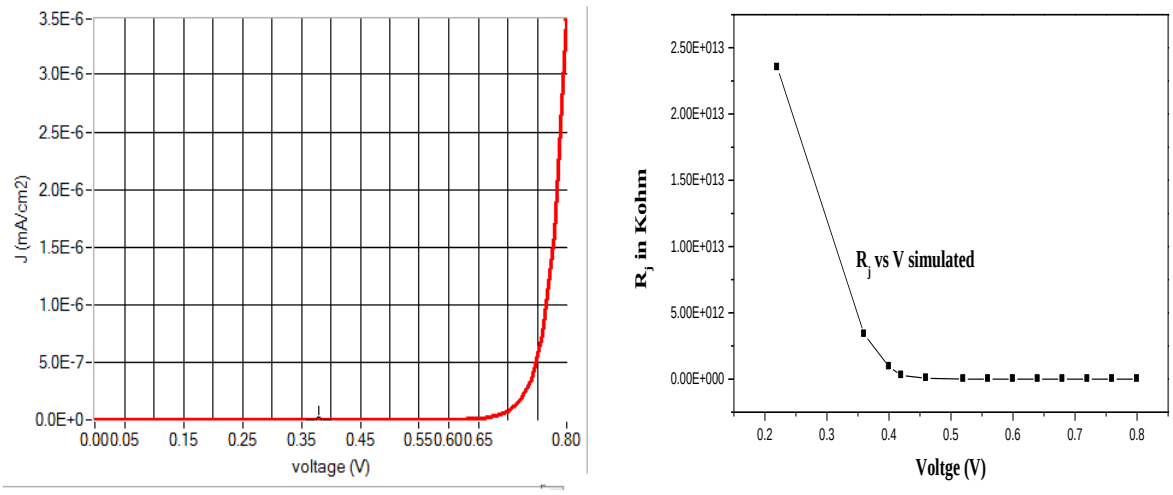

(a) (b)

Fig. 5.11. (a) Dark J-V characteristics of Al/Beet/Cu using SCAPS, **(b)** Rj vs V for Al/Beet/Cu using SCAPS.

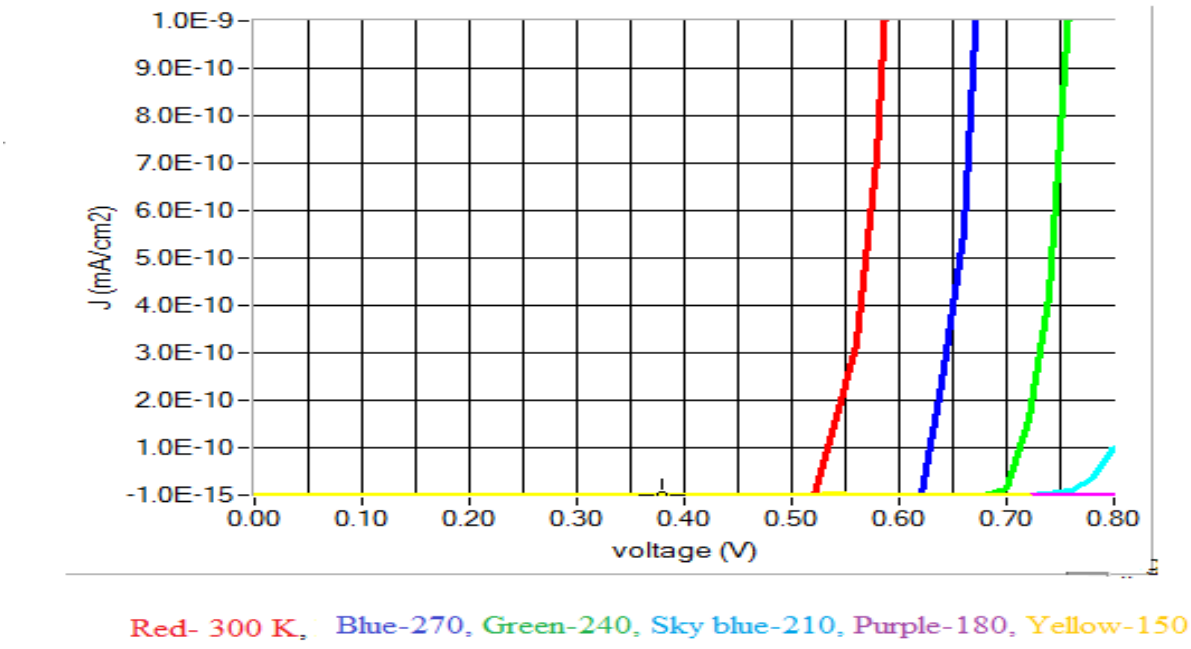

Fig. 5.12. Temperature dependent J-V of Al/Beet/Cu using SCAPS

Table 5.3 Comparison of the electrical parameters of the device extracted from experimental by AK Das et al and simulated results [1].

Electrical parameters	Experimental	Simulated
R_s (KΩ)	1.10 [1]	0.64
Φ (eV)	0.73 [1]	0.69
V_{th} (V)	0.75 [1]	0.70
T_i (K)	133 [1]	Nearly 140
N_t (cm^{-3})	$1.25x10^9$	
n_o (cm^{-3})	$1.8x10^9$	
μ ($cm^2v^{-1}\ s^{-1}$)	124.54	

5.3.8 Determination of maximum cut-off frequency in one dimensional geometry of the device

The maximum cut-off frequency of an MIM diode coupled to an antenna is calculated with the help of Sanchez theoretical model. Sanchez introduced a theoretical model [47] to calculate the cut-off frequency of a MIM diode. In this model the equivalent circuit of the MIM diode is a parallel combination of junction resistance R and capacitance C, shown in Fig. 5.13. The mathematical expression of cut-off frequency [47] is given as follows in equation (5.8).

$$f = \frac{1}{2\pi RC} \qquad (5.8)$$

Where; $C = \frac{k\varepsilon_o A}{d}$

We found that the dielectric constant K= 3.9 for SiO_2, K= 15 for TiO_2 and K= 9 for Al_2O_3[48], again we found that the values of dielectric constants for betanin, Cur-M and Indigo are 2.81, 2 and 4.3 respectively [23, 24, 49].

Table 5.4 Calculated values of Cut-off frequency for MIM diodes using different insulating layers

Diode	Dielectric constant (K)	Capacitance (C)	Cut-off frequency for 1Ω	Cut-off frequency for 1kΩ
Al/SiO_2/Cu	3.9	10.62×10^{-15} F	14×10^{12}	14×10^{9}
Al/TiO_2/Cu	15	40.85×10^{-15} F	3.8×10^{12}	3.8×10^{9}
Al/Al2O_3/Cu	9	24.50×10^{-15} F	6.49×10^{12}	6.49×10^{9}
Al/Beet/Cu	2.81	7.65×10^{-15} F	20.8×10^{12}	20.8×10^{9}
Al/Cur-M/Cu	2	5.45×10^{-15} F	29×10^{12}	29×10^{9}
Al/Indigo/Cu	4.3	11.7×10^{-15} F	12.7×10^{12}	12.7×10^{9}

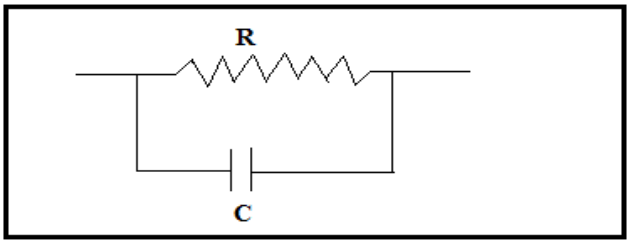

Fig. 5.13. Equivalent circuit of a MIM diode.

Table. 5.4 show that the values of capacitance and cut-off frequency of MIM diodes with different insulating layers. Here all the values are calculated in same ambient conditions (d= 13 nm, A= 4μm^2). From the above theoretical prediction, we may also say that Al/Beet/Cu MIM diode has a great potential in energy harvesting rectifier and rectenna application. Again, we may fabricate a one-dimensional Al/Beet/Cu Schottky diode and Al/TiO_2/Beet/Cu diode using FTO or silicon as a substrate shown in Fig. 5.14. This one-dimensional geometry of the reported diode will be of very low junction capacitance, which will increase the cut-off frequency. This ensures the potential of this diode in future research in high frequency communication system. But the main problem of this device is its area and instability in current (current decreases with time). Though the zero-bias resistance of Al/Beet/Cu is much smaller than some previously reported MIM diodes, but this value is high enough for a better use of optoelectronic system. These three reasons are the main restrictions to its implementation in the rectifier system. It should be optimized corresponding these problems before its implementation.

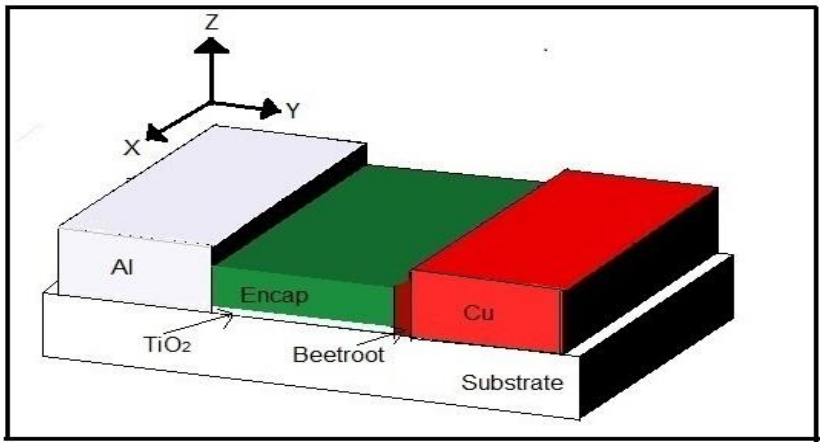

Fig. 5.14. One dimensional geometry of the diode.

5.4 Conclusion

In this chapter we have demonstrated organic dye active layer based single layer thin film diode and its comparison with TiO_2 based inorganic thin film diode. The experimental results show that Al/Beet/Cu diode shows better FOMs among all the natural dye-based diodes and TiO_2 based diode. The present reported diode exhibits an acceptable low voltage large signal and small signal nonlinearities with asymmetry of 17.6 at 0.85 V, maximum rate of change of nonlinearity of 6 and sensitivity of 25.6 A/W at 0.7 V. The maximum sensitivity of the diode is higher than earlier reported diodes. A validation with experimental curves was conducted once the major Al/Beetroot/Cu parameters required for the simulation were extracted from the logarithmic characteristic, and a good agreement was seen. The trap density and carrier concentration were found $1.25x10^9$ cm^{-3} and $1.8x10^9$ cm^{-3} respectively with the mobility 124.54 $cm^2v^{-1}s^{-1}$ for Al/Beetroot/Cu. It was proven by the parabolic behaviour of the dI/dV versus V plot that all-natural dye-based Schottky diodes may be affected in some way by the quantum tunnelling phenomena. For this device f_{NL}> 3 and f_{SENS}> 7 A/W, and from the FOMs of the diode we may conclude that, the diode has a great potential to the researchers in energy harvesting rectifier application. In order to have a predictive behavior and to have a better understanding of the physical processes and mechanisms influencing the effectiveness of the appliance under examination

5.5 References

1. Das AK, Mandal R, Mandal DK. The current transport mechanism of Al/Beetroot/Cu used as an organic semiconductor Schottky diode is superior than natural dye-based thin film devices. Microelectronic Engineering. 2022 May 15;261:111816.
2. Das AK, Mandal R, Chakraborty K, Mandal DK. Impact of ZnO nanoparticles on electrical characteristics of herbal dye-based organic Schottky diode. Bulletin of Materials Science. 2022 Aug 23;45(3):164.
3. Das AK, Mandal R, Chakraborty K, Mandal DK. Electrical Characteristics of a Turmeric Dye-Based Organic Thin Film Device and the Effect of Light on Barrier Height. Materials Proceedings. 2022 Aug 9;10(1):11.
4. Das A K, Mandal R, Chakraborty K and Mandal D K 2019 *IJIKC ISSN* **7** 2454-2415
5. Sen S, Manik NB. Effects of two different solvents on Schottky barrier of organic device. Journal of Physics Communications. 2021 Sep 24;5(9):095010.
6. Al-Ahmadi NA. Metal oxide semiconductor-based Schottky diodes: a review of recent advances. Materials Research Express. 2020 Mar 9;7(3):032001.
7. Kawano K, Sakai J, Yahiro M, Adachi C. Effect of solvent on fabrication of active layers in organic solar cells based on poly (3-hexylthiophene) and fullerene derivatives. Solar Energy Materials and Solar Cells. 2009 Apr 1;93(4):514-8.
8. Chakraborty K, Das A, Mandal R, Mondal DK. Interpretation of trap-assisted conduction with estimation of electrical parameters of thin indigo film-based semiconducting device. Bulletin of Materials Science. 2021 Jun;44(2):92.
9. Chakraborty K, Das A K, Mandal R and Mondal D K 2020 *Trans. Tianjin Univ*. **26** 265
10. Chakraborty K, Das A, Mandal R, Mandal DK. An analytical study on low voltage regime of natural organic semiconductor based device: Physics of trap energy and ideality factor. Solid State Communications. 2021 Jan 1;323:114080.
11. Etor D, Dodd LE, Wood D, Balocco C. An ultrathin organic insulator for metal–insulator–metal diodes. IEEE Transactions on Electron Devices. 2016 Jun 20;63(7):2887-91.
12. Das AK, Mandal R, Mandal DK. Impact of HTM on lead-free perovskite solar cell with high efficiency. Optical and Quantum Electronics. 2022 Jul;54(7):455.
13. Simmons JG. Conduction in thin dielectric films. Journal of Physics D: Applied Physics. 1971 May 1;4(5):613.
14. Fisher JC, Giaever I. Tunneling through thin insulating layers. Journal of Applied Physics. 1961 Feb 1;32(2):172-7.

15. Champlin KS, Eisenstein G. Cutoff frequency of submillimeter Schottky-barrier diodes. IEEE Transactions on Microwave Theory and Techniques. 1978 Jan;26(1):31-4.
16. Heiblum M. Tunneling hot electron transfer amplifiers (THETA): Amplifiers operating up to the infrared. Solid-State Electronics. 1981 Apr 1;24(4):343-66.
17. Masalmeh SK, Stadermann HK, Korving J. Mixing and rectification properties of MIM diodes. Physica B: Condensed Matter. 1996 Feb 1;218(1-4):56-9.
18. Krishnan S, Bhansali S, Stefanakos E, Goswami Y. Thin film metal-insulator-metal junction for millimeter wave detection. Procedia Chemistry. 2009 Sep 1;1(1):409-12.
19. Gustafson TK, Schmidt RV, Perucca JR. Optical detection in thin-film metal-oxide-metal diodes. Applied Physics Letters. 1974 Jun 15;24(12):620-2.
20. Rad S, Sharbati MT, Behrouz S, Nekoei AR. Fabrication of non-doped red organic light emitting diode using naturally occurring Curcumin as a donor-acceptor-donor (DAD) emitting layer with very low turn-on voltage. Iranian Journal of Science. 2015 Sep 6;39(3):297-304.
21. Bouzidi A, Yahia IS, El-Sadek MS. Novel and highly stable indigo (CI Vat Blue I) organic semiconductor dye: Crystal structure, optically diffused reflectance and the electrical conductivity/dielectric behaviors. Dyes and Pigments. 2017 Nov 1;146:66-72.
22. Dakhel AA, Cassidy S, Jasim KE, Henari FZ. Synthesis and characterisation of curcumin–M (M= B, Fe and Cu) films grown on p-Si substrate for dielectric applications. Microelectronics Reliability. 2015 Feb 1;55(2):367-73.
23. Usha P Kumar S, Khedkar NK, Jagtap B, Singh TP. The effects of cryogenic treatment on cutting tools. InIOP Conference Series: Materials Science and Engineering 2017 Aug 1 (Vol. 225, No. 1, p. 012104). IOP Publishing.
24. Maraghechi P, Foroughi-Abari A, Cadien K, Elezzabi AY. Enhanced rectifying response from metal-insulator-insulator-metal junctions. Applied Physics Letters. 2011 Dec 19;99(25).
25. Weerakkody AD, Sedghi N, Mitrovic IZ, Van Zalinge H, Noureddine IN, Hall S, Wrench JS, Chalker PR, Phillips LJ, Treharne R, Durose K. Enhanced low voltage nonlinearity in resonant tunneling metal–insulator–insulator–metal nanostructures. Microelectronic Engineering. 2015 Nov 1;147:298-301.
26. Bhatt K, Kumar S, Tripathi CC. Highly sensitive Al/Al2O3/Ag MIM diode for energy harvesting applications. AEU-International Journal of Electronics and Communications. 2019 Nov 1;111:152925.

27. Metcalfe DD, Sampson HA, Simon RA, Lack G, editors. Food allergy: adverse reaction to foods and food additives. John Wiley & Sons; 2013 Oct 28.
28. Manohar CM, Kundgar SD, Doble M. Betanin immobilized LDPE as antimicrobial food wrapper. Lwt. 2017 Jul 1;80:131-5.
29. Herbach KM, Stintzing FC, Carle R. Betalain stability and degradation—structural and chromatic aspects. Journal of food science. 2006 May;71(4):R41-50.
30. Fowler RH, Nordheim L. Electron emission in intense electric fields. Proceedings of the Royal Society of London. Series A, Containing Papers of a Mathematical and Physical Character. 1928 May 1;119(781):173-81.
31. Slovick BA, Bean JA, Krenz PM, Boreman GD. Directional control of infrared antenna-coupled tunnel diodes. Optics express. 2010 Sep 27;18(20):20960-7.
32. Bareib M, Tiwari B N, Hochmeister A, Jegert G, Zschieschang U, Klauk H et al. 2011 *IEEE Trans. Microw. Theory Tech.* **59** 20751
33. Bareib M, Ante F, Kälblein D, Jegert G, Jirauschek C, Scarpa G et al. 2012 *ACS nano*. **27** 2853
34. Gadalla MN, Abdel-Rahman M, Shamim A. Design, optimization and fabrication of a 28.3 THz nano-rectenna for infrared detection and rectification. Scientific reports. 2014 Mar 6;4(1):4270.
35. Periasamy P, Berry JJ, Dameron AA, Bergeson JD, Ginley DS, O'Hayre RP, Parilla PA. Fabrication and characterization of MIM diodes based on Nb/Nb2O5 via a rapid screening technique. Advanced Materials. 2011 Jul 19;23(27):3080-5.
36. Berland B. Photovoltaic Technologies Beyond the Horizon: Optical Rectenna Solar Cell, Final Report, 1 August 2001-30 September 2002. National Renewable Energy Lab. (NREL), Golden, CO (United States); 2003 Feb 1.
37. Brinkman WF. Dynes RC and Rowell JM. Journal of Applied Physics. 1970;1970:41.
38. Gupta SK, Koiry SP, Chauhan AK, Padma N, Aswal DK, Yakhmi JV. Self-assembled and electrochemically deposited mono/multilayers for molecular electronics applications. Applied surface science. 2009 Oct 30;256(2):407-13.
39. Sreeja S, Pesala B. Performance enhancement of betanin solar cells co-sensitized with indigo and lawsone: A Comparative Study. ACS omega. 2019 Nov 11;4(19):18023.
40. Esfandiari P, Bernstein G, Fay P et al. 2015 *Infrared Technology and applications* XXXI *Int. Soc. Opt. Photonics* **5783** 470

41. Been J A, Tiwari B, Bernstein G H, Fay P and Porod W 2009 *J. Vac. Sci. Technol. B: Microelectronics and Nanometer Structures Prossesing, Measurement and phenomena* **27** 11
42. Rahman M A, Issa K, Zia M F, Alduraibi M, Siraj M, Ragheb A et al. 2018 *Micro Nano lett.* **13** 680
43. Zia M, Abdel-Rahman M, Al-Khalli N, Debbar N. Fabrication and Characterization of Vanadium/Vanadium Pentoxide/Vanadium ($V/V_2O_5/V$) Tunnel Junction Diodes. Acta Physica Polonica A. 2015 Apr;127(4):1289-91.
44. Aldrigo M, Dragoman M, Modreanu M, Povey I, Iordanescu S, Vasilache D, Dinescu A, Shanawani M, Masotti D. Harvesting Electromagnetic Energy in the ${V} $-Band Using a Rectenna Formed by a Bow Tie Integrated With a 6-nm-Thick Au/HfO 2/Pt Metal–Insulator–Metal Diode. IEEE Transactions Electron Devices. 2018 May 22;65(7):2973-80.
45. Moliton A, Rammal W, Lucas B. A new method for the determination of electronic mobility in organic materials associated with optoelectronic devices. Europhysics Letters. 2005 Nov 4;72(5):754.
46. Lucas B, El Amrani A, Moliton A, Skaiky A, El Hajj A, Aldissi M. Charge transport properties in pentacene films: Evaluation of carrier mobility by different techniques. Solid-state electronics. 2012 Mar 1;69:99-103.
47. Sanchez A, Davis Jr CF, Liu KC, Javan A. The MOM tunneling diode: Theoretical estimate of its performance at microwave and infrared frequencies. Journal of Applied Physics. 1978 Oct 1;49(10):5270-7.
48. Hemmetter A, Yang X, Wang Z, Otto M, Uzlu B, Andree M, Pfeiffer U, Vorobiev A, Stake J, Lemme MC, Neumaier D. Terahertz rectennas on flexible substrates based on one-dimensional metal–insulator–graphene diodes. ACS Applied Electronic Materials. 2021 Aug 27;3(9):3747-53.
49. Shityakov S, Roewer N, Förster C, Broscheit JA. In silico modeling of indigo and tyrian purple single-electron nano-transistors using density functional theory approach. Nanoscale Research Letters. 2017 Dec;12:1-8.

Chapter 6

Impact of ZnO nanoparticles on electrical characteristics herbal dye based organic Schottky diode

6.1 Introduction

6.2 Materials and methods

6.3 Results and discussion

6.4 Conclusion

6.5 References

6.1 Introduction

In the previous chapters we have discussed that researchers' interest in fabricating a MIM and Schottky diode with organic materials as the active layer has grown [1-6]. However, existence of high trapping tendency, charge carrier recombination, enhanced effect of series resistance and high barrier height at metal-organic semiconductor interface limits its development in optoelectronic applications. Gradually, researchers are tasked with improving the performance of an organic Schottky diode based on herbal dyes by lowering the barrier height(ϕ_b), series resistance (R_s) and trap energy (E_c). When the barrier height at the metal -organic semiconductor junction is high enough, current conduction is poor, resulting in a high threshold voltage (V_{th}). Most organic Schottky diodes have a voltage at which current conduction obeys Ohm's law and I-V characteristics are virtually linear, but above this voltage I-V characteristics are non-linear due to non-ohmic current conduction. This voltage is recognized as the threshold voltage (V_{th}). To improve the efficiency of the herbal dye based organic device, threshold voltage should be optimized. According to some prior research, the trapping of charge carriers affects the increase in threshold voltage [7-8]. Charges are captured at trap centres and recombined in current conduction through herbal dye based organic thin film devices. Two significant conditions for collecting charges and recombination are trap state energy and trap state density. Trap energy, barrier height and threshold voltage can all be reduced using a variety of approaches. Incorporation of nanoparticles in the organic-metal Schottky diode is one of them. However, no significant research has been conducted which reports on the influence of ZnO nanoparticles on the threshold voltage (V_{th}), ϕ_b and trap energy (E_c) of an organic Schottky diode based on herbal dyes. It has been assessed the impact of incorporating zinc oxide nanoparticles within the herbal dye on the threshold voltage (V_{th}), ϕ_b and E_c of a herbal dye based organic Schottky diode in this paper. ZnO is a broad band gap semiconductor with a distinctive nanostructure and unique features like high heat conductivity, high electron mobility and high transparency. The zinc oxide (ZnO) nanoparticle has a high exciton binding energy (60 meV) [9] and optical transparency [10]. ZnO was chosen for integration into the herbal dye based organic Schottky diode because of all of the above intriguing features. It is observed at a variety of natural pigments in this study, including betanin (beetroot), curcumin (turmeric) and indigo dyes. Different organic Schottky diodes were fabricated by dissolving all the above dyes in a viscous solution of PVA. The organic Schottky devices were then made by incorporating ZnO nanoparticles into each of the herbal pigments. For both types of fabricated diodes, it has been calculated the threshold voltage (V_{th}), barrier height (ϕ_b) series

resistance (R_s) and trap energy (E_c). Barrier height(ϕ_b) of an organic Schottky diode at metal-organic dye junction is analysed by using the interfacial barrier height at the metal-organic dye contact. Barrier height is defined as the difference between the energy band of the natural dye based organic semiconductor and the fermi level of the metal electrode [11]. The Richardson-Schottky model based on thermionic emission theory [12] has been utilized to investigate the charge injection process of this diode in this work. Finally, we examined the electrical characteristics of other natural dye-based thin film diodes and discovered that the Al/beetroot/Cu device outperforms our previously published Al/indigo/Cu and Al/turmeric/Cu devices significantly. The work will be fruitful to enrich the information regarding the further application of herbal dyes and as well the significance of the ZnO nanoparticles in different segments of optoelectronic development applications.

6.2 Materials and methods

In this experiment, the red beetroot pastes and mixture of ZnO with red beet root paste is used as insulating layer. In actuality this red beetroot obtains a taproot of red beetroot plant. Structure of betanin which present in the beetroot dye shown in Fig. 1. Here it has also been used zinc oxide (ZnO) and polyvinyl alcohol (PVA). It has been procured PVA from Loba Chemie Pvt. Ltd. and ZnO obtained from Adnano Technologies private limited (Shimoga-577222, karnataka, india). In this experiment the FTO coated glass with resistivity 15 Ωcm-2 as substrate and Al and Cu as two electrodes are utilized. Specification of the used ZnO nanoparticles is developed as: APS = 30-80 nm, SSA = 110-120 m^2/g, molecular weight = 81.408 g/mol, melting point = 1975^{o}c, bulk density = 0.69 g/cm3. SEM images, EDX and chemical structure of zinc oxide nanoparticles are shown in Fig. 6.1

At first, it has been taken 20 mL distilled water in a beaker and then 4 g of PVA is mixed with it by stirring with a magnetic stirrer for 40 min at 80 ^{0}C. It is used PVA as an inert blinder to produce a gel-like viscous solution. Viscosity and molecular weight of PVA are 98 and 1,15,000 respectively. 6 mL beetroot juice solution is mixed with the prepared PVA solution and then the solution is divided into two identical parts in two clean beakers. One beaker is placed aside, which contains beetroot dye solution. In the other beaker 6 mg of zinc oxide nanoparticles is added to prepare Beet + ZnO solution.

FTO coated glass used as a substrate material for the fabrication of the Al/Beetroot/Cu and Al/Beetroot +ZnO/Cu diodes. The FTO glass was chemically polished by acetone. At that time native oxide of Al and Cu wafers was removed in HF: H_2O (1:10) solution and finally the wafers were rinsed in deionised water for one minute. The Cu layer was deposited as base electrode using thermal evaporation process. The dye (Beetroot) was coated onto Cu substrate using a spin coater at 2000 rpm and then, the film was dried at 50 ^oC for one hour to let the moisture. Here beet root (betanin) dye thin film of 50 μ m was deposited. Thickness of the Al electrode is about 0.005 mm and thickness of the beetroot +ZnO dye layer is about 50 μm. The same thin film spin-coated on the Al, and finally to make an Al/Beetroot/Cu diode, these two electrodes are put together. At last, this Al/beet root/Cu device has been dried for 10 hour. In the similar way Al/Beetroot +ZnO/Cu surface type Schottky diode was fabricated and its schematic circuit shown in Fig. 6.2.

SEM IMAGES

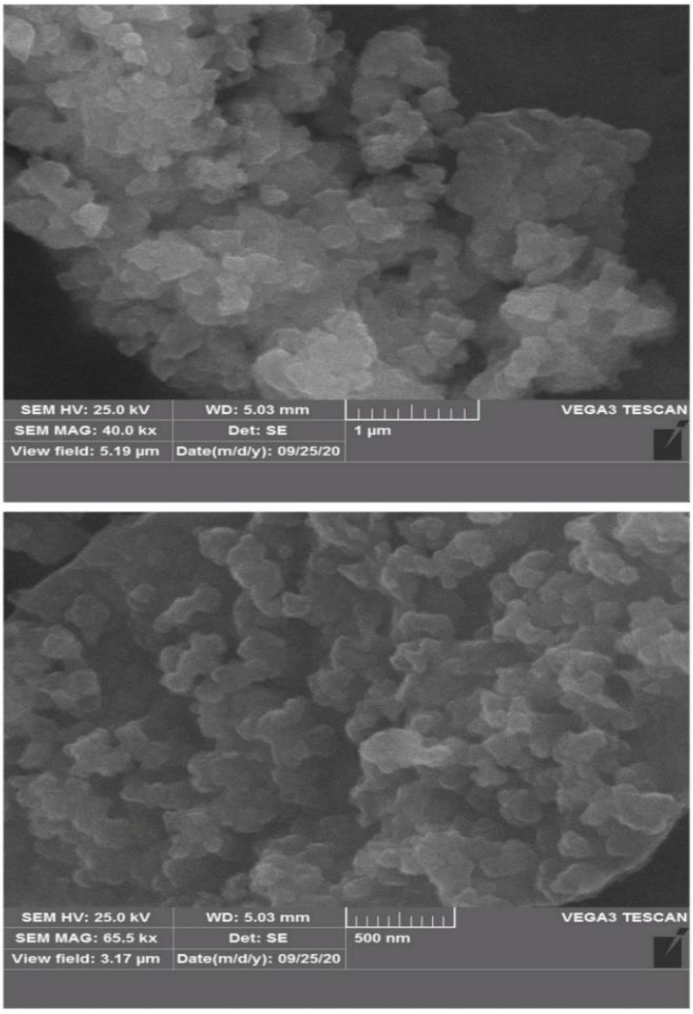
SEM HV: 25.0 kV
WD: 5.03 mm
VEGA3 TESCAN
SEM MAG: 40.0 kx
Det: SE
1 µm
View field: 5.19 µm
Date(m/d/y): 09/25/20
SEM HV: 25.0 kV
WD: 5.03 mm
VEGA3 TESCAN
SEM MAG: 65.5 kx
Det: SE
500 nm
View field: 3.17 µm
Date(m/d/y): 09/25/20

(a)

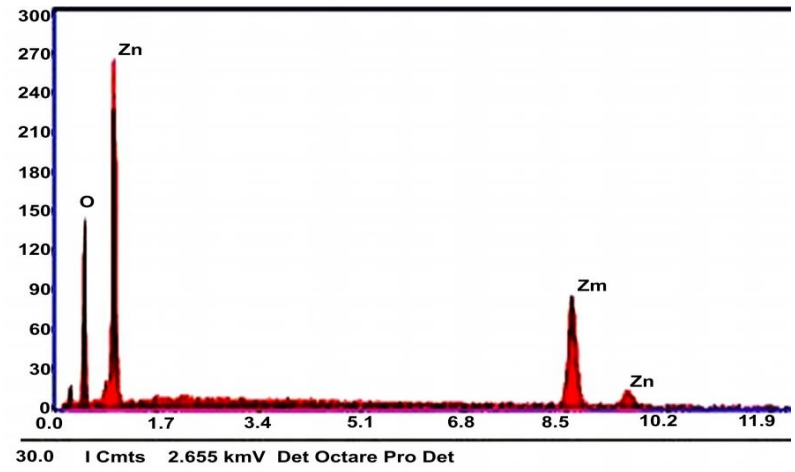

(b)

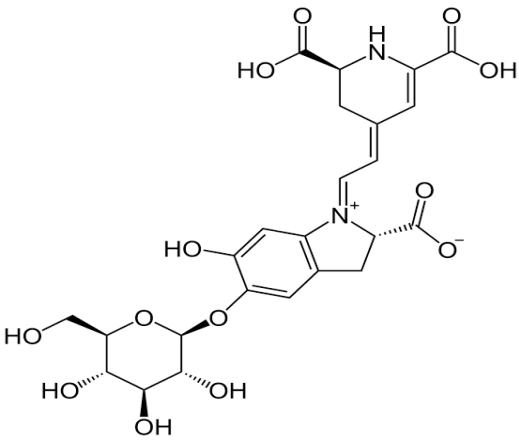

(c)

eZAF Smart Quant Results

Element	Weight %	Atomic %
0K	39.61	72.83
Znk	80.39	27.17

Fig. 6.1 (a) SEM images of ZnO and (b) EDX of ZnO and (c) chemical structure of betanin

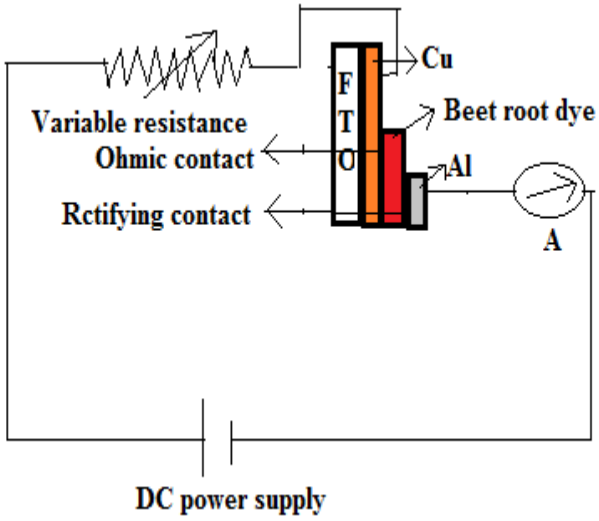

Fig. 6.2 I-V measurement circuit where beetroot has been selected as active layer with and without ZnO nanoparticles.

6.3 Results and discussions

The dark I vs V characteristics of both the natural dye based organic diodes with and without ZnO are shown in Fig. 6.3(a)-(d) respectively. It has been observed that the I-V curves are highly non-linear with quite low dark current for all the reported natural dyes. But for the incorporation of ZnO nanoparticles with the herbal dyes, the obtained current is greater in comparison. From all the I-V characteristics we observed that current conduction varies after a particular transition voltage is reached. This particular value of the bias voltage can be treated as threshold voltage (V_{th}) of the device. For different dye based Schottky diodes, this voltage is different.

Using thermionic emission theory, we can analyse the I vs V characteristics and current through the natural dye based organic semiconductor Schottky diode can be described as the following Eqs. (6.1-6.3) [13-18]:

$$I = I_0\left(exp\left(\frac{qV}{nkT}\right) - 1\right) \qquad (6.1)$$

where I_0 is the saturation current, given by

$$I = AA^* T^2 \exp\left(-\frac{q\phi}{kT}\right) \qquad (6.2)$$

and

$$A^* = \left(\frac{4\pi q m^* k^2}{h^3}\right) \qquad (6.3)$$

Here A* is the Richardson constant, and its obtained value is 120 Acm^{-2} K^{-2}, calculated from the saturation current of the device. From the interpolation of the exponential slope of current I at zero bias voltage, we can determine the reverse saturation current. The ϕ at metal- herbal dye (organic semiconductor) junction can be determined by the Eq. (6.4) [19-22] :

$$\phi = \frac{kT}{q} \ln \frac{AA^{*}T^{2}}{I_0} \qquad (6.4)$$

The dark I-V characteristics of the herbal dye based organic diodes with and without ZnO nanoparticles are shown in Fig. 6.3(a)-(d) respectively. From all the dark I-V characteristics it has been observed the amount of electric current flowing through the reported devices is increased due to the presence of zinc oxide nanoparticles. These increments of electric charge carrier conduction can be attributed due to the trap filling process. Current conduction mechanism through a natural dye based organic device can be influenced by various factors. Among all these factors, thickness of the dye film and presence of traps are the most important factor in these types of organic devices. In this study the film thickness is relatively high. Thickness of the active layer should be selected in such a way that the thinner layer production can accumulate and conduct carriers frequently. In present experiment, such thickness has been chosen to overcome the problem related to poor charge collection of the dye-based organic semiconductor. The aforementioned parameter has quite significant impact on device performance based on Schottky formation. E. Verna et al. investigated that due to increasing film thickness resistivity decreases from 17.99 Ωcm to 1.48 Ωcm and carrier concentration increases from 2.14 x 10^{16} to 4.02x 10^{17} cm^{-3}. Ahmadi et al. shows that increasing layer thickness of the sample reduces Schottky barrier which prevents the active formation of deep level traps in organic semiconductors [23-25]. We know that natural dye based organic materials are solids that are amorphous, disordered, and have weak intermolecular bonding. In natural dye based organic Schottky diodes, traps are present inherently. As a result, these types of organic diodes are trap prone, which are distributed randomly between the HOMO and LUMO of the organic layers [26, 27]. When we incorporate the ZnO nanoparticle the traps are filling by them, as a consequence there is an increment in current conduction in these devices.

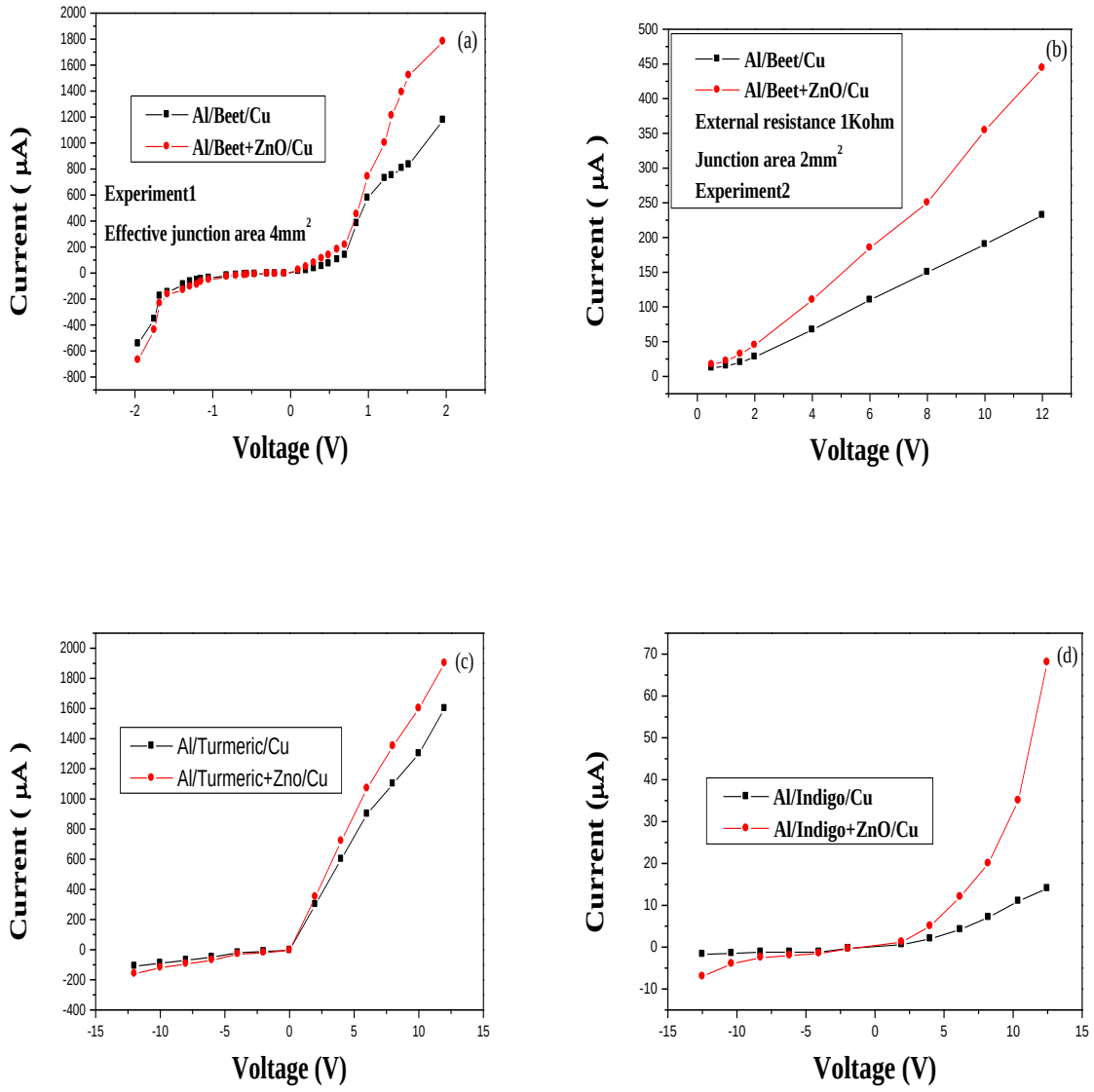

Fig. 6.3 Dark I-V characteristics of (a) beetroot dye with and without ZnO where the metal organic junction area is 4 mm^2 (b) beetroot dye with and without ZnO where the metal organic junction area is 2 mm^2 and external resistance is 1 KΩ, (c) turmeric dye with and without ZnO (d) indigo dye with and without ZnO.

The semi-logarithmic I-V characteristics of all the reported devices are shown in Fig. 6.4(a)-(d) respectively. When forward bias voltages are larger than kT/q, then extrapolated intercepts of all these plots at zero bias gives the saturation current for these reported devices. Using these values of saturation currents, we have calculated barrier heights (ϕ) of all the reported devices. From Fig. 6.4 we observed that saturation current (I_0) increases due to the presence of zinc oxide nanoparticles, which causes the decrease in barrier heights as obtained in Eq. (6.4).

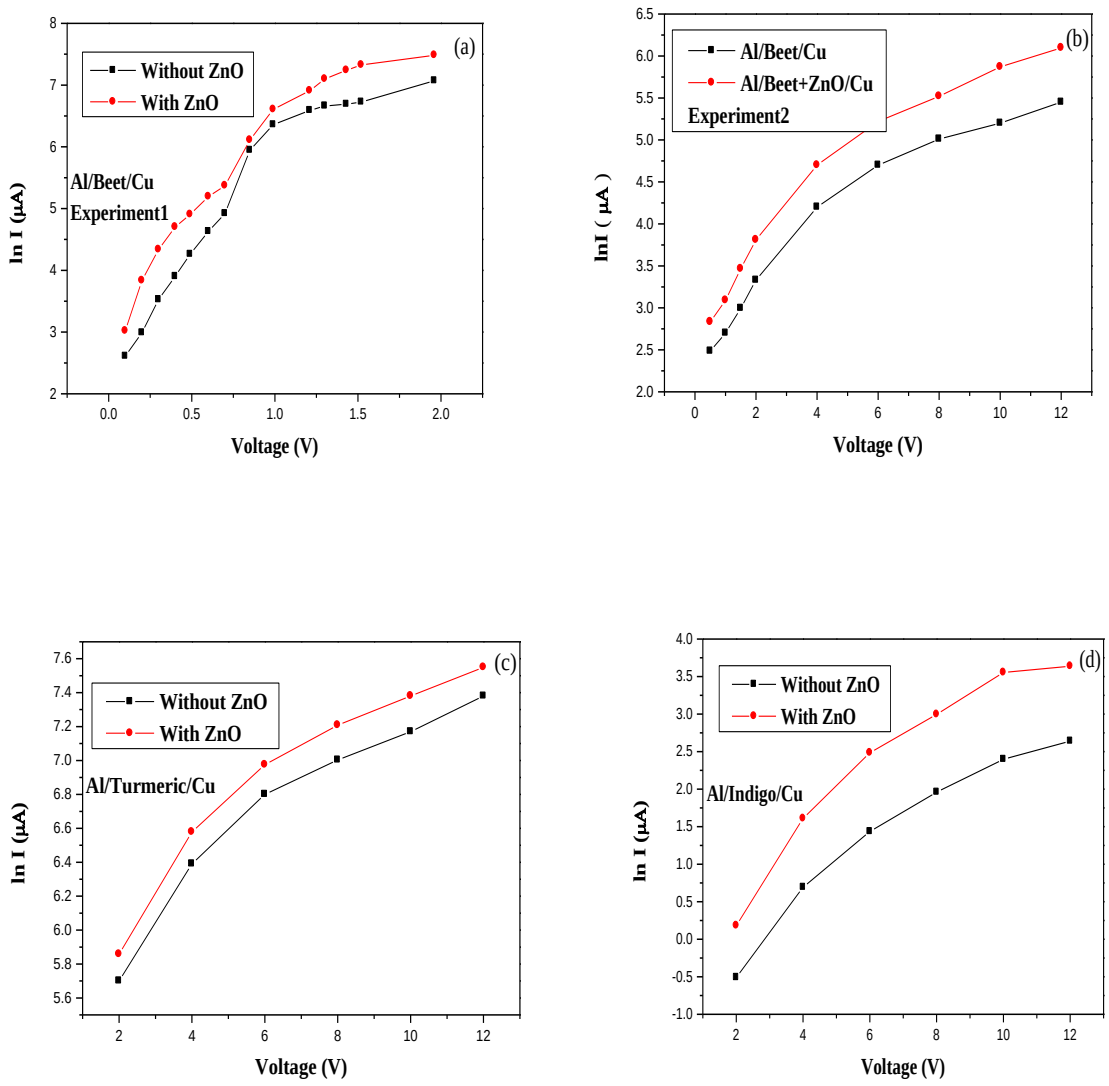

Fig. 6.4 Semi-logarithmic dark I-V characteristics of (a) beetroot dye with and without ZnO where the metal organic junction area is 4 mm^2 (b) beetroot dye with and without ZnO where the metal organic junction area is 2 mm^2 and external resistance is 1 KΩ (c) turmeric dye with and without ZnO (d) indigo dye with and without ZnO.

Barrier heights of the reported Al/Beet/Cu and Al/Beet+ZnO/Cu devices can also be computed using Norde function. Norde function F (V) can be expressed as Eq. (6.5)[28, 29]:

$$F(V) = \left(\frac{V}{X}\right) - \frac{kT}{q}\ln\left(\frac{I(V)}{AA^{*}T^{2}}\right) \qquad (6.5)$$

where X is the first integer greater than n. I (V_0) is the value of current for which Norde function is minimum, and F (V_0) is the minimum value of the Norde function, where V_0 represents the corresponding voltage. We calculated the barrier height of the device in absence and presence of zinc oxide nanoparticles using the eq. (6.6).

$$\phi = F(V_0) + \left(\frac{V_0}{X}\right) - \frac{kT}{q} \qquad (6.6)$$

In Fig. 6.5 from the plot of Norde function we observed that barrier height of Al/Beet/Cu device reduces due to the presence of zinc oxide nanoparticles, which agrees with the values of barrier height computed from the dark I-V characteristics of the reported diode.

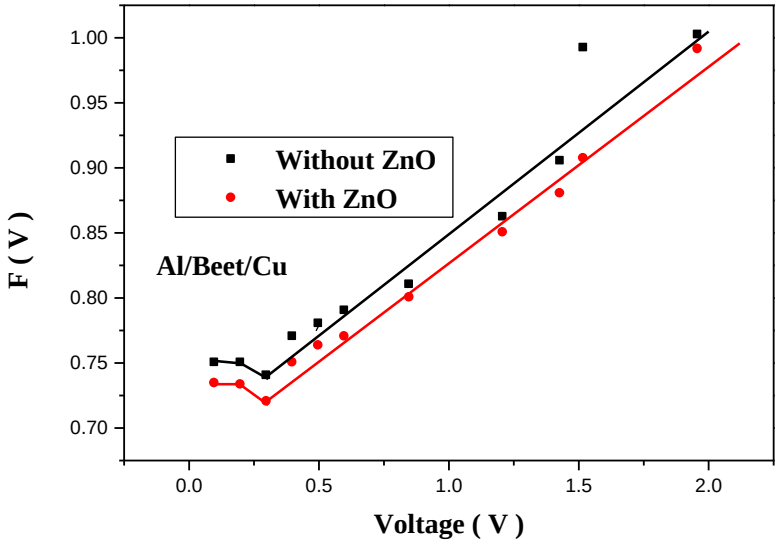

Fig. 6.5 Norde function F (V) - V plot for beetroot dye with and without ZnO where the metal organic junction area is 4 mm^2.

The variation of junction resistance ($R_j = dV/dI$) with bias voltage (V) is shown in Fig. 6.6. At a certain applied voltage the junction becomes minimum, which is called series resistance (R_s) of the device. From Fig. 6.6 we observed that the value of R_s in absence and presence of ZnO is 48.78 KΩ and 20.62 KΩ respectively. Which confirms that ZnO nanoparticles will reduce the series resistance (R_s) of an organic Schottky diode.

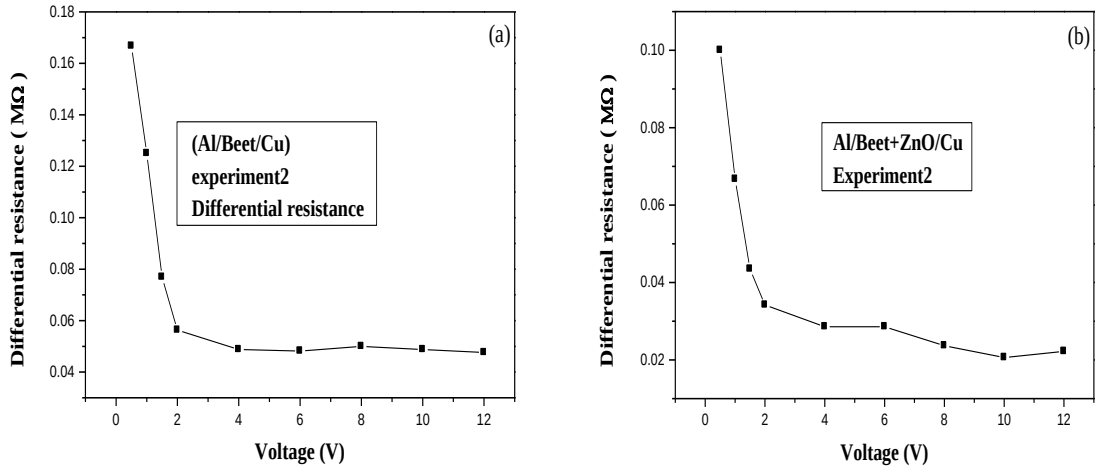

Fig. 6.6 Plot of variation of R_j with applied bias of Al/Beet/Cu (a) in absence of ZnO (b) in presence of ZnO.

We have calculated trap energy from the ln I - ln V plot of Al/Beet/Cu diode which shown in Fig. 6.7. The trap charge concentration N_t can be expressed as

$$N_t(\varepsilon) = N_0 \exp [-\varepsilon / kT] \quad (6.7)$$

where ε is depth of traps below conduction band mobility edge and T_c is the temperature of trap distribution (i.e., $T_c = E_c / k$, where E_c is the characteristic trap energy). $m = T_c / T$, where T is the room temperature. We have calculated the trap energy using the equation which can be expressed as [30]

$$E_c = mkT \quad (6.8)$$

Trap energy E_c can be measured from the value of m, which can be estimated from ln I- ln V plot of Al/Beet/Cu organic Schottky diode. In current conduction process through the organic Schottky traps carry out a significant role. Presence of traps causes the immobilization in majority charge carriers, motion [31-32]. As a consequence of these trapping states there is an internal resistive property arises inside the organic Schottky diode. We found that R_s, E_c and ϕ are high enough for organic Schottky diodes based on herbal dyes in our previous research [33-35]. The values of threshold voltage (V_{th}) trap energy (E_c) , series resistance (R_s) and barrier height (ϕ) of some metal-organic semiconductor junction Schottky diodes are shown in table 1. From this table we observed that the values of R_s, E_c and ϕ are reduced because of the presence of ZnO nanoparticle.

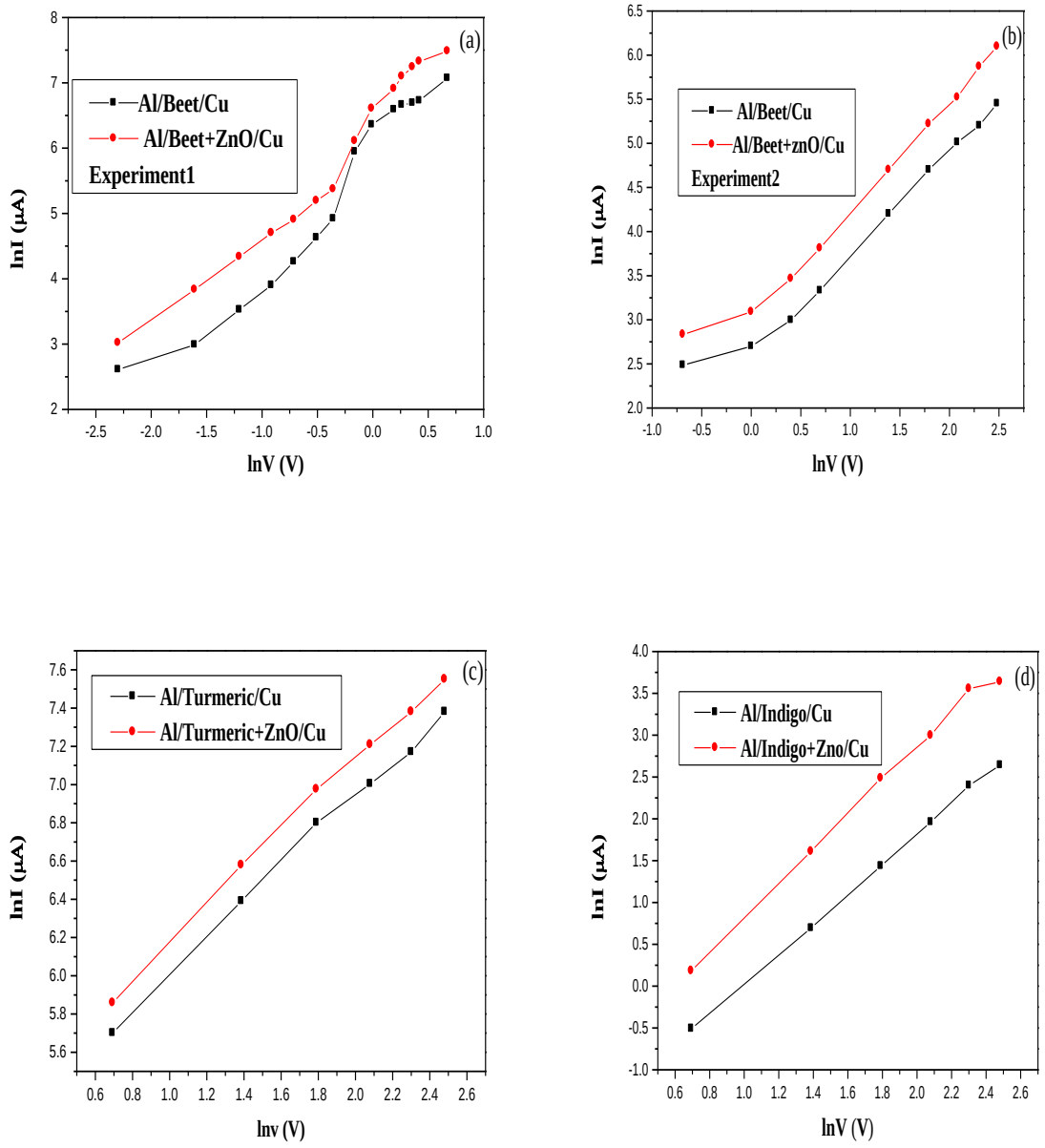

Fig. 6.7 ln I- ln V plot of (a) beetroot dye with and without ZnO where the metal organic junction area is 4 mm^2, (b) beetroot dye with and without ZnO where the metal organic junction area is 2 mm^2 and external resistance is 1 KΩ, (c) turmeric dye with and without ZnO, (d) indigo dye with and without ZnO.

Table 6.1. Different electrical parameters of the natural dye-based devices.

Device	V_{th} (volt)	R_s (KΩ)	E_c (eV)	ϕ (eV) from I-V characteristics	ϕ(eV) using Norde function
Al/Beet/Cu	0.74	1.46	0.021	0.75	0.78
Al/Beet+Zno/Cu expt1	0.45	0.92	0.016	0.72	0.75
Al/Beet/Cu	1.02	48.78	0.036	0.732	
Al/Beet+Zno/Cu Expt2	0.8	20.62	0.032	0.72	
Al/Turmeric/Cu	1.07	8	0.031	0.738	
Al/Turmeric+ZnO/Cu	0.5	3	0.025	0.715	
Al/Indigo/Cu	1.5	430	0.045	0.802	
Al/Indigo+ZnO/Cu	0.65	210	0.042	0.78	

6.4 Conclusion

The effect of ZnO on V_{th}, R_s, E_c and ϕ of natural dye-based organic Schottky diodes is investigated in this study. The measurement of electrical properties of a variety of herbal pigments, including beetroot, turmeric and indigo with and without the incorporation of ZnO is done. It is clearly noticed that the incorporation of ZnO nanoparticles reduced all of the aforementioned parameters. The barrier height for all known organic devices with and without ZnO is calculated using dark I-V characteristics and the Norde function. From these two approaches the calculated values are very similar to one another. Based on the consistency of the data, it is concluded that employing zinc oxide nanoparticles reduced the barrier height (ϕ) at the metal-herbal dye (organic semiconductor) junction. When ZnO nanoparticles are injected, they occupy a wide range of trap states, which reduces the trap energy (E_c) and series resistance (R_s). As a result, the threshold voltage (V_{th}) was decreased, and the device's electrical conductivity improved.

6.5 References

1. Shah M, Karimov KS, Ahmad Z, Sayyad MH. Electrical characteristics of A1/CNT/NiPc/PEPC/Ag surface-type cell. Chinese Physics Letters. 2010 Oct 1;27(10):106102.
2. Okur S, Yakuphanoglu F, Ozsoz M, Kadayifcilar PK. Electrical and interface properties of Au/DNA/n-Si organic-on-inorganic structures. Microelectronic engineering. 2009 Nov 1;86(11):2305-11.
3. Shah M, Sayyad MH, Karimov KS, Wahab F. Electrical characterization of the ITO/NiPc/PEDOT: PSS junction diode. Journal of Physics D: Applied Physics. 2010 Sep 21;43(40):405104.
4. Yakuphanoglu F. Controlling of silicon–insulator–metal junction by organic semiconductor polymer thin film. Synthetic metals. 2010 Jul 1;160(13-14):1551-5.
5. Yakuphanoglu F. Photovoltaic properties of the organic–inorganic photodiode based on polymer and fullerene blend for optical sensors. Sensors and Actuators A: Physical. 2008 Feb 15;141(2):383-9.
6. Yakuphanoglu F, Kandaz M, Senkal BF. Inorganic–organic photodiodes based on polyaniline doped boric acid and polyaniline doped boric acid: nickel (II) phthalocyanine composite. Sensors and Actuators A: Physical. 2009 Aug 3;153(2):191-6.
7. Lampert MA. Simplified theory of space-charge-limited currents in an insulator with traps. Physical Review. 1956 Sep 15;103(6):1648.
8. Mark P, Helfrich W. Space-charge-limited currents in organic crystals. Journal of Applied Physics. 1962 Jan 1;33(1):205-15.
9. Roy VA, Djurišić AB, Chan WK, Gao J, Lui HF, Surya C. Luminescent and structural properties of ZnO nanorods prepared under different conditions. Applied physics letters. 2003 Jul 7;83(1):141-3.
10. Chen QH, Zhang WG. Continuous preparation of decorated nano zinc oxide organic sols with intense luminescence. Journal of non-crystalline solids. 2007 Mar 15;353(4):374-8.
11. Armbrust N, Schiller F, Güdde J, Höfer U. Model potential for the description of metal/organic interface states. Scientific Reports. 2017 Apr 20;7(1):46561.
12. Sze S M and Ng K K 2007 Physics of the semiconductor devices, 3rd ed. (New York: Wiley, 2007), pp. 159-181.
13. Svensson J, Campbell EE. Schottky barriers in carbon nanotube-metal contacts. Journal of applied physics. 2011 Dec 1;110(11).

14. Sen S, Manik NB. Effect of back electrode on trap energy and interfacial barrier height of crystal violet dye-based organic device. Bulletin of Materials Science. 2020 Dec;43(1):60.
15. Sen S, Manik NB. Effect of carboxyl-functionalized single walled carbon nanotubes on the interfacial barrier height of malachite green dye based organic device. Physics International. 2019 Jan 1;10(1):1-7.
16. Shah M, Karimov KS, Ahmad Z, Sayyad MH. Electrical characteristics of A1/CNT/NiPc/PEPC/Ag surface-type cell. Chinese Physics Letters. 2010 Oct 1;27(10):106102.
17. Harrabi Z, Jomni S, Beji L, Bouazizi A. Distribution of barrier heights in Au/porous GaAs Schottky diodes from current–voltage–temperature measurements. Physica B: Condensed Matter. 2010 Sep 1;405(17):3745-50.
18. Al-Ta'ii HM, Amin YM, Periasamy V. Calculation of the electronic parameters of an Al/DNA/p-Si schottky barrier diode influenced by alpha radiation. Sensors. 2015 Feb 26;15(3):4810-22.
19. Yıldırım M. Determination of contact parameters of Au/n-Ge Schottky barrier diode with rubrene interlayer. Politeknik Dergisi. 2017;20(1):165-73.
20. Güzeldir B, Sağlam M, Ateş A, Türüt AB. Determination of the some electronic parameters of nanostructure copper selenide and Cu/Cu3Se2/n-GaAs/In structure. Journal of Alloys and Compounds. 2015 Apr 5;627:200-5.
21. Sen S, Manik NB. Characterization of Electrical Parameters of Copper Phthalocyanine Based Organic Electronic Device in Presence of Fullerene Nanoparticles. Advanced Materials Research. 2021 Dec 9;1167:35-42.
22. Islam ZU, Tahir M, Syed WA, Aziz F, Wahab F, Said SM, R. Sarker M, Md Ali SH, Sabri MF. Fabrication and photovoltaic properties of organic solar cell based on zinc phthalocyanine. Energies. 2020 Feb 21;13(4):962.
23. Veena E, Bangera KV, Shivakumar GK. Effective role of thickness on structural, electrical and optical properties of lead sulphide thin films for photovoltaic applications. Materials Science and Engineering: B. 2017 Sep 1;223:64-9.
24. Al-Ahmadi NA, Al-Jawhari HA. Effect of epitaxial layer thickness on the electrical properties of Ti/n-AlGaAs grown by MBE. Results in physics. 2016 Jan 1;6:67-9.
25. Park SG, Lee WJ, Song MJ, Shin J, Kim TW. Effects of the Thickness of N, N′-diphenyl-N, N′-di (m-tolyl)-benzidine on the Electro-Optical Characteristics of Organic Light-Emitting Diodes. Materials. 2019 Mar 22;12(6):966.

26. Haldar A, Maity S, Manik NB. Effect of C 60 on methyl red and crystal violet dye-doped photovoltaic device. Ionics. 2008 Jun;14:263-7.
27. Scher H, Montroll EW. Anomalous transit-time dispersion in amorphous solids. Physical Review B. 1975 Sep 15;12(6):2455.
28. Shah M, Sayyad MH, Karimov KS, Wahab F. Electrical characterization of the ITO/NiPc/PEDOT: PSS junction diode. Journal of Physics D: Applied Physics. 2010 Sep 21;43(40):405104.
29. Harrabi Z, Jomni S, Beji L, Bouazizi A. Distribution of barrier heights in Au/porous GaAs Schottky diodes from current–voltage–temperature measurements. Physica B: Condensed Matter. 2010 Sep 1;405(17):3745-50.
30. Haldar A, Maity S, Manik NB. Effect of back electrode on photovoltaic properties of crystal-violet-dye-doped solid-state thin film. Ionics. 2008 Sep;14:427-32.
31. Chakraborty S, Manik NB. Effect of single walled carbon nanotubes on the threshold voltage of dye based photovoltaic devices. Physica B: Condensed Matter. 2016 Jan 15;481:209-16.
32. Kawano K, Sakai J, Yahiro M, Adachi C. Effect of solvent on fabrication of active layers in organic solar cells based on poly (3-hexylthiophene) and fullerene derivatives. Solar Energy Materials and Solar Cells. 2009 Apr 1;93(4):514-8.
33. Chakraborty K, Das A, Mandal R, Mondal DK. Interpretation of trap-assisted conduction with estimation of electrical parameters of thin indigo film-based semiconducting device. Bulletin of Materials Science. 2021 Jun;44(2):92.
34. Chakraborty K, Das AK, Mandal R and Mandal DK . 2020 *Transactions of Tianjin University*. **26** 265
35. Chakraborty K, Das A, Mandal R, Mandal DK. An analytical study on low voltage regime of natural organic semiconductor based device: Physics of trap energy and ideality factor. Solid State Communications. 2021 Jan 1;323:114080.

Chapter 7

The impact of the shape of zinc oxide nanoparticles on electrical parameters of natural dye based FTO/Beetroot/ Al Schottky diode

7.1 Introduction

In the previous chapter we have discussed on the impact of ZnO nanoparticles on natural dye-based organic semiconductor diodes. In this chapter we have discussed the impact of morphology of ZnO Np on natural dye-based organic semiconductor Schottky diodes. For this purpose, we have used ZnO Np's of Spherical and cylindrical in geometry. Semiconducting zinc oxide (ZnO) nanoparticle is a unique material and attracted to the researchers due to its high electron mobility, thermal conductivity and good transparency. The exciton binding energy of ZnO is 60 meV [1] and its optical transparency [2] is high. Because of all these properties, zinc oxide nanoparticles have been chosen for the fabrication of Schottky diodes [3] and solar cells [4]. The high value of excitonic binding energy of Zinc oxide leads to extreme stability of excitons at high temperature [5] and enables the device to function at low threshold voltage. The morphology-dependent electron mobility of zinc oxide nanoparticles is another key characteristic. By altering their morphology, nanoparticles with a sufficient band gap for a certain device application can be created. Absorption is affected by the materials effective surface area, which affects the direct band gap. According to the Burstein-Moss effect, all states close to the conduction band are crowded, pushing the absorption edge of semiconducting nanoparticles to higher energies. Changes in the morphological growth can have an impact on this [6]. At higher temperatures, an n-type semiconductor material with a larger band gap is ideal for the creation of a Schottky barrier. Zinc oxide is compatible with metal-semiconductor Schottky diode as a classical semiconductor with a wide band gap. Many metals, including Ag [7], Au [8], Pd [9], and Pt [10,11], have been used to make ZnO-based Schottky barrier diodes. The barrier height for all these metal-semiconductor Schottky diodes is around 0.6-0.8 eV, and ideality factor is around 1.5 [7-11]. Synthesizing ZnO nanoparticles with various morphologies took a lot of time and effort. Zhang et al. [12]. reported flower-shaped, prism-shaped, rod-shaped ZnO nanoparticles. Optoelectronics, sensors, and photocatalysis are just a few of the uses for zinc oxide (ZnO) nanoparticles. ZnO nanoparticles' shape significantly influences both their characteristics and potential uses. Electrical conductivity and optical characteristics vary across various ZnO nanostructures. For instance, ZnO nano shuttles have the lowest electrical conductivity out of all nanostructures, whereas ZnO nanorods have the highest [13]. Surface morphology and particle size have an impact on ZnO nanoparticle structural parameters such as lattice constants, crystallite size, micro strain, and other associated structural parameters [13]. The size of the nanoparticles, surface morphology, pH levels of the preparation solution, synthetic solvents, and annealing

temperatures are the primary factors that predict the creation of various nanostructured ZnO materials [13]. The morphological impacts of ZnO on the metal-organic semiconductor junction physics of FTO/Beet/Al, FTO/beet+ZnO/Al and the morphological effects of ZnO nanoparticles on the rectifying electrical properties of FTO/ZnO/Al Schottky diodes, respectively, have not yet been studied.

For this purpose, in this work we have fabricated FTO/ZnO/Al to examine the effect of ZnO nanomorphology on metal-inorganic Schottky diode parameters. We have also fabricated FTO/Beet/Al and FTO/Beet + ZnO/Al diodes to analyse the effect ZnO nanomorphology on herbal dye based organic Schottky diode parameter. The rectifying nature of the I-V characteristics of the reported devices was consistent with the Schottky diode. With the variation of the shape of ZnO nanoparticles, a significant change in diode behaviour as well as electrical parameters like barrier height (ϕ), series resistance (R_s), and trap energy (E_c) were explored. In order to gain better understanding of the charge transport mechanism within the device, we examined the I-V characteristics using thermionic emission theory.

A. K. Das et al, fabricated natural herbal dye based organic semiconductor Schottky diodes [14-17] and organic semiconductor HTM based perovskite solar cell [18]. Natural dye-based organic semiconductor diodes provide numerous advantages over inorganic semiconductor diodes, including enhanced performance, cost-effectiveness, lightweight, biocompatibility, tuneable characteristics, flexibility, and versatility. But the values of R_s, n and ϕ for natural herbal dye-based organic semiconductor Schottky diodes are high enough, as we have seen in certain literature and in our published works [14- 29]. Therefore, lowering the value of R_s, n, and ϕ is one of the key objectives of this study. In order to create an organic semiconductor Schottky diode based on natural herbal beetroot dye, we incorporated ZnO nanoparticles with beetroot dye. This demonstrates a notable drop in the Schottky diode's R_s, n and ϕ. Which boost the mobility and current conduction through the natural beetroot dye based Schottky diode. But there are ZnO nanoparticles of many forms. Now, we want to determine which ZnO nanoparticle forms are more efficient. We have therefore employed two distinct morphological (cylindrical and spherical) nanoparticles. For both types of Schottky diodes, it has been found that the presence of spherical ZnO nanoparticles reduces R_s, ϕ and n more than cylindrical ZnO nanoparticles do.

7.2 Materials and Methods

7.2.1 Fabrication of FTO/ZnO/Al based inorganic Schottky diode

In this experiment we have used FTO coated glass with resistivity 15 Ωcm^{-2} as substrate and Al and FTO as two electrodes. At first, 4 g of PVA is dissolved with 20 mL of distilled water in a clean beaker by swirling with a magnetic stirrer for 40 minutes at 80 °C. We created a thick gel-like solution using PVA as an inert blinder. PVA has a viscosity of 98 and a molecular weight of 1,15,000. Then, two identical portions of this solution are separated into two beakers. PVA solution is combined with 8 mg of ZnO(S) nanoparticles in one beaker, and 8 mg of ZnO(C) nanoparticles in the other beaker. To make ZnO solution, the solutions were then mixed with a magnetic stirrer for 40 minutes at 80 °C.

Glass with FTO coating was employed as the base material to create the FTO/ZnO/Al diode. Acetone was used to chemically polish the FTO glass. Al wafers' native oxide was then removed using an HF: H_2O (1:10) solution, and the wafers were then washed for a minute in deionized water. ZnO was applied to the FTO substrate using a spin coater at 2000 revolutions per minute, and the film was then allowed to dry at 50 ^oC for an hour then then it is cooled at room temperature for four hours. A 50 µm thick thin layer of ZnO was formed here. The Al electrode has a thickness of around 0.055 mm. Finally, these two electrodes are sandwiched to create an FTO/ZnO/Al diode by having the same thin film spin-coated on both the Al and ZnO. This device has finally been dried for 10 hours.

7.2.2 Fabrication of FTO/Beet/Al based organic Schottky diode with and without ZnO

In this experiment, the insulating layer was made of red beetroot paste and a combination of red beetroot paste and ZnO. We have first poured 30 mL of distilled water into a clean beaker, and then we have added 6 g of PVA and stirred with a magnetic stirrer for 40 minutes at 80 ^0C. We created a thick gel-like solution using PVA as an inert blinder. PVA has a viscosity of 25-32 cps and a molecular weight of 1,15,000. The produced PVA solution is combined with 9 mL of beetroot juice solution before being divided into three identical portions in three beakers. The beaker containing the beetroot dye solution is set aside. In the other two beakers 6 mg of zinc oxide nanoparticles of different morphology is added to prepare Beet + ZnO solution.

Using a spin coater at 2000 rpm, the dye (beetroot) was deposited to the FTO substrate. The film was then dried at 50 ^0C for an hour to remove the moisture. A 50 µm thin coating of beet

root dye was placed here. The beetroot + ZnO dye layer has a thickness of around 50 µm, while the Al electrode is about 0.055 mm thick. To create an FTO/Beetroot/Al diode, the same thin film is spin-coated on the Al, and then these two electrodes are sandwiched together. This Al/Beet root/Cu device has finally been dried for 10 hours in a dark place at room temperature. The FTO/Beetroot + ZnO/Al surface type Schottky diode was created in a similar manner. Fig 7.1. Shows the flow chart and sandwiched configuration of the device.

ZnO nanoparticles' XRD patterns were captured during analytical tests using a Bruker D8 X-Ray Diffractometer with CuKα (λ= 1.5418A) radiation. The ZnO nanoparticles' microscopic images were captured using a Hitachi S-4800 scanning electron microscope (SEM). A computer interfaced Keithley 2400 Source Meter was used to characterize the current-voltage (I-V) properties of the reported Schottky barrier diodes. The electrical properties of the diodes, were assessed by rectifying I-V characteristic curves.

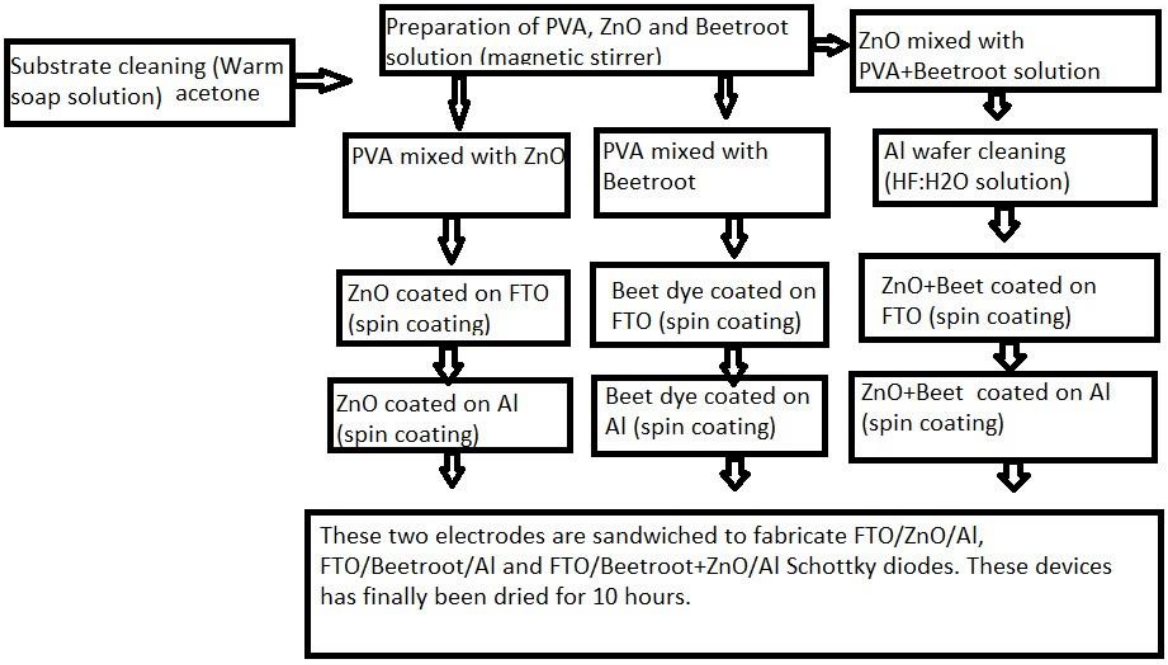

(a)

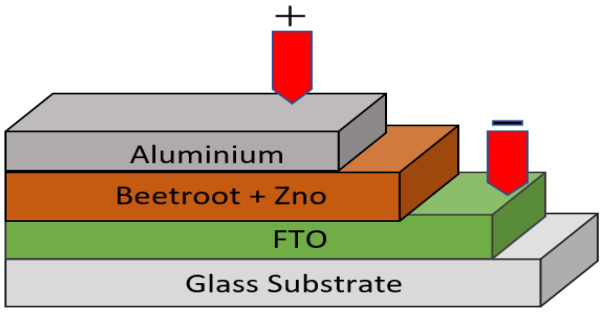

(b)

Fig. 7.1 (a) Flow chart of the diodes fabrication and (b) Sandwiched configuration of the FTO/Beetroot+ZnO/Al diode

7.3 Results and discussion

SEM images XRD and EDX of ZnO nanoparticles are shown in Fig. 7.2. Which shows that our used ZnO nanoparticles are different in morphology, one is spherical and another is cylindrical. Using EDX we find the weight% and atomic% of Zn and O are 80.39, 39.61, 27.17 and 72.83 respectively. The crystallite size was estimated from the basic Scherrer equation [30],

$$D = \frac{K\lambda}{\beta \cos\theta} \tag{7.1}$$

where D is the average crystallite size, λ is the x-ray wavelength, β is the x-ray peak's width on the 2θ axis, which is typically measured as full width at half maximum (FWHM) after the error caused by instrumental broadening has been properly corrected (subtraction of variances), is the Bragg angle, and K is the so-called Scherrer constant. The diffraction line indices, the size distribution of the crystallites, and the definition of β—FWHM or integral breadth—that is actually utilized all affect K [31]. K can range in value between 0.62 and 2.08. K = 0.9 was employed in this study. Table 7.1 displays the technical specifications of the utilized ZnO nanoparticles.

(a)

SEM IMAGES

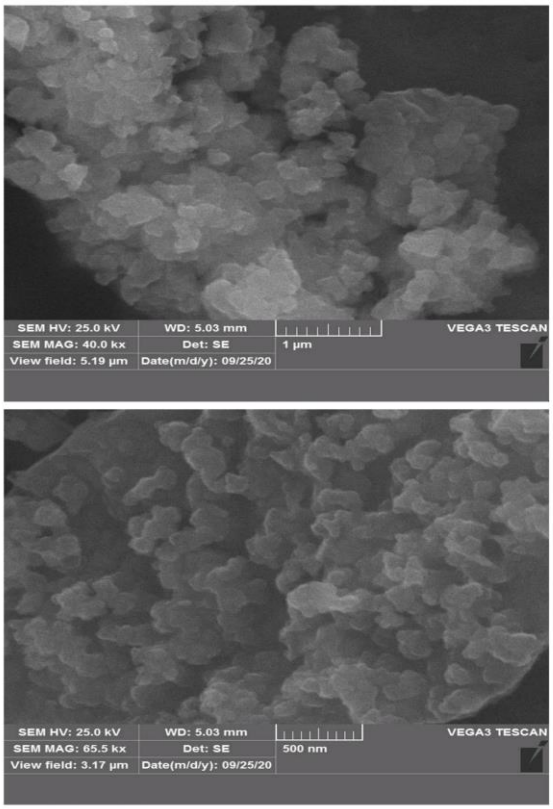

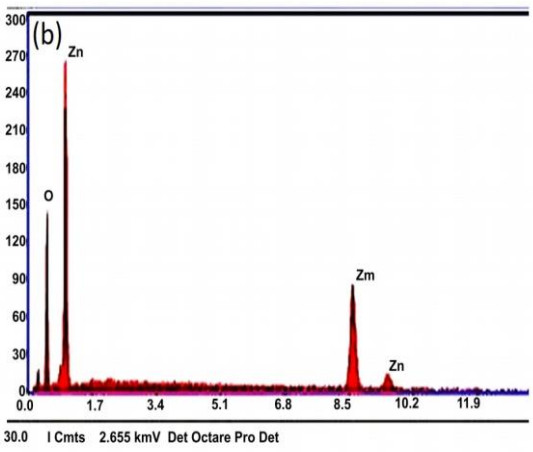

eZAF Smart Quant Results

Element	Weight %	Atomic %
0K	39.61	72.83
Znk	80.39	27.17

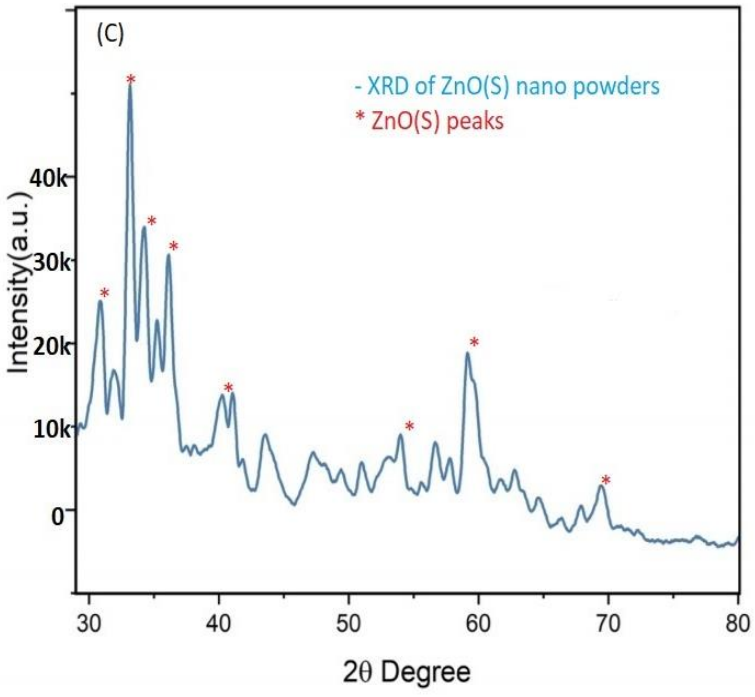

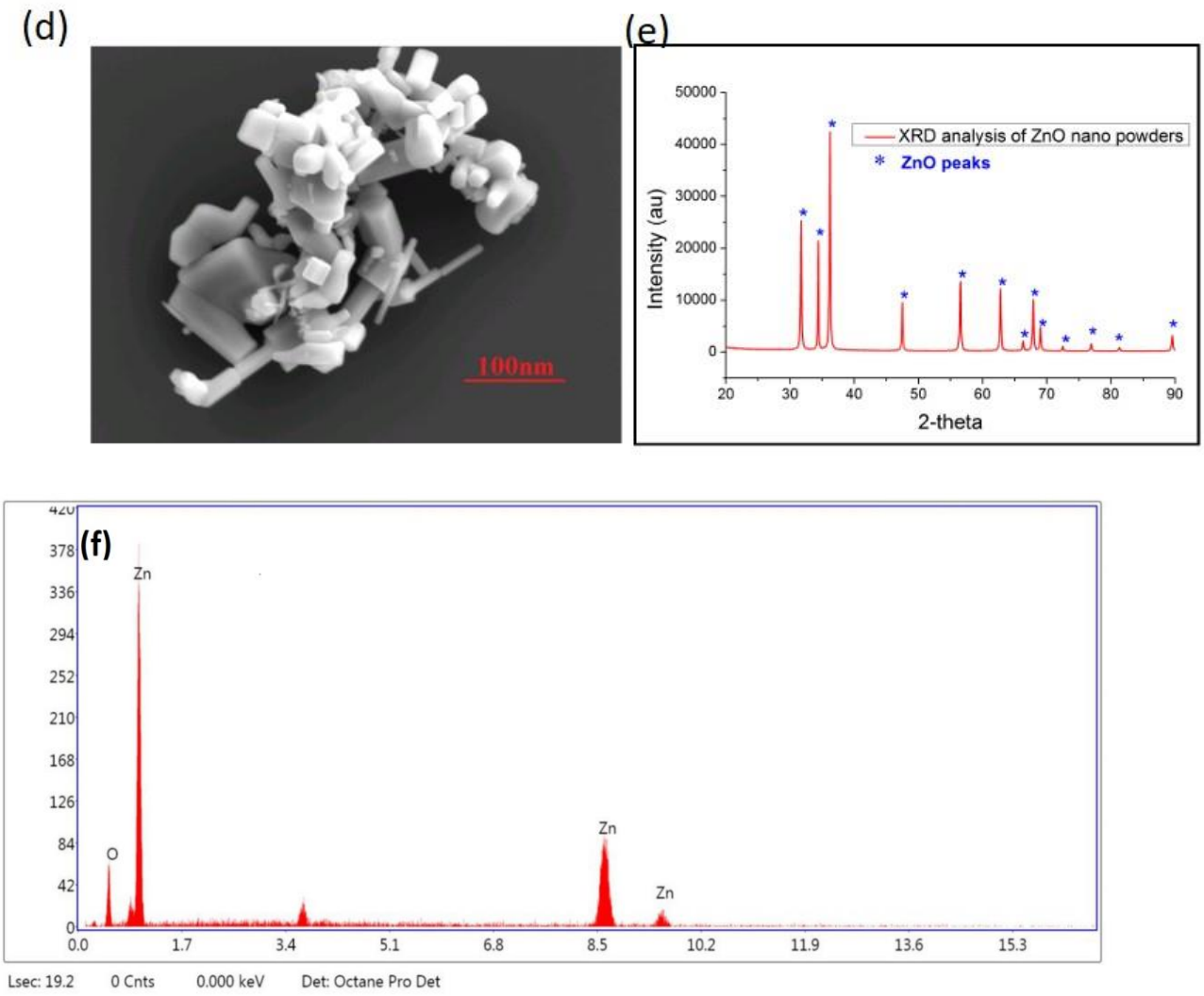

eZAF Smart Quant Results

Element	Weight %	Atomic %
O K	22.25	53.90
ZnK	77.75	46.10

Fig. 7.2 (a) SEM images of ZnO(S), (b) EDX of ZnO(S), (c) XRD of ZnO(s), (d) SEM image of ZnO(c), (e) XRD of ZnO(c) and (f) EDX of ZnO(c).

Table 7.1 Specification of the used ZnO nanoparticles

Physical properties	ZnO(S) spherical	ZnO(C) cylindrical
Purity	99.9 %	99.5 %
Molecular weight	81.408 g/mol	81.39 g/mol
Bulk density	0.69 g/cm^3	5.61 g/cm^3
Average particle size	50-80 nm	70 -85 nm
Physical form	Powder	Powder
Morphology	Spherical	Cylindrical
Colour	Milky white	Milky white

Fig. 7.2 depicts the dark I vs. V properties of organic devices based on natural dyes with ZnO nanoparticles of different morphology. For all of the described natural dyes, we have observed that the curves are significantly non-linear and have a rather modest dark current. However, the resulting current is noticeably larger when ZnO nanoparticles are combined with the dyes. There is a certain transition voltage after which current conduction varies among all the I-V characteristics we have seen. The device's threshold voltage (V_{th}) can be thought of as this specific bias voltage value. This voltage varies for different dye-based Schottky diodes.

Using thermionic emission theory, we can analyse the dark I vs V characteristics and current through the natural dye based organic semiconductor Schottky diode can be described as the following Eqs. (7.2-7.4) [32-37]:

$$I = I_0 \left(\exp\left(\frac{qV}{nkT}\right) - 1\right) \qquad (7.2)$$

where I_0 is the saturation current, given by

$$I_0 = AA^* T^2 \exp\left(-\frac{q\phi}{kT}\right) \qquad (7.3)$$

and

$$A^* = \left(\frac{4\pi q m^* k^2}{h^3}\right) \qquad (7.4)$$

Here A* is the Richardson constant, and its obtained value is 120 Acm^{-2} K^{-2} for organic beetroot dye and 32 Acm^{-2} K^{-2} for ZnO calculated from the saturation current of the device. From the interpolation of the exponential slope of current I at bias voltage V = 0, we can determine the

reverse saturation current. The barrier height at metal-organic semiconductor junction for all the natural dye-based devices with and without ZnO nanoparticles can be determined by the Eq. (7.5) [38-41]:

$$\phi = \frac{kT}{q} \ln \frac{AA^* T^2}{I_0} \qquad (7.5)$$

Figures 7.3(a)-3(b) illustrate the dark I-V characteristics of organic Schottky diodes based on herbal dyes with ZnO nanoparticles of different morphology. Considering all the dark I-V characteristics we noticed, the reported devices' higher current flow is caused by the presence of spherical zinc oxide nanoparticles. These increases in electric current can be attributed to the process of filling several traps. Many factors can affect the current conduction process through an organic device based on natural dyes. The existence of traps is the most crucial feature in these kinds of organic devices out of all of these. We are aware that organic compounds used to make natural dyes are amorphous, disordered solids with weak intermolecular interactions. Traps are a built-in feature of organic Schottky diodes that use natural dyes. Due to their random distribution between the HOMO and LUMO of the organic layers, these kinds of organic devices are trap-prone [42, 43]. There is an increase in current conduction in these devices when we introduce ZnO nanoparticles because they fill the traps.

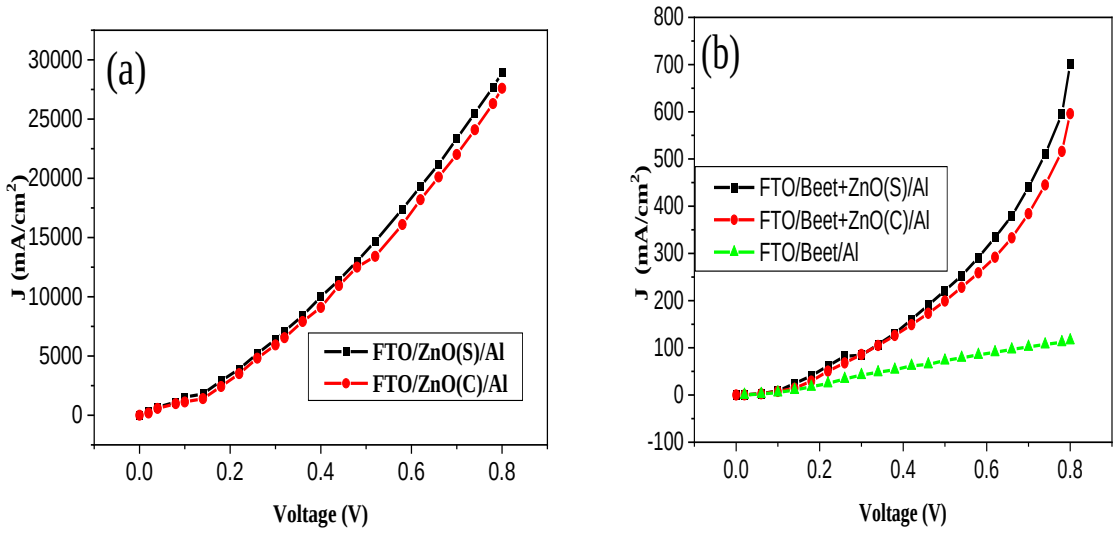

Fig. 7.3 (a) J-V characteristics of FTO/ZnO(s)/Al and FTO/ZnO(C)/Al Schottky diode. (b) J-V characteristics of FTO/Beet/Al with and without ZnO.

Fig. 7.4(a)–(b), respectively, displays the semi-logarithmic J–V characteristics of all the reported devices. When forward bias voltages are greater than kT/q, the saturation current for the given devices is revealed by extrapolating intercepts of all these numbers at zero bias. Using these saturation current values, we calculated the barrier heights (ϕ) of all the devices that were reported. As seen in Fig.4, the presence of zinc oxide (ZnO) nanoparticles causes saturation current (I_o) to increase, which lowers barrier heights.

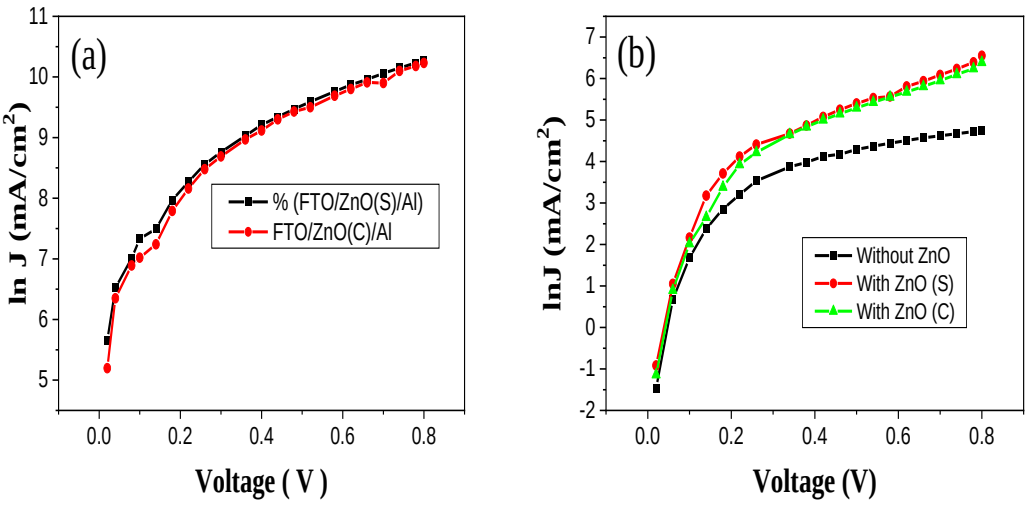

Fig. 7.4 Semi-logarithmic dark J-V characteristics (a) FTO/ZnO/Al (b) FTO/Beet/Al with and without ZnO.

Barrier heights of the reported FTO/Beet/Al and FTO/Beet+ZnO/Al devices can also be computed using Norde function. Norde function F (V) can be expressed as Eq. (7.6) [44, 45]:

$$F\,(V) = \left(\frac{V}{X}\right) - \frac{kT}{q}\ln\left(\frac{I(V)}{AA^{*}T^{2}}\right) \qquad (7.6)$$

where X is the first integer greater than n. I (V_0) is the value of current for which Norde function is minimum, and this minimum value of Norde function is F (V_0) where V_0 represents the

corresponding voltage. We have calculated the barrier height of the device in absence and presence of zinc oxide nanoparticles using the eq. (7.7).

$$\phi = F\,(V_0) + \left(\frac{V_0}{X}\right) - \frac{kT}{q} \qquad (7.7)$$

We can see in Fig. 7.5 from the plot of the Norde function that the introduction of zinc oxide nanoparticles causes the barrier height of the FTO/Beet/Al device to decrease, which is consistent with the values of barrier height calculated from the dark J-V characteristics of the reported device.

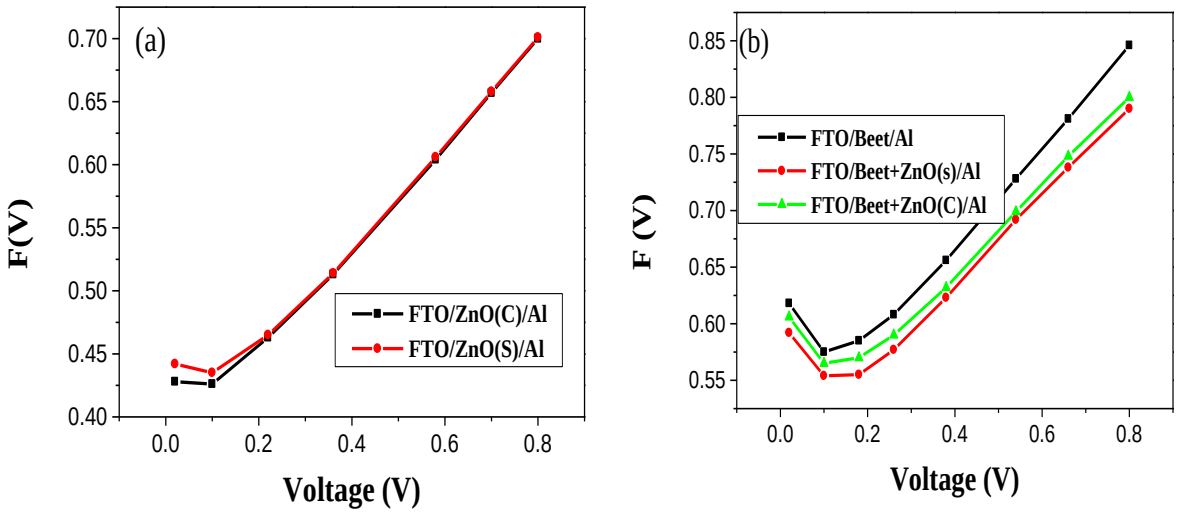

Fig. 7.5 Norde's function F(V) vs V plot of (a) FTO/ZnO/Al (b) FTO/Beet+ZnO/Al.

Fig. 7.6 depicts the variation of junction resistance (R_j = dV/dI) with bias voltage (V). The junction becomes lowest at a specific applied voltage, which is known as the device's series resistance (R_s). We can see from Fig. 7.5 that the value of R_s for FTO/ZnO(C)/Al is 1.86 Ω and for FTO/ZnO(S)/Al is 1.84 Ω. Again, the values of R_s for FTO/Beet/Al, FTO/Beet+ZnO(C)/Al and FTO/Beet+ZnO(S)/Al are 580 Ω, 60.6Ω and 51.7 Ω respectively. This demonstrates that the reduction in series resistance when ZnO nanoparticles with a spherical morphology are present is greater than when ZnO nanoparticles with a cylinder morphology are present.

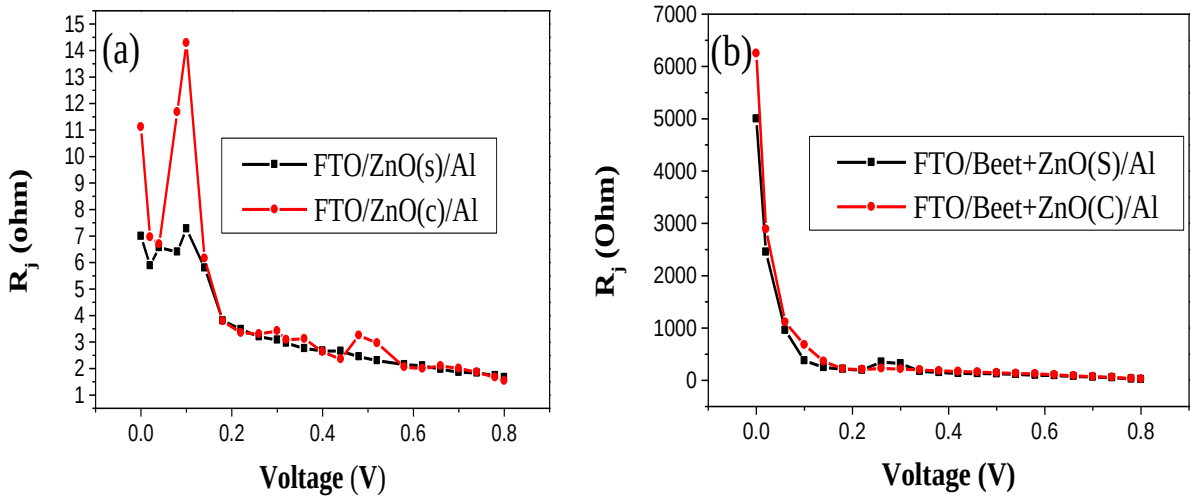

Fig. 7.6 Plot of variation of R_j with applied bias of (a) FTO/ZnO/Al (b) FTO/Beet + ZnO/Al.

We have calculated trap energy from the ln I - ln V plot of Al/Beet/Cu diode which shown in Fig. 7.7 The trap charge concentration N_t can be expressed as [46]

$$N_t(\varepsilon) = N_0 \exp\left[-\frac{\varepsilon}{kT}\right] \qquad (7.8)$$

where T_c is the temperature of the trap distribution and ε is the depth of traps below the conduction band mobility edge (i.e., $T_c = E_c / k$, where E_c is the typical trap energy). As T is the ambient temperature, $m = T_c / T$. Using the equation 14 [47], we were able to compute the trap energy.

$$E_c = mkT \qquad (7.9)$$

The value of m, which may be determined from the ln I- ln V plot shown in Fig. 6 of the reported Schottky diode, can be used to calculate the trap energy E_c. Traps play an important part in the current conduction process via the organic Schottky. The presence of traps causes the majority of charge carriers to become immobile [48-49]. An intrinsic resistance property emerges inside the organic Schottky diode as a result of these trapping states. In prior research we observed that the series resistance and trap energy for organic Schottky diodes based on herbal dyes are high enough [50-52]. Table 1 shows the values of electrical parameters of reported Schottky diodes measured in different methods. Due to the presence of ZnO nanoparticles, the values of R_s, E_c, ϕ and V_{th} are reduced in this table. This reduction is greater for spherical ZnO nanoparticles than for cylindrical ZnO nanoparticles.

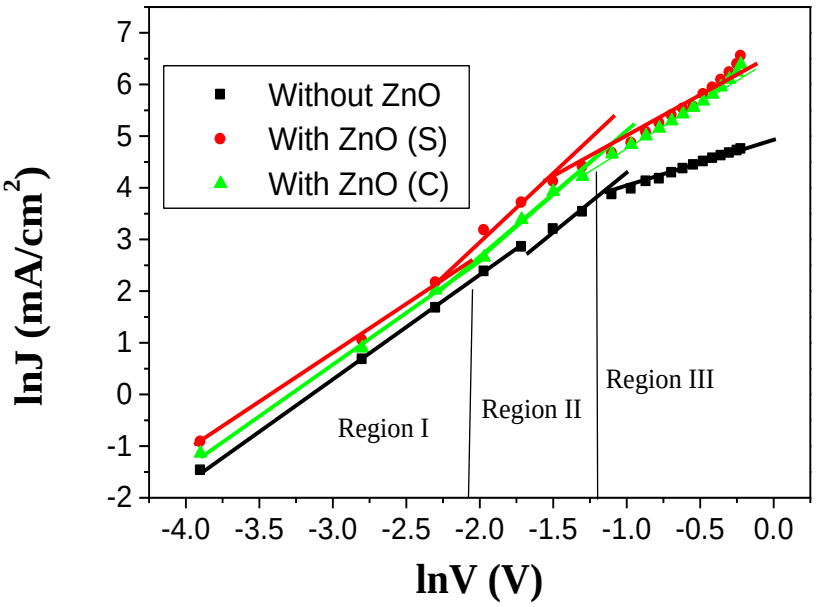

Fig. 7.7 ln I- ln V characteristics of Beetroot dye with and without ZnO nanoparticles.

Eqs. (7.10)-(7.12), which Cheung [53] derived from Eqs. (4) and (5) were used to calculate the series resistance (R_s), ideality factor(n) and barrier height (ϕ):

$$\frac{dV}{dln(I)} = (\frac{nkT}{q}) + IR_s \qquad (7.10)$$

$$H(I) = V - (\frac{nkT}{q}) \ln(\frac{I_0}{T^2AA^*}) \qquad (7.11)$$

and

$$H(I) = IR_s + n\phi \qquad (7.12)$$

The series resistance and ideality factor were calculated using the slope and intercept of the dV/dln(I) vs. I plot, and the potential barrier height was calculated using the intercept of the H(J) vs. J curve (Fig. 7.8). Table 7.2 shows the measured ϕ, n, R_s and V_{th} for FTO/ZnO/Al and FTO/Beet+ZnO/Al Schottky diodes in presence of ZnO nanoparticles with various morphologies. The ideality factor in these devices is not equal to one, indicating divergence from ideal behavior. This difference is most likely due to multigenerational recombination in the junction area via interface traps [54]. The values of ideality factor 1.77, 1.4 and 1.7 imply that the interface is not totally intimate metal-semiconductor, and that some trapping states in the interfacing layer must exist [55], which can act as localized generation-recombination centers. The density of trapping states grows as the disorder in the nanoparticle structure increases, resulting in a high ideality factor. Because the cylinder-like ZnO nanoparticles have

a more disorder structure, the ideality factor is larger here. FTO/ZnO(S)/Al and FTO/ZnO(C)/Al Schottky diodes have barrier heights of 0.43 and 0.49 eV respectively. Again, for FTO/Beet+ZnO(C)/Al and FTO/ Beet+ZnO(S)/Al Scottky diodes the barrier heights are 0.589 eV and 0.57 eV respectively. According to Schottky- Mott's hypothesis [56], the barrier height (ϕ) is closely correlated with the work function of the metal and the electron affinity of the semiconductor. The difference between the metal work function and semiconductors electron affinity at the Schottky limit is known as the barrier height [57]. The lnI vs. lnV graphs shown in Fig. 6 were used to demonstrate the implementation of charge transport mechanism. The slopes of these logarithmic characteristic curves reflect three distinct regions. Region I is represented by the bias voltage V< 0.26 Volt, where current varies virtually linearly. As a result, the region is ohmic, and quantum tunnelling outperforms thermionic emission for charge transport. Region-II, where current varies exponentially, is defined by a bias voltage ranging from 0.26 to 0.6 Volt. Charge transport in this region is mostly based on recombination tunnelling [58-60]. Region-III is represented by a bias voltage V> 0.6 Volt, in which maximal charge transportation occurs due to space charge limited current. By interfering with the mobility of carriers, the rate of recombination can be visualised. To gain a better understanding of the device interface carrier mobility, the slope of region-III evaluated. According to these slopes, the carrier mobility of a device based on spherical ZnO nanoparticles is larger than that of a device based on cylindrical ZnO nano particles. From the carrier mobility and electrical characteristic parameters shown in Table 1 we observed that spherical ZnO nanoparticles based organic device can perform better than cylindrical ZnO nanoparticles based organic device. Thus, to reduce the barrier height, series resistance and trap energy of an organic Schottky diode the spherical ZnO nanoparticles with regular structure can be more effective than cylindrical ZnO nanoparticles.

A comparison of suggested diodes to various previously reported Schottky diodes and Schottky diodes based on natural dyes is shown in Table 3. The values of n, R_s, ϕ and E_c are significantly better, as we have shown. Because of the high value of the beetroot molecule's dipole moment [14] and the presence of spherical ZnO nanoparticles, our reported FTO/Beetroot + ZnO(s) /Al diode performs significantly better than previously reported diodes. Table 4 Percentage error, mean and standard deviation values of electrical parameters of the natural herbal dye-based Schottky diodes.

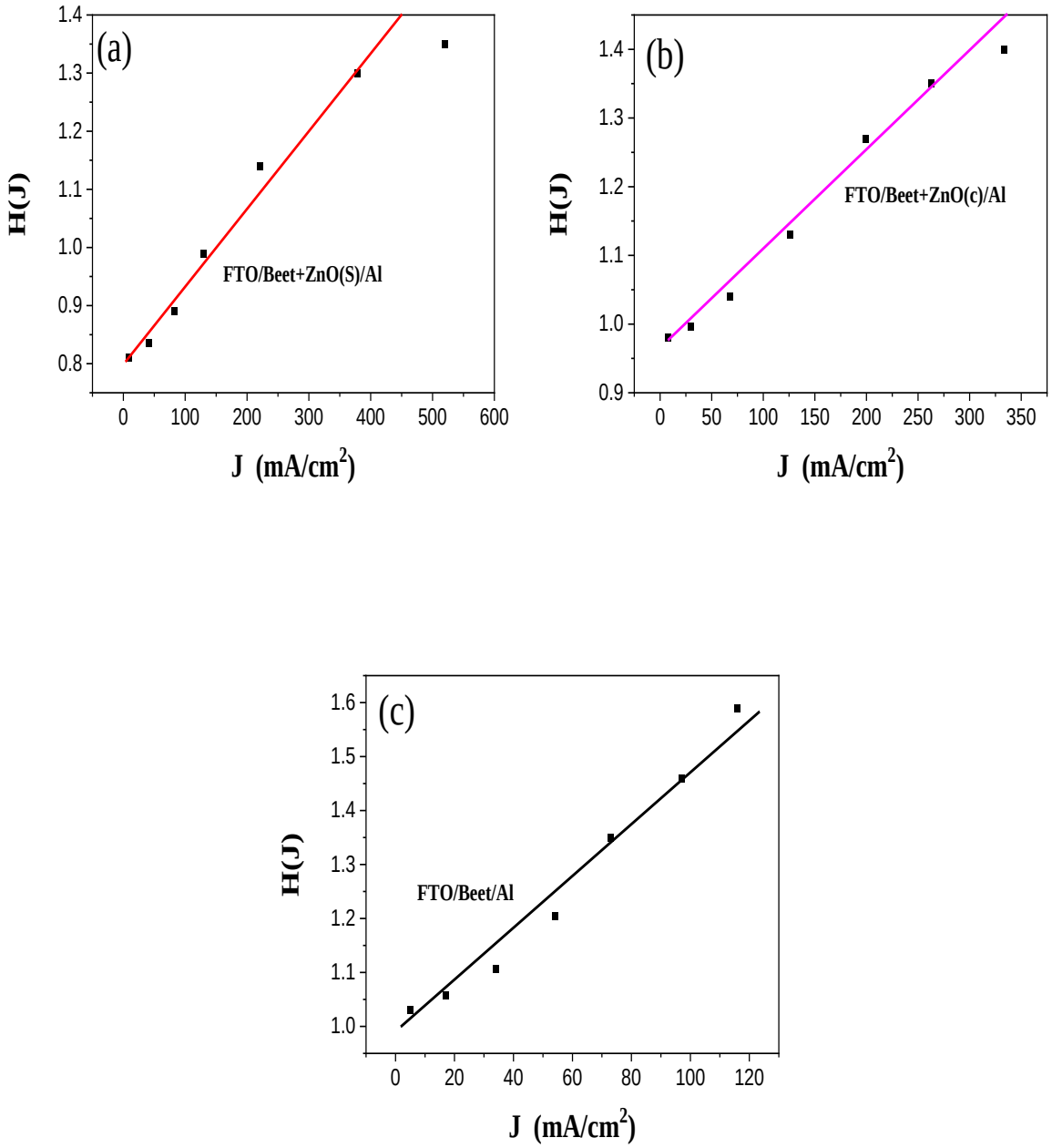

Fig. 7.8 H(J) vs J plot of (a) FTO/Beet+ZnO(S)/Al, (b) FTO/Beet+ZnO(C)/Al and (c) FTO/Beet/Al Schottky diodes.

Table 7.2 Electrical characteristic parameters of the reported Schottky diodes.

Methods	FTO/ZnO(S)/Al	FTO/ZnO(C)/Al	FTO/Beet/Al	FTO/Beet +ZnO(s)/Al	FTO/Beet +ZnO(C)/Al
From J-V	n = 1.65 ϕ = 0.43 Rs = 1.84	n = 1.68 ϕ = 0.49 Rs = 1.86	n = 1.77 ϕ = 0.65 Rs = 580	n = 1.4 ϕ = 0.6 Rs = 52	n = 1.7 ϕ = 0.62 Rs = 61
From H-J	ϕ = 0.42 Rs = 1.98	ϕ = 0.447 Rs = 2.1	ϕ = 0.62 Rs = 589	ϕ = 0.56 Rs = 98	ϕ = 0.60 Rs = 115
From Norde function	Φ = 0.45	Φ = 0.459	Φ = 0.598	Φ = 0.57	Φ = 0.589
Trap energy in eV	-	-	0.052	0.046	0.048

Table 7.3 Comparison of proposed diodes with some previously reported Schottky diodes and natural dye based Schottky diodes

Schottky	n	R_s	Φ (eV)	E_c (eV)
Organic Schottky [20-25]	2-11			
Al/L5 HZ-doped Schottky [19]	42.9, 18.8, 20	$3x10^6$, $2x10^7$, $1.2x10^7$Ω	0.78, 0.81, 0.75	
Al/Indigo/Cu [14]	11.65	0.43 MΩ	0.80	
Al/Turmeric/Cu [14]	6.56	8 KΩ	0.74	
Al/Beetroot/Cu [14]	4.5	1.1 KΩ	0.73	
Al/TiO_2/Cu [14]	3.75	198 K Ω	0.76	
FTO/ZnO(S)/Al [this work]	1.65	1.84 Ω	0.43	
FTO/Beetroot/Al [this work]	1.77	580.00 Ω	0.65	0.052
FTO/Beetroot+ZnO(S)/Al [this work]	1.40	98.00 Ω	0.60	0.046

Table 7.4 Percentage error, mean and standard deviation values of electrical parameters of the natural herbal dye-based Schottky diodes

Device	parameters	Mean	SD	Percentage Error (%)
FTO/Beetroot/Al	n	1.77	0.030	1.7
	Φ (eV)	0.623	0.026	4.2
	Rs (Ω)	584.50	6.36	1.1
	Ec (eV)	0.052	0.002	3.8
FTO/Beetroot+ZnO(c)/Al	n	1.70	0.06	3.5
	Φ (eV)	0.603	0.016	2.6
	Rs (Ω)	88	38.18	4.3
	Ec (eV)	0.0483	0.0015	3.1
FTO/Beetroot+ZnO(s)/Al	n	1.40	0.1	7.1
	Φ (eV)	0.58	0.021	3.6
	Rs (Ω)	75	32.53	4.3
	Ec (eV)	0.0463	0.0015	3.2

7.4 Conclusions

Different morphologies of ZnO nanoparticles have been used to make Schottky diodes. To examine the impact of ZnO nanoparticle architecture on the metal organic semiconductor surface, several device parameters were calculated. The calculated values of ideality factor (n), barrier height (Φ), trap energy (E_c), and series resistance (R_s) of FTO/Beetroot/Al have been 1.77, 0.65 eV, 0.052 eV, and 589, respectively. These values change to 1.7, 0.62 eV, 0.048 eV, and 61 when cylindrical ZnO is incorporated with beetroot dye. When spherical ZnO nanoparticles are used in place of cylinder-shaped ZnO, the values of n and R_s drop from 1.7 to 1.4 and 61 to 52, respectively. In the reported Schottky diodes, these were explained with the help of trap energy and carrier mobility. The electrical parameters were calculated in different methods. It was found that these methods were comparable to one another. As the data are reliable, we may draw the conclusion that using ZnO nanoparticles decreased the barrier height at the metal–organic interaction. The ZnO nanoparticles based organic and

inorganic Schottky diodes demonstrate that there are less trap energy and small series resistance with higher carrier mobility within the metal-organic semiconductor interface for the spherical morphology. Using spherical ZnO instead of cylindrical ZnO results in a 17% greater reduction in Rs. The disclosed devices' mobility and current conductivity are enhanced by this lowering. The ZnO nanoparticles used in this study are not perfectly spherical; if they were, this increase would be more obvious. Trap energy decreases significantly when spherical ZnO is utilized rather than cylindrical ZnO. Spherical ZnO nanoparticle injection results in a wide range of trap states being occupied, which lowers the trap energy and series resistance. The device conductivity increased and the threshold voltage was lowered as a result.

7.5 References

1. Roy VA, Djurišić AB, Chan WK, Gao J, Lui HF, Surya C. Luminescent and structural properties of ZnO nanorods prepared under different conditions. Applied physics letters. 2003 Jul 7;83(1):141-3.
2. Chen QH, Zhang WG. Continuous preparation of decorated nano zinc oxide organic sols with intense luminescence. Journal of non-crystalline solids. 2007 Mar 15;353(4):374-8.
3. Allen MW, Alkaisi MM, Durbin SM. Metal Schottky diodes on Zn-polar and O-polar bulk ZnO. Applied physics letters. 2006 Sep 4;89(10).
4. Middya S, Layek A, Dey A, Ray PP. Morphological impact of ZnO nanoparticle on MEHPPV: ZnO based hybrid solar cell. Journal of Materials Science: Materials in Electronics. 2013 Nov;24:4621-9.
5. Chen Y, Bagnall DM, Koh HJ, Park KT, Hiraga K, Zhu Z, Yao T. Plasma assisted molecular beam epitaxy of ZnO on c-plane sapphire: Growth and characterization. Journal of Applied Physics. 1998 Oct 1;84(7):3912-8.
6. Abdollahi Y, Abdullah AH, Zainal Z, Yusof NA. Synthesis and characterization of Manganese doped ZnO nanoparticles. International Journal of Basic & Applied Sciences. 2011;11(4):62-9.
7. Polyakov AY, Smirnov NB, Kozhukhova EA, Vdovin VI, Ip K, Heo YW, Norton DP, Pearton SJ. Electrical characteristics of Au and Ag Schottky contacts on n-ZnO. Applied physics letters. 2003 Aug 25;83(8):1575-7.
8. Yuan G, Ye Z, Zhu L, Huang J, Qian Q, Zhao B. Gold schottky contacts on n-type ZnO thin films with an Al/Si(100)substrates. Journal of crystal growth. 2004 Jul 15;268(1-2):169-73.
9. Von Wenckstern H, Kaidashev EM, Lorenz M, Hochmuth H, Biehne G, Lenzner J, Gottschalch V, Pickenhain R, Grundmann M. Lateral homogeneity of Schottky contacts on n-type ZnO. Applied physics letters. 2004 Jan 5;84(1):79-81.
10. Ip K, Gila BP, Onstine AH, Lambers ES, Heo YW, Baik KH, Norton DP, Pearton SJ, Kim S, LaRoche JR, Ren F. Improved Pt⁄Au and W⁄Pt⁄Au Schottky contacts on n-type ZnO using ozone cleaning. Applied physics letters. 2004 Jun 21;84(25):5133-5.
11. Ip K, Heo YW, Baik KH, Norton DP, Pearton SJ, Kim S, LaRoche JR, Ren F. Temperature-dependent characteristics of Pt Schottky contacts on n-type ZnO. Applied Physics Letters. 2004 Apr 12;84(15):2835-7.
12. Zhang J, Sun, Yin, Su H, Liao, Yan. Control of ZnO morphology via a simple solution route. Chemistry of Materials. 2002 Oct 21;14(10):4172-7.

1 3. Ahmad AA, Alsaad AM, Aljarrah IA, Al-Bataineh QM, Telfah AD. Optical, electronic, and structural properties of different nanostructured ZnO morphologies. The European Physical Journal Plus. 2022 Jun 30;137(6):752.

14. Das AK, Mandal R, Mandal DK. The current transport mechanism of Al/Beetroot/Cu used as an organic semiconductor Schottky diode is superior than natural dye-based thin film devices. Microelectronic Engineering. 2022 May 15;261:111816.

15. Das AK, Mandal R, Chakraborty K, Mandal DK. Impact of ZnO nanoparticles on electrical characteristics of herbal dye-based organic Schottky diode. Bulletin of Materials Science. 2022 Aug 23;45(3):164.

16. Das AK, Mandal R, Chakraborty K, Mandal DK. Electrical Characteristics of a Turmeric Dye-Based Organic Thin Film Device and the Effect of Light on Barrier Height. Materials Proceedings. 2022 Aug 9;10(1):11.

17. Das AK, Mandal R, Chakrabarty K, Mandal DK. IJIKC ISSN **7** 2454-2415(2019).

18. Das AK, Mandal R, Mandal DK. Impact of HTM on lead-free perovskite solar cell with high efficiency. Optical and Quantum Electronics. 2022 Jul;54(7):455.

19. Olyaee HG, Foot PJ, Montgomery V. Electrical properties and I–V characteristics of 5, 14-dihydro-5, 7, 12, 14-tetraazapentacene doped Schottky barrier diode. Journal of Theoretical and Applied Physics. 2015 Dec;9:315-9.

20. Kanicki J. METAL-POLYACETYLENE SCHOTTKY BARRIER DIODES. Molecular crystals and liquid crystals. 1983 Mar 1.

21. Grant PM, Tani T, Gill WD, Krounbi M, Clarke TC. Properties of metal/polyacetylene Schottky barriers. Journal of Applied Physics. 1981 Feb 1;52(2):869-72.

22. Turut A, Köleli F. Semiconductive polymer-based Schottky diode. Journal of applied physics. 1992 Jul 15;72(2):818-9.

23. Nazarova IB, Krinichnyi VI, Goldenberg LM. Schottky diodes based on poly (p-phenylene) and poly (1, 4-dipyrrolobenzene). Synthetic metals. 1993 Feb 1;53(3):399-402.

24. Misra SC, Chandra S. Electronic applications of semiconducting polymers. Indian J.Chem 1994 **33A**, 583

25. Chen SA, Fang Y, Lee HT. Polyacrylic acid-doped polyaniline as p-type semiconductor in Schottky barrier electronic device. Synthetic metals. 1993 Apr 12;57(1):4082-6.

26. Chakraborty K, Das AK, Mandal R, Mandal DK, Transactions of Tianjin University2020 **26**, 265

27. Chakraborty K, Das A, Mandal R, Mondal DK. Interpretation of trap-assisted conduction with estimation of electrical parameters of thin indigo film-based semiconducting device. Bulletin of Materials Science. 2021 Jun;44(2):92.
28. Sen S, Manik NB. Effects of two different solvents on Schottky barrier of organic device. Journal of Physics Communications. 2021 Sep 24;5(9):095010.
29. Al-Ahmadi NA. Metal oxide semiconductor-based Schottky diodes: a review of recent advances. Materials Research Express. 2020 Mar 9;7(3):032001.
30. Scherrer PJ. Estimation of the size and internal structure of colloidal particles by means of röntgen. Nachr. Ges. Wiss. Göttingen. 1918;2:96-100.
31. Langford JI, Wilson AJ. Scherrer after sixty years: a survey and some new results in the determination of crystallite size. Journal of applied crystallography. 1978 Apr 1;11(2):102-13.
32. Svensson J, Campbell EE. Schottky barriers in carbon nanotube-metal contacts. Journal of applied physics. 2011 Dec 1;110(11).
33. Sen S, Manik NB. Effect of back electrode on trap energy and interfacial barrier height of crystal violet dye-based organic device. Bulletin of Materials Science. 2020 Dec;43(1):60.
34. Sen S, Manik NB. Effect of carboxyl-functionalized single walled carbon nanotubes on the interfacial barrier height of malachite green dye based organic device. Physics International. 2019 Jan 1;10(1):1-7.
35. Shah M, Karimov KS, Ahmad Z, Sayyad MH. Electrical characteristics of A1/CNT/NiPc/PEPC/Ag surface-type cell. Chinese Physics Letters. 2010 Oct 1;27(10):106102.
36. Harrabi Z, Jomni S, Beji L, Bouazizi A. Distribution of barrier heights in Au/porous GaAs Schottky diodes from current–voltage–temperature measurements. Physica B: Condensed Matter. 2010 Sep 1;405(17):3745-50.
37. Al-Ta HM. ii, YM Amin and V. Periasamy. Sensors. 2015;15:3.
38. Yildirim MN, Karaman A, Alca IK. Determination of the mechanical behavior of laminated wood products under different temperatures. Pro Ligno. 2020 Dec 1;16(4).
39. Güzeldir B, Sağlam M, Ateş A, Türüt AB. Determination of the some electronic parameters of nanostructure copper selenide and Cu/Cu3Se2/n-GaAs/In structure. Journal of Alloys and Compounds. 2015 Apr 5;627:200-5.
40. Sen S, Manik NB. Characterization of Electrical Parameters of Copper Phthalocyanine Based Organic Electronic Device in Presence of Fullerene Nanoparticles. Advanced Materials Research. 2021 Dec 9;1167:35-42.

41. Islam ZU, Tahir M, Syed WA, Aziz F, Wahab F, Said SM, R. Sarker M, Md Ali SH, Sabri MF. Fabrication and photovoltaic properties of organic solar cell based on zinc phthalocyanine. Energies. 2020 Feb 21;13(4):962.
42. Haldar A, Maity S, Manik NB. Effect of C 60 on methyl red and crystal violet dye-doped photovoltaic device. Ionics. 2008 Jun;14:263-7.
43. Scher H, Montroll EW. Anomalous transit-time dispersion in amorphous solids. Physical Review B. 1975 Sep 15;12(6):2455.
44. Das AK, Manik NB, Mandal R, Mandal DK. The impact of the shape of zinc oxide nanoparticles on electrical parameters of natural dye-based FTO/Beetroot/Al Schottky diode. Journal of Materials Science: Materials in Electronics. 2023 Sep;34(25):1745.
45. Harrabi Z, Jomni S, Beji L, Bouazizi A. Distribution of barrier heights in Au/porous GaAs Schottky diodes from current–voltage–temperature measurements. Physica B: Condensed Matter. 2010 Sep 1;405(17):3745-50.
46. Yang J, Meisner GP, Chen L. Strain field fluctuation effects on lattice thermal conductivity of ZrNiSn-based thermoelectric compounds. Applied physics letters. 2004 Aug 16;85(7):1140-2.
47. Haldar A, Maity S, Manik NB. Effect of back electrode on photovoltaic properties of crystal-violet-dye-doped solid-state thin film. Ionics. 2008 Sep;14:427-32.
48. Chakraborty S, Manik NB. Effect of single walled carbon nanotubes on the threshold voltage of dye based photovoltaic devices. Physica B: Condensed Matter. 2016 Jan 15;481:209-16.
49. Kawano K, Sakai J, Yahiro M, Adachi C. Effect of solvent on fabrication of active layers in organic solar cells based on poly (3-hexylthiophene) and fullerene derivatives. Solar Energy Materials and Solar Cells. 2009 Apr 1;93(4):514-8.
50. Chakraborty K, Das A, Mandal R, Mondal DK. Interpretation of trap-assisted conduction with estimation of electrical parameters of thin indigo film-based semiconducting device. Bulletin of Materials Science. 2021 Jun;44(2):92.
51. Chakraborty K, Das AK, Mandal R, Mondal DK. Transactions of Tianjin University 2020 **26,** 265 .
52. Chakraborty K, Das A, Mandal R, Mandal DK. An analytical study on low voltage regime of natural organic semiconductor based device: Physics of trap energy and ideality factor. Solid State Communications. 2021 Jan 1;323:114080.
53. Cheung SK, Cheung NW. Extraction of Schottky diode parameters from forward current-voltage characteristics. Applied physics letters. 1986 Jul 14;49(2):85-7.

54. Campos M, Bulhoes LD, Lindino CA. Gas-sensitive characteristics of metal/semiconductor polymer Schottky device. Sensors and Actuators A: Physical. 2000 Dec 1;87(1-2):67-71.
55. Yakuphanoglu F. Electrical characterization and interface state density properties of the ITO/C70/Au Schottky diode. The Journal of Physical Chemistry C.2007Jan 25;111(3):1505-7.
56. Schottky W. Halbleitertheorie der sperrschicht. Naturwissenschaften. 1938 Dec;26(52):843-.
57. Mott NF. Note on the contact between a metal and an insulator or semi-conductor. InMathematical Proceedings of the Cambridge Philosophical Society 1938 Oct (Vol. 34, No. 4, pp. 568-572). Cambridge University Press.
58. Koteeswara Reddy N, Ahsanulhaq Q, Kim JH, Hahn YB. Behavior of n-ZnO nanorods/p-Si heterojunction devices at higher temperatures. Applied Physics Letters. 2008 Jan 28;92(4).
59. Klason P, Nur O, Willander M. Electrical characteristics and stability of gold and palladium Schottky contacts on ZnO nanorods. Nanotechnology. 2008 Oct 29;19(47):475202.
60. Kim DC, Han WS, Cho HK, Kong BH, Kim HS. Multidimensional ZnO light-emitting diode structures grown by metal organic chemical vapor deposition on p-Si. Applied Physics Letters. 2007 Dec 3;91(23).

Chapter 8

Conclusion

8.1 Summary

8.2 Findings

8.3 Conclusion

8.4 Scope of the future work

8.1 Summary

The primary objective of this thesis is to explore the semiconducting properties of natural dye-based organic materials and investigate the **charge transport mechanisms in natural dye-based organic semiconductor Schottky diodes**. In this thesis, we explore the semiconducting behaviour of natural herbal dyes, specifically Indigo, Turmeric, and Beetroot. These dyes are less studied compared to other organic materials like Polyacetylene. To analyse their electrical properties, we have fabricated metal-organic semiconductor junction devices (Al / Indigo / Cu, Al / Turmeric / Cu, and Al / Beetroot / Cu) and examined their dark I-V characteristics. Additionally, we determined the band gap of the dye molecules using absorption spectra, which lying within the semiconductor range. Finally, we discuss the charge transport mechanism in natural dye-based organic Schottky diodes. Furthermore, we have done a comparative study on the electrical conductivity, and carrier mobility of organic semiconductor Schottky diodes based on natural dyes.

The electrical characteristics of the devices have been evaluated using I-V characteristics, Cheung function, and Norde function measurements. For the current transport mechanism, we have discussed Schottky Emission (SE), Poole-Frenkel effect (PFE), Gaussian Distribution (GD), and quantum tunnelling. We have also calculated the insulating temperature of our fabricated devices, and some experimental results have been verified through simulation studies.

The performance and applications of natural dye-based organic semiconductor devices in optoelectronics are limited by high barrier height, high series resistance, high trap energy, and low current conduction at the metal-organic semiconductor interface. One way to address these challenges is by incorporating nanoparticles, such as zinc oxide (ZnO), into the organic layer.

This thesis investigates the impact of ZnO nanoparticles on the electrical characteristics of organic Schottky diodes derived from herbal dyes. The results for natural herbal dye-based organic Schottky diodes have been compared with previously reported typical organic Schottky diodes. Additionally, this thesis explores potential explanations for the observed impact of ZnO nanoparticle's shape on organic Schottky diodes.

We have designed our present work into eight chapters.

The ***Chapter 1*** establishes the goal of the research. This chapter presents simplified discussions of the interwork covered in the thesis. The purpose of this study is to discuss the analytical

explanation of the charge transfer mechanism via the natural digest organic semiconductor Schottky diode. This chapter has covered the overall introduction, motivation, and aims of the entire study. The significance of the present work is also discussed. The overall structure of the thesis study has also been detailed.

Chapter 2 provides a detailed overview of Schottky diodes based on organic semiconductors. Review of previous history including notable studies with theoretical and experimental clarification has been clarified. The properties of organic semiconductors are divided into two groups: electrical structure and chemical properties. The focus has been on the exciton production process and its subsequent recombination. A thorough description of the various recombination processes has also been discussed. It has been stated that the cause of recombination at the interfacial regime is Langevin recombination. On the other hand, photons are produced by thermal agitation caused by Auger recombination. The focus has been on various experimental and theoretical modeling approaches related to the charge transport mechanism in organic semiconductors. CTE generation, dissociation, and charge conduction with various recombination types are generally discussed. We have also been discussed about the ZnO nanoparticles in thin film electronics.

The detailed fabrication and characterization of the Al/Turmeric/Cu diode presented in this work were covered in ***chapter 3*** of this thesis. The experiment's excellent outcome demonstrates how to improve the device's rectification ratio. Our obtained rectification ratio (asymmetry) of 30 at the 4V bias voltage. The conclusion drawn from the energy gap between HOMO and LUMO of the curcumin molecule and temperature dependent I-V characteristics observation is that the turmeric dye molecule behaves like a semiconductor. Al/Turmeric/Cu device's series resistance reduces as temperature rises and the presence of light also reduces the threshold voltage. So, the device might be accepted in optoelectronic applications based on the calculated values of nonlinearity, sensitivity.

In ***chapter 4***, we have fabricated Al/Beetroot/Cu device for the first time and conclude that the electrical characteristics of an organic thin-film device based on herbal dyes that works as a Schottky diode at room temperature and as a MIM below 140 K. Our device's ideality factor of 4.5 and maximum asymmetry of 17.6 at 0.85 V establish it as a viable option for use as an organic Schottky diode in rectifying applications. The device performs better than the organic Schottky diodes that have been previously reported. Additionally, we have fabricated an Al/TiO_2/Cu surface type Schottky diode in this chapter to compare it with organic dye-based

organic diodes. First conclusion of this chapter is semiconducting behaviour of beetroot dye molecules which is one of the primary goals of this investigation. In this Al/Beetroot/Cu device, quantum tunnelling and trap-assisted current conduction were observed. We also observed that GD and SE might work well in the charge transportation mechanism. There is a theoretical prediction of this device's insulating temperature. Finally, we have conducted a comparative analysis of various natural dye-based thin-film diodes and observed that Al/beetroot/Cu exhibits markedly better electrical properties than our fabricated indigo and turmeric based devices.

Chapter 5 covered the in-depth construction of a thin-film diode based on natural dyes, in which Ag is substituted with Cu and natural dye layers (betanin, curcumin, and indigo) for Al_2O_3. We have also fabricated another (Al/TiO_2/Cu) diode under the same ambient conditions, and we have compared the rectifying parameters of these two diodes. In order to confirm experimentally the observation of quantum tunnelling through the current conduction mechanism of a series of natural dye based Schottky diodes, this work compares all of the Schottky diodes based on natural dyes. We have found that a single layer Al/Beet/Cu diode has the highest sensitivity of 25.7 A/W at 0.7 V and a superior low bias asymmetry of 18 at 0.85 V, which makes it a good option for high-speed optoelectronic use. In this study, the trap density, carrier density, and mobility of the active layer (beetroot dye) were measured using Poisson's equation. Once more, we proposed a one-dimensional organic semiconductor Schottky diode based on natural dyes. We also covered simulation studies in this chapter to confirm the experimental findings. The electrical properties obtained from the simulated and experimental data are fairly similar to each other.

ZnO was selected for incorporation into the organic Schottky diode based on herbal dyes due to all of the aforementioned fascinating characteristics which we have discussed in ***Chapter 6***. We have fabricated various natural herbal dye-based organic Schottky diodes using viscous PVA solution to dissolve each of the aforementioned dyes. ZnO nanoparticles were then added to each of the herbal pigments to create the organic Schottky devices. The series resistance (R_s), trap energy (E_c), barrier height (ϕ_b), threshold voltage (V_{th}), and trap energy (E_c) for both kinds of fabricated diodes have been calculated. The interfacial barrier height at the metal-organic dye contact is used to calculate the barrier height (ϕ_b) of an organic Schottky diode at that junction. Within this ***chapter 6*** lastly, we have investigated a comparative study of the electrical properties of three natural dye-based thin-film diodes and found that the

Al/beetroot/Cu device performs substantially better than our fabricated Al/indigo/Cu and Al/turmeric/Cu devices. The work will be beneficial in enhancing knowledge about the potential uses of herbal dyes going forward and the importance of ZnO nanoparticles in various optoelectronic devices development applications.

Organic semiconductor diodes based on natural dyes have many benefits over inorganic semiconductor diodes, such as improved performance, affordability, lightweight design, biocompatibility, tuneable features, flexibility, and versatility. But as we have seen in some literature and in our discussed chapters, the values of Rs, n, and ϕ for organic semiconductor Schottky diodes based on natural herbal dyes are sufficiently high. Thus, one of the main goals of this study is to reduce the values of Rs, n, and ϕ. We have incorporated ZnO nanoparticles with beetroot dye to create an organic semiconductor Schottky diode based on a natural herbal beetroot dye. This shows a significant decrease in the R_s, n, and ϕ of the Schottky diode. which increase the Schottky diode's mobility and current conduction through the use of natural beetroot dye. However, ZnO nanoparticles come in a variety of geometrical shapes. The goal at this point is to identify the more effective ZnO nanoparticle forms which we have discussed in ***Chapter 7***. Thus, we have used two different morphological (spherical and cylindrical) nanoparticles. It has been observed that spherical ZnO nanoparticles reduce Rs, ϕ, Ec and n more than cylindrical ZnO nanoparticles do for both types of Schottky diodes.

8.2 Findings

The entire work involves in charge transport mechanism of natural dye-based organic semiconductor Schottky diodes. For this we have fabricated and characterized the natural dye-based organic semiconductor Schottky diodes. We observed that the I-V characteristics of all the three natural dye-based diodes discussed here are asymmetric in nature. The electronic parameters of Al/Turmeric/Cu Schottky diode have been evaluated at first by current-voltage method at room temperature. Also, the electronics properties of Al/Turmeric/Cu device have been investigated by temperature dependent current-voltage (I-V) measurements at different temperature using another diode. The average values of ideality factor, series resistance and shunt resistance have been observed to be about 6.562, 8 kΩ and 105 kΩ, respectively, from forward bias current-voltage characteristics. High value of Rectification Ratio as found to be maximum 30 at 4 V indicates that this junction has potential to be used as a good rectifier. As the diode shows high rectification ratio at low voltage, this may be used as a good rectifier at

low voltage application. The maximum sensitivity was found $0.1V^{-1}$ under an applied bias 5V and $4.3V^{-1}$ at -2V. The interesting result obtained in this present work is that the series resistance decreases with temperature and current increases with temperature. At 65^oCR_s is 56 kΩ and at 28^oCR_s is 1.06 MΩ and the energy difference between HOMO and LUMO is 2.95 eV (at 420 nm). These findings indicate that turmeric behaves like a semiconductor and has a potential to be used as organic semiconductor diode. Turmeric contains diarylheptanoids and phenolic compounds. These molecules contribute to its semiconducting behaviour. Also, it is suggesting that this diode can be used as a good rectifier in electronics and solar cell applications.

Then the development and characterization of Al/Beetroot/Cu device has been presented. The electronic parameters of the diode are retrieved using a thermionic emission approach from the I-V characteristics. Furthermore, the computed values of ideality factor (n), barrier height (ϕ) and series resistance (Rs) of Al/Beetroot/Cu using the Cheung and Cheung functions are 4.5, 0.73 eV and 1.10 KΩ, respectively. The values of R_s in these two different approaches are very similar (shown in table 1), but a discrepancy in values of n confirms the existence of high R_s and high interface state density. The band gap of the betanin molecule present in beetroot is 2.1 eV. The electronic properties of the Al/beetroot/Cu device have been investigated in the temperature range 293-323 K and the findings shown in Table 8.1. These findings indicate that the betanin molecule is a semiconductor with a band gap lower than TiO_2, and the linear behaviour of the ϕ vs 1/n graph confirms the device is a Schottky diode. Moreover, we found that the reverse leakage current is dominated by Schottky emission (SE) over Poole-Frenkle emission (PFE), and from the temperature dependent I-V, the values of β are noticeably closer to β_{SE} than β_{PFE}. Which concludes from the findings of the Table 8.3 and Table 8.4 that at high temperature SE is dominant PFE and at very low temperature PFE dominant SE. At 140 K, the beetroot dye behaves like an insulator and the quantum tunnelling effect dominates over the thermionic emission. On the other hand, at room temperature, the dye behaves like a semiconductor and thermionic emission dominates quantum tunnelling. As a result, at room temperature and higher, the device could be a Schottky diode. The G(V) vs V plot was used to explain the existence of the dye's trapping effect. There is a significant reduction in R_s, E_c, and ϕ that has been gained in the use of beetroot dye over some previously reported organic dyes which shown in Table 8.5. When we utilise beetroot dye instead of indigo dye, the value of n and Rs decreases from 11.65 to 4.5 and 430 KΩ to 1.1 KΩ, respectively, according to the comparison analysis. The trap energy drops from 0.0732 to 0.021 eV once more. The

theoretically estimated value of the insulating temperature for Al/Beetroot/Cu is 133 K. As a result, we may conclude that Al/Beetroot/Cu exhibits significantly better electrical properties than herbal dye-based thin film diodes such as Al/Turmeric/Cu and Al/Indigo/Cu.

Table 8.1 The calculated electrical parameters of Al/Beetroot/Cu in two different methods.

Method	Barrier height(φ)	Series Resistance(Rs)	Ideality factor(n)
I-V Experimental	0.73 eV	1.46 KΩ	9.5
dV/dlnI vs I		1.10 KΩ	4.5
H (I) vs I	0.751 eV	1.087 KΩ	

Table 8.2 Temperature dependent electrical parameters of Al /Beetroot /Cu.

Temperature (K)	Barrier height(φ) eV	Series Resistance (Rs) KΩ	Ideality factor(n) from I-V
293	0.22	333	15.1
298	0.25	173	12.1
308	0.41	80	9.1
313	0.57	45	8.7
318	0.61	27	8.4
323	0.72	10.53	7.1

Table 8.3 Represents the comparison of theoretical and experimental value of β for three natural dye based thin film diode.

Thin film diode	Experimental β ($eVm^{1/2} V^{-1/2}$)	Theoretical β_{SE} ($eVm^{1/2} V^{-1/2}$)	Theoretical β_{PFE} ($eVm^{1/2} V^{-1/2}$)
Al/Beetroot/Cu	$3.069x10^{-5}$	$2.25x10^{-5}$	$4.5x10^{-5}$
Al/Indigo/Cu	$0.45x10^{-5}$	$1.825x10^{-5}$	$3.65x10^{-5}$
Al/Turmeric/Cu	$0.52x10^{-5}$	$0.514x10^{-5}$	$1.013x10^{-5}$

Table 8.4 Represents temperature dependence of β for Al/Beetroot/Cu

Temperature (K)	293	298	308	313	318	323
β ($eVm^{1/2} V^{-1/2}$)	$0.59x10^{-5}$	$0.53x10^{-5}$	$0.65x10^{-5}$	$0.71x10^{-5}$	$0.78x10^{-5}$	$0.89x10^{-5}$

Table 8.5 Values of E_c and barrier height for different dyes used in organic Schottky device.

Device and used dye	Trap energy (E_c) in eV	Barrier height from I-V in eV	Series resistance (s) in kΩ
ITO/CV/Al [52]	0.044	0.80	
ITO/CV/Al-M [52]	0.034	0.77	
Al/Turmeric/Cu [53]	0.028	0.825	
Al/Indigo/Cu[45]	0.073	0.87	127
ITO/RB/Al-M [55]	0.086	0.95	202
ITO/MR/Al-M[55]	0.076	0.99	439
Al/Beetroot/Cu [this work]	0.021	0.732	1.1 and 1.46

Again, for this Al/Beetroot/Cu device f_{NL}> 3 and f_{SENS}> 7 A/W, and from the Table 8.6 using the FOMs of the diode we may conclude that, the diode has a great potential to the researchers in energy harvesting rectifier application. In order to have a predictive behaviour and to have a better understanding of the physical processes and mechanisms influencing the effectiveness of the appliance under examination. Significant consistency has been obtained in experimental observation and simulation study. From the parabolic behaviour of the dI/dV vs V plot we may conclude that all the three natural dye-based Schottky diodes may affected in some way by the quantum tunnelling phenomena. Two different linear zones with varying slopes of ϕ vs n graph for Al/Beetroot/Cu device demonstrates the existence of two different charge transport processes corresponding to two different temperature ranges. Which concludes that the GD model could be useful.

Table 8.6 FOMs comparison between natural dye-based diodes with Al/TiO_2/Cu

diode	I (μA) at 2V	f_{ASYM}	f_{NL}	f_{SENS} (A/W)	Zero bias resistance
Al/Indigo/Cu	0.6	Increases with bias	3	0.4	2.57MΩ
Al/Turmeric/Cu	300	30	1.9	4.3	12.8kΩ
Al/Beet/Cu	1180	17.6	5.998	25.7	23.26kΩ
Al/TiO_2/Cu	8	Increases with bias		0.4	436kΩ

Again, we observed that due to the incorporation of ZnO nanoparticles the R_s, n, and ϕ of the Schottky diode have significantly decreased, which increase the charge carrier's mobility and current conduction in the natural beetroot dye-based Schottky diode. The findings on the impact of ZnO nanoparticles on electrical characteristics of herbal dye based organic Schottky diode shown in Table 8.7 and these findings conclude that, when ZnO nanoparticles are injected, they occupy a wide range of trap states, which reduces the trap energy (E_c) and series resistance (R_s). As a result, the threshold voltage (V_{th}) was decreased, and the device's electrical

conductivity improved. Finally, we observed the influence of ZnO nanoparticle morphology on various electrical properties of the organic semiconductor Schottky diodes based on herbal dyes and the findings are shown in Table 8.8.

Table 8.7. Findings of different electrical parameters of the natural dye-based devices with and without ZnO nanoparticles.

Device	**V_{th} (volt)**	**R_s (KΩ)**	**E_c (eV)**	**ϕ (eV) from I-V characteristics**	**ϕ(eV) using Norde function**
Al/Beet/Cu	0.74	1.46	0.021	0.75	0.78
Al/Beet+Zno/Cu expt1	0.45	0.92	0.016	0.72	0.75
Al/Beet/Cu	1.02	48.78	0.036	0.732	
Al/Beet+Zno/Cu Expt2	0.8	20.62	0.032	0.72	
Al/Turmeric/Cu	1.07	8	0.031	0.738	
Al/Turmeric+ZnO/Cu	0.5	3	0.025	0.715	
Al/Indigo/Cu	1.5	430	0.045	0.802	
Al/Indigo+ZnO/Cu	0.65	210	0.042	0.78	

Table 8.8 Findings of electrical characteristic parameters of the reported Schottky diodes with the incorporation of spherical and cylindrical ZnO nanoparticles.

Methods	**FTO/ZnO(S)/Al**	**FTO/ZnO(C)/Al**	**FTO/Beet/Al**	**FTO/Beet +ZnO(s)/Al**	**FTO/Beet +ZnO(C)/Al**
From J-V	n = 1.65 ϕ = 0.43 Rs = 1.84	n = 1.68 ϕ = 0.49 Rs = 1.86	n = 1.77 ϕ = 0.65 Rs = 580	n = 1.4 ϕ = 0.6 Rs = 52	n = 1.7 ϕ = 0.62 Rs = 61
From H-J	ϕ = 0.42 Rs = 1.98	ϕ = 0.447 Rs = 2.1	ϕ = 0.62 Rs = 589	ϕ = 0.56 Rs = 98	ϕ = 0.60 Rs = 115
From Norde function	Φ = 0.45	Φ = 0.459	Φ = 0.598	Φ = 0.57	Φ = 0.589
Trap energy in eV	-	-	0.052	0.046	0.048

From the findings of Table 8.8 we may conclude that spherical ZnO nanoparticles have been found to reduce Rs, n and ϕ more than cylindrical ZnO nanoparticles do for both types of Schottky diodes. There have been reductions of 91%, 11.5%, and 8% in series resistance (R_s), trap energy (E_t), and barrier height (ϕ), in that order.

8.3 Conclusion of the work

In this thesis we have studied the **charge transport mechanism in natural dye-based organic semiconductor Schottky diodes** and found the semiconducting property of natural herbal dyes like turmeric, indigo, and beetroot. The natural dyes show the semiconducting property which has been concluded from the band gap measurement using absorption spectra and temperature dependent dark I-V characteristics. The linear behaviour of the ϕ vs 1/n graph confirms the device is a Schottky diode. Moreover, we found that the reverse leakage current is dominated by Schottky emission (SE) over Poole-Frenkle emission (PFE), and from the temperature dependent I-V, the values of β are noticeably closer to β_{SE} than β_{PFE}. Which concludes that at high temperature SE is dominant PFE and at very low temperature PFE dominant SE. At 140 K the beetroot dye behaves like insulator and the observed parabolic conductance concludes that quantum tunnelling takes an important role in charge transportation. Using Poisson's equation, we extract the mobility, carrier concentration, and trap density in Al/beetroot/Cu Schottky diodes. The mobility is notable for reaching 124.54 $cm^2/V \cdot s$, indicating effective charge transport. The diode is a potential rectifier due to its sensitivity, nonlinearity, and asymmetric current-voltage characteristics. Again, a simulation study was run using the SCAPS 1d program to confirm the findings of the experiment. The value of conductivity and forward bias current is quite low for all these natural herbal dye-based organic semiconductor devices. Again, we observed that due to the incorporation of ZnO nanoparticles the R_s, n, and ϕ of the Schottky diode have significantly decreased, which increase the charge carrier's mobility and current conduction in the natural beetroot dye-based Schottky diode. Finally, we may conclude that spherical ZnO nanoparticles have been founded to reduce R_s, n and ϕ more than cylindrical ZnO nanoparticles do for both types of Schottky diodes. There have been reductions of 91%, 11.5%, and 8% in series resistance (R_s), trap energy (E_t), and barrier height (ϕ), in that order.

8.4 Scope of the future work

8.4.1 Challenges and current research

One of our approaches involved studying biodegradable natural herbal organic semiconductor-based electronics. This thesis provides valuable insights into nonconventional biodegradable organic electronic materials. The current conduction is highly dependent on the barrier height at the metal–organic semiconductor junction. The goal of this thesis is to investigate the current conduction mechanism through natural dye-based organic semiconductor devices, aiming to

reduce this barrier height and series resistance to enhance device performance. Charge carrier mobility is restricted by high series resistance. We also encountered a challenge where the forward bias current decreases over time in all our fabricated devices using Turmeric, Indigo, and Beetroot dyes, resulting in poor forward bias current. For, organic semiconductor devices to be efficient, strategies to lowering R_s and increasing the forward bias current are essential. Charge transport is impeded by trap states present in the organic semiconductor layer. It is crucial to look into trap energy levels and minimize their effects. We observed that ZnO nanoparticles affects barrier height, trap energy, and series resistance because of its distinct nanostructure. While natural dyes derived from beetroot have been studied extensively, other natural dyes, like indigo and turmeric, also show promise. Research on their behaviour in organic devices is an exciting area to pursue in the future.

8.4.2 Future Directions

Researchers must continue to optimize barrier height, reduce series resistance, and minimize trap energy. For this we can optimise the thickness of the dye layer. In our fabricated device thickness of the dye layer is high enough, so it should be optimised to decrease the trap energy. For this, researchers can observe the I-V characteristics by varying the dye layer's thickness. Researchers can also observe the electrical parameters by varying the junction area between organic semiconductor and metal electrode. Novel approaches, including hybrid materials and interface engineering, can lead to breakthroughs. Again, in our fabricated device we have used Al, Cu and FTO as electrodes which are not biodegradable. In light of future development of implantable and biocompatible electronics, Al and Cu substrates must be replaced with organic counterparts. Starch, composed of complex carbohydrates, can be proposed as suitable candidate for biodegradable, recyclable electronic device operation.

Herbal dye-based organic semiconductors can serve as sensors, photodetectors, and energy harvesters. Integrating these functionalities within a single device is an exciting challenge.

Bridging the gap between lab-scale demonstrations and large-scale production is essential. Collaboration with industry partners can accelerate commercialization.

Organic semiconductors based on natural herbal dyes provide a flexible and sustainable platform for electronics of the future. As scientists continue to explore their characteristics and uses, we should anticipate ground-breaking discoveries that will completely transform the industry.

Remember, the colourful natural herbal dyes may hold the key to our technological future!

List of publication

Publications included in the thesis

Part of the work presented in this thesis have been published or submitted for publication by the author:

[1] **Das AK**, Mandal R, Chakraborty K, Mandal DK. Electrical Characteristics of a Turmeric Dye-Based Organic Thin Film Device and the Effect of Light on Barrier Height. Materials Proceedings. 2022 Aug 9;10(1):11.

[2] **Das AK**, Mandal R, Mandal DK. The current transport mechanism of Al/Beetroot/Cu used as an organic semiconductor Schottky diode is superior than natural dye-based thin film devices. Microelectronic Engineering. 2022 May 15;261:111816.

[3] **Das AK**, Mandal R, Chakraborty K, Mandal DK. Impact of ZnO nanoparticles on electrical characteristics of herbal dye-based organic Schottky diode. Bulletin of Materials Science. 2022 Aug 23;45(3):164.

[4] **Das AK**, Manik NB, Mandal R, Mandal DK. The impact of the shape of zinc oxide nanoparticles on electrical parameters of natural dye-based FTO/Beetroot/Al Schottky diode. Journal of Materials Science: Materials in Electronics. 2023 Sep;34(25):1745.

[5] **Das AK**, Manik NB, Mandal DK, Rkashit S, Mandal R. A natural dye-based Schottky diode with observed quantum tunnelling and determined trap density, mobility, and excellent sensitivity and nonlinearity. Bulletin of Materials Science. 2024 Mar 23;47(2):60.

Other publications

[1] **Das AK**, Mandal R, Mandal DK. Impact of HTM on lead-free perovskite solar cell with high efficiency. Optical and Quantum Electronics. 2022 Jul;54(7):455.

[2] Chakraborty K, **Das A**, Mandal R, Mandal DK. An analytical study on low voltage regime of natural organic semiconductor based device: Physics of trap energy and ideality factor. Solid State Communications. 2021 Jan 1;323:114080.

[3] Chakraborty K, **Das AK**, Mandal R, Mandal DK. Investigation on the Trap Signature in Organic Semiconductor Turmeric Film Through Current–Voltage Analysis. Transactions of Tianjin University. 2020 Aug;26(4):265-72.

[4] Chakraborty K, **Das A**, Mandal R, Mondal DK. Interpretation of trap-assisted conduction with estimation of electrical parameters of thin indigo film-based semiconducting device. Bulletin of Materials Science. 2021 Jun;44(2):92.

[5] Chakraborty K, Mandal R, **Das A**, Mandal DK. A unified realization of the modified Einstein equation approach in organic semiconductors: theoretical interpretation and experimental validation. Indian Journal of Physics. 2023 Sep;97(10):3033-40.

[6**] Das A K**, Mandal R, Chakrabarty K, Mandal DK. IJIKC ISSN 7 (2019) 2454-2415.

Presentation at International / National conferences

[1] Design and fabrication of an indigo dye based organic thin film, A.K. Das, R. Mandal, K. Chakraborty, D.K Mandal. In RAICMHAS-2019 international conference.

[2] The current voltage characteristics of herbal dye based organic thin film, A.K. Das, R. Mandal, K. Chakraborty, D.K Mandal. In national conference on the emerging trends 2020, held at Jadavpur University.

Workshop Attendant

[1] One day seminar on Recent Trends in Pressure Vessels Design & Operation, organized by Department of Mechanical Engineering, Jadavpur University-2017.